2009

# Validation of remotely-sensed soil moisture observations for bare soil at 1.4 GHz:A quantitative approach through radiative transfer models to characterize abrupt transitions caused by a ponding event in an agricultural field,modifications to radiative transfer models,and a mobile groundbased system

Cihan Erbas
*Iowa State University*

## Recommended Citation

Erbas, Cihan, "Validation of remotely-sensed soil moisture observations for bare soil at 1.4 GHz:A quantitative approach through radiative transfer models to characterize abrupt transitions caused by a ponding event in an agricultural field,modifications to radiative transfer models,and a mobile groundbased system" (2009). *Graduate Theses and Dissertations*. 10834.
https://lib.dr.iastate.edu/etd/10834

# Validation of remotely-sensed soil moisture observations for bare soil at 1.4 GHz:

## A quantitative approach through radiative transfer models to characterize abrupt transitions caused by a ponding event in an agricultural field, modifications to the radiative transfer models, and a mobile ground-based system

by

**Cihan Erbas**

A dissertation submitted to the graduate faculty

in partial fulfillment of the requirements for the degree of

DOCTOR OF PHILOSOPHY

Major:  Electrical Engineering

Program of Study Committee:
Brian Hornbuckle, Major Professor
Robert Weber
Mani Mina
James Evans
Robert Horton

Iowa State University

Ames, Iowa

2009

To

my parents,

Sultan and Salman Erbas

who made all of this possible.

# TABLE OF CONTENTS

## LIST OF FIGURES

### Chapter 1

### Chapter 2

## Chapter 3

## Chapter 4

# LIST OF TABLES

## Chapter 1

## Chapter 4

# ABSTRACT

Soil moisture controls the physical processes that exchange mass and energy between the atmosphere and the land surface in the hydrologic cycle. Improved observations of soil moisture may lead to dramatic improvements in weather forecasting, seasonal climate prediction, and our understanding of the physical, chemical and biological processes that occur within the soil. Recent advances in remote sensing have shown that microwave radiometry is a suitable approach to retrieve soil moisture. However, the quantitative aspects of remotely-sensed soil moisture observations are not well-known, and validation of remotely-sensed measurements is an important challenge. In this dissertation, we describe efforts made at Iowa State University to establish the framework needed for the validation of remotely-sensed soil moisture observations. In the process of developing this framework, we engineered new tools that can be used by both our research group and the wider remote sensing community, and we discovered new science. The first tool is a direct-sampling digital L-band radiometer system. This radiometer system is the world's first truly mobile ground-based system. The other tools are radiative transfer models that have been modified in order to be applied to the most general remote sensing situations. An incoherent radiative transfer model was modified to include the contributions of a semi-infinite layer, and a coherent radiative transfer model was modified to account for abrupt transitions in the electrical properties of a medium. The models were verified against each other and the code was written in a user-friendly format. We demonstrated the use of these tools in determining the effect of the transient ponding of water in an agricultural field on the remote sensing signal. We found that ponding was responsible

for a 40 K change in the L-band horizontally-polarized brightness temperature. We were able to model this change with both modified coherent and incoherent radiative transfer models. Finally we gave an example of how these tools could be used to quantitatively compare remote sensing observations with models.

# CHAPTER 1.  OVERVIEW

This chapter introduces the proposed study along with the description of the global hydrologic cycle, land water and energy balances, the impact of soil moisture on the global hydrologic cycle, global change, soil moisture and global change interaction, basics of microwave radiometry, which includes sections on Planck’ s Law, brightness temperature and emissivity, the importance of L-band for radiometric soil moisture measurements, and the vegetation and surface roughness effects on microwave measurements. The format of the dissertation is also provided.

In order to fully understand the subsequent chapters, it is imperative to include a brief overview that covers the goal and significance of this study, hypotheses, methodology, and how it could be used for future research. The introduction part highlights the key concepts such as validation, error quantization, diurnal error change, and describes the flow of the analysis. Then the hydrologic cycle and its components are explained in detail. Land energy and water balances along with the interaction between their components and soil moisture are discussed. Particular emphasis is devoted to global change and how soil moisture plays a role in climate change. Microwave radiometry, its basic concepts, and the effects on microwave measurements such as surface roughness and vegetation cover are investigated. Finally, the contents of the next chapters are summarized.

## 1.1 Introduction

A growing body of evidence supports the assertion that soil moisture and the associated exchange of moisture and energy between the land surface and the atmosphere has a significant impact on precipitation patterns [1], droughts and floods [2], physical, chemical and biological processes that occur within the soil [3], and weather forecasting and seasonal climate prediction [4].

Microwave radiometry offers a unique opportunity to improve modeling of land-atmosphere interaction since it is sensitive to the presence of liquid water. Microwave frequencies are ideal for soil moisture retrieval since the dielectric constant of soil, which determines the emissive properties of the surface, changes with soil moisture. L-band is shown to be the most suitable frequency band for soil moisture observations because the emitting depth of the soil is relatively large and vegetation/surface roughness effects are smallest in this frequency band [5].

In spite of the apparent usefulness of radiometry, the quantitative aspects of remotely-sensed soil moisture observations are not well known. There is a good agreement within the scientific and engineering communities that validation of remotely-sensed measurements is an important challenge. We first need to improve quantitative value of the measurements before these observations can be truly useful, since it is not possible to advance scientific understanding without an advanced understanding of the observations. Hence, validation is a necessary step before remote sensing can effectively contribute to further scientific developments, and before it can improve our capability to predict global water and energy cycles. We define validation as

**Validation:** the determination of the space-time statistical structure of the uncertainty of an algorithm or model output.

This definition has the advantage that we can utilize mathematics, statistics and physics in order to quantify uncertainties. Any scientific developments and decision making that are based on uncertainties will be compromised and lack credibility if we cannot quantify these uncertainties.

In this study, we

- Develop a validation procedure for remotely-sensed observations of soil at L-band by first considering the simplest case: observations of bare soil. For the bare soil case, variations in the soil variables such as soil moisture profile, temperature profile and roughness can lead to errors in the remotely-sensed soil moisture measurement. The simultaneous changes of these variables might cause constructive and destructive effects on the measured brightness temperature. In order to best understand these effects, we observe the full diurnal variation of the relationship between soil moisture, temperature, and roughness and microwave emission. Diurnal microwave observations are quite rare [6]. This analysis differs significantly from most previous studies, which focused on remotely-sensed measurements of soil moisture at only one point of the day. The results of our research will be a starting point for the validation of soil moisture observations and provide an enhanced analysis of the cumulative effect of the major soil parameters such as soil moisture, soil temperature and roughness on the brightness temperature by integrating theoretical models, statistical analysis as well as remotely-sensed and in-situ measurements. This study focuses on the small-scale measurements of bare soil. Once the small-scale interactions in a basic system are understood, then it will be possible in the future to extend the method to vegetated soil, and then to larger scales, which will lead to advances in our capability to predict global water and energy cycles.

- Aim to increase the value of the future L-band satellite observations by quantifying the errors associated with these observations. Validation of remote sensing technologies must occur before these observations can be used to maximize the science return of the future L-band satellite radiometers.
- Present a potential method to determine optimal overpass time of future L-band satellite missions. The optimal overpass time for future satellite missions is still an unresolved issue. A typical selection is 6AM/6PM since temperature gradients in the soil and vegetation are smallest, which yields a more uniform temperature distribution, near sunrise and sunset. The first L-band satellite mission, the European Space Agency’ s (ESA) Soil Moisture and Ocean Salinity (SMOS) mission, will have a 6AM/6PM overpass time [7]. However, one recent study [8] showed that this overpass time might not provide the smallest error in soil moisture retrieval and more research should be conducted. Our approach in this analysis could be a basis to determine the optimal overpass time (by detecting the time of the day where the minimal error between the radiobrightness models and the measured brightness temperature occurs). However, further investigation need to be performed in order to include all of the significant effects such as Faraday rotation, the temperature gradient within the soil and vegetation, the soil moisture gradient, the vegetation water content, intercepted precipitation and dew formation.

- Study the validation of the remotely-sensed observations of soil moisture through the investigation of the error between the radiative transfer models and the radiometric soil moisture measurements. We look for answers to the following questions:

  “Does the error vary diurnally?”

  “Is the error maximum or minimum at a certain time?”

  “What changes are happening within the soil while the amount of the error is changing?”

We hypothesize that:

“Remotely-sensed observations of soil moisture can be best validated through the use of a rigorous statistical methodology that accounts for the variability in the data.”

- Utilize four radiative transfer models: the Fresnel model, the incoherent model, the coherent model, and the transmission line model, which is another coherent model, with a land surface process model that produces the soil moisture and soil temperature profiles, which are two critical inputs to all models. Then we develop programming codes for the radiative transfer models through Fortran and MATLAB routines, and verify the agreement between the models using hypothetical configurations that have known emission characteristics. Upon the application of the models to an L-band brightness temperature dataset that was collected in Michigan in 2001, we perform the error analysis. Examination of the diurnal error pattern reveals the model that produces the least error.
- Modify two of the radiative transfer models, which are the incoherent model and the coherent model. For the incoherent model, we include the semi-infinite layer effect in

the theoretical model equations. We generalize the semi-infinite layer contribution for N layers. For the coherent model, we modify the original programming code such that it could be applied to an air-water-soil case.

- Introduce world' s first truly ground-based system. The Iowa State University Direct Sampling L-Band Digital Radiometer (DSDR) was built at The University of Michigan, Ann Arbor in 2005. We provide a detailed description of the radiometer along with the overview of noise characterization of devices, and other types of radiometers.
- Produce a MATLAB tool that allows the user to apply the radiative transfer models in one main program. By choosing different options within the main program such as the model, dielectric mixing model, soil surface roughness, and the plot choice, it is possible to compute and plot the brightness temperature for a specular surface and a rough surface.

## 1.2 Global Hydrologic Cycle

The global hydrologic cycle is the exchange of water between earth and the atmosphere [9, 10, 11, 12]. Figure 1 and Table 1 show the global hydrologic cycle and Earth' s estimated water inventory, respectively.

Water moves from the surface into the atmosphere through evaporation, by which water changes from its liquid form to its gas form (vapor). Evaporation occurs on the ocean surface as well as the surfaces of other open water such as lakes, reservoirs, and plant /bare soil surfaces. The energy that a water molecule needs to break through the water surface called latent energy, which is provided by solar radiation. The molecule absorbs latent energy as it goes through the phase change from liquid to vapor. Evaporation therefore requires a supply of energy to occur.

Plants also transfer water vapor into the atmosphere through their leaves by transpiration. Soil moisture is pulled up by the plant roots and transported to the stems and leaves. Some of that water is released in the form of water vapor from the leaf openings. Since it is difficult to separate the evaporation and the transpiration processes, the term evapotranspiration is used to combine these two phenomena [13].

As moist air is elevated, it cools and its capacity to hold water decreases. The air becomes saturated when its capacity to hold water is reached. Continued cooling beyond saturation causes condensation, which is the change of state from water vapor to liquid, to form clouds. The clouds and the water vapor are advected in the atmosphere by winds and moved over the Earth. The amount of condensed water increases as the clouds further cool and precipitation begins in the form of rain, snow, drizzle or hail, depending on the air temperature.  Most of the water evaporated from the ocean returns directly back to the ocean as precipitation.

After the water reaches the ground, it infiltrates into the soil, possibly percolating down to the groundwater zone or it may run off the surface towards a stream channel:

Infiltration refers to the entry of water into the soil profile, which consists of a mixture of solid, liquid and gaseous materials [16], from the soil surface [17]. One important parameter to describe the infiltration process is the infiltration rate, which is defined as the

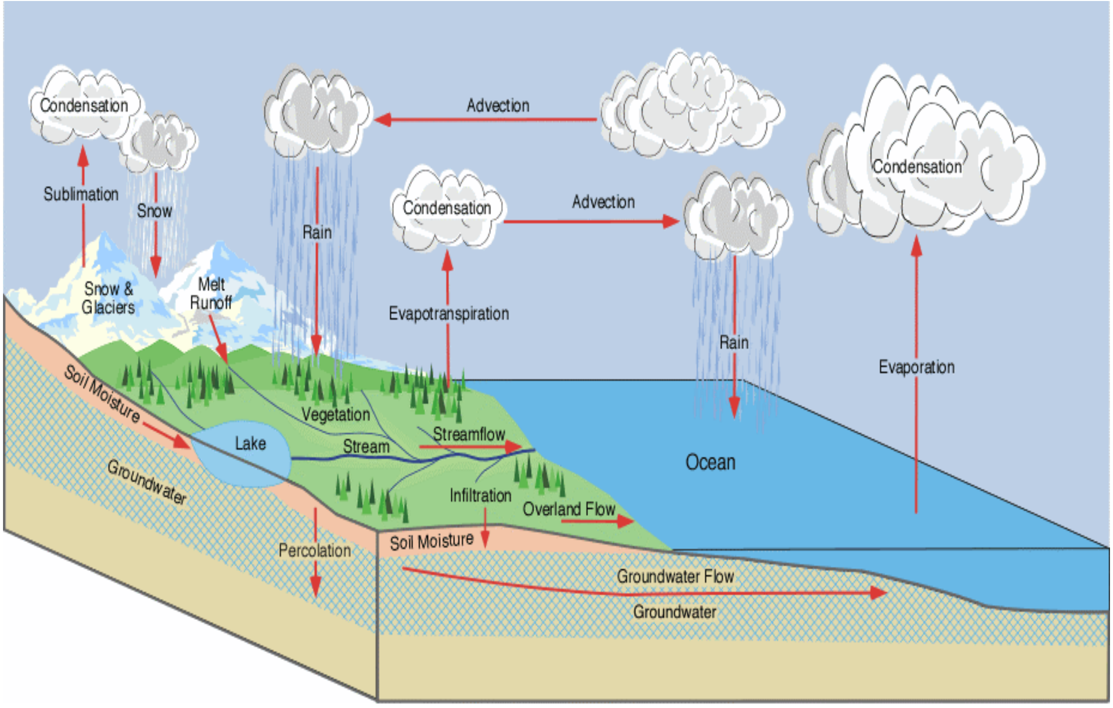

**Figure 1. Global hydrologic cycle [14].**

flux density of water passing through the soil surface and flowing into the soil profile [18]. With a continuous supply of precipitation, the infiltration rate decreases with time until it reaches a constant rate. During infiltration, a sharp boundary between the wetted region and the dry region occurs. This distinct interface between the wet and dry sections is called wetting front [19].

Some of the factors that influence infiltration are vegetation cover, soil moisture content, land use practices, surface roughness, cracks and crusts, soil texture, bulk density, hydraulic conductivity, porosity, root systems, the viscosity of water, soil and water temperature, and soil chemistry [20]. Water that infiltrates into the soil provides water for vegetation, and decreases soil erosion and the movement of the pollutants into surface water systems.

**Table 1. Earth' s estimated water inventory [15].**

| RESERVOIR | VOLUME ($10^6$ km$^3$) | % OF TOTAL |
|---|---|---|
| Oceans | 1370 | 97.25 |
| Ice caps and glaciers | 29 | 2.05 |
| Deep groundwater (750-4000 m) | 5.3 | 0.38 |
| Shallow groundwater (<750 m) | 4.2 | 0.30 |
| Lakes | 0.125 | 0.01 |
| Soil moisture | 0.065 | 0.005 |
| Atmosphere | 0.013 | 0.001 |
| Rivers | 0.0017 | 0.0001 |
| Biosphere | 0.0006 | 0.00004 |
| TOTAL | 1408.7 | 100 |

Percolation is defined as the movement of water through the soil profile [21]. When the infiltrating water passes through the unsaturated zone (or vadose zone/zone of aeration), which is the layer where voids are filled with both air and water, and water pressure is smaller than the atmospheric pressure, it permeates downward due to gravity until it reaches the saturated zone. The saturated zone is area of ground in which all voids are filled with water, and the water pressure is greater than the atmospheric pressure. Between the saturated and the unsaturated zones lies the water table, where the water pressure is equal to the atmospheric pressure. The soil water becomes groundwater when it reaches the water table. Figure 2 illustrates the unsaturated and the saturated zones. The unsaturated zone consists of root zone, intermediate zone, and capillary zone. The root zone is where roots of the plants are found, and is about a meter or so thick [22]. The zone near the water table is the capillary zone. Capillary forces draw water upward from the water table producing a zone that is wetter than the intermediate zone, which is the region located between the root zone and the capillary zone. The height of this zone depends on the pore size. The saturated zone is restricted by the impermeable rock that minimally transmits water through its interconnected voids. A rock is considered impermeable if its permeability (hydraulic conductivity) is less than 0.01 meters per day [23].

The soil water gathers minerals and loses excess bacteria and $CO_2$ as it percolates downward through the soil [24]. Groundwater returns to the surface by flowing into lakes, rivers and the oceans. The flow of groundwater is expressed in centimeters per day, meters per year, or even centimeters per year.

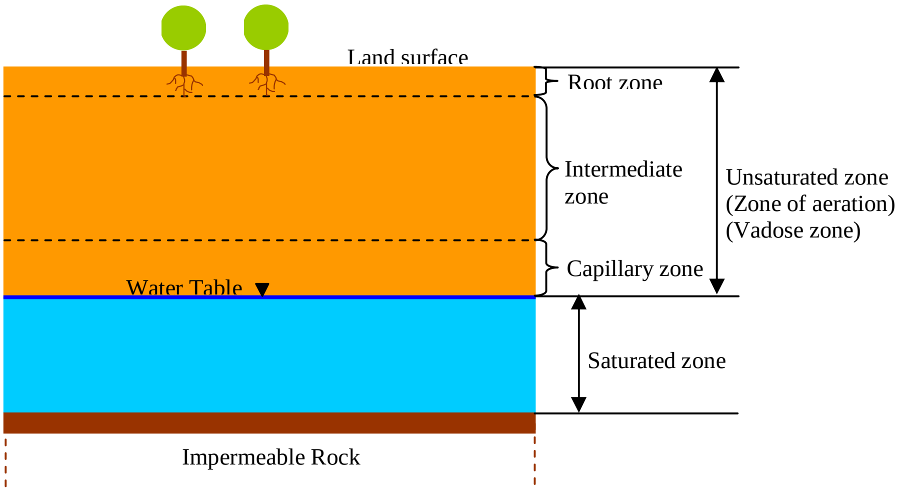

**Figure 2. Illustration of the zones through the ground [22, 25]. Not drawn to scale.**

Runoff is the water that flows over the land surface, enters the surface water systems, and eventually reaches the oceans by streamflow. It can result from precipitation, snowmelt, groundwater flow, interflow, and return flows from water used for irrigation purposes. When the precipitation rate exceeds the infiltration rate of the soil, the water begins to fill the pores on the soil surface, and surface storage (retention) occurs. If the precipitation further exceeds infiltration and the soil infiltration capacity, which is the maximum rate of infiltration into the soil, is reached, water begins to run across the land. This process is called surface runoff or overland flow, where the water flows in a shallow sheet. A large portion of the surface runoff enters stream channels, of which excessive amounts might cause riverine flooding.

As the runoff returns the water to the oceans, it completes the hydrologic cycle, and the circulation continues through evaporation of the liquid water on the Earth’ s surface.

## 1.3 Land Water and Energy Balances

The land water balance for a surface soil layer is given as

$$\frac{dS}{dt} = P - E - R_s - R_g \tag{1}$$

where $dS/dt$ is the time-change of water content within the layer (such as changes in soil moisture, snow content, ice content, surface water, groundwater), $P$ is the precipitation, $E$ is the evapotranspiration, $R_s$ is the surface runoff, and $R_g$ is the drainage or groundwater runoff (percolation), depending on the soil depth.

The land energy balance for a surface soil layer is expressed as

$$\frac{dH}{dt} = R_n - \lambda E - SH - G \tag{2}$$

where $dH/dt$ is the time-change of energy within the surface layer (such as temperature change, phase change), $R_n$ is the net radiation, $\lambda E$ is the latent heat flux (latent energy of vaporization $\lambda$ times the evapotranspiration $E$), $SH$ is the sensible heat flux, and $G$ is the ground heat flux to deeper layers.

The land water and energy balances are coupled through the evapotranspiration term, because during the evapotranspiration process, latent energy is absorbed by water molecules, and water vapor is transferred into the atmosphere. Energy is therefore transported through water vapor. Figure 3 illustrates the land water and energy balances for a soil layer.

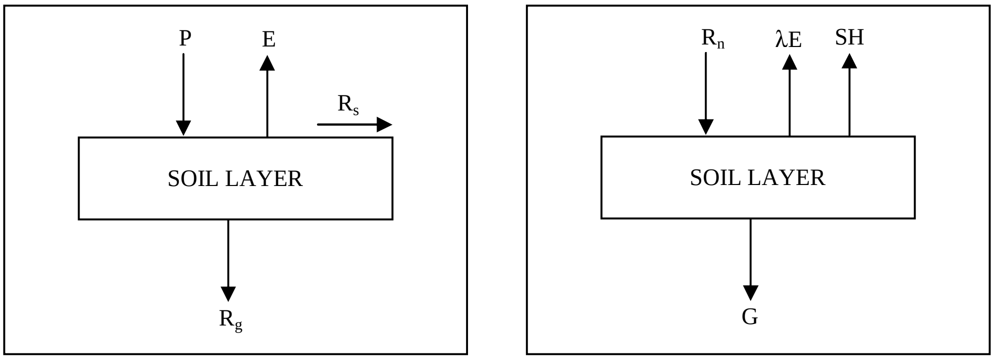

**Figure 3. Land water and energy balances for a soil layer.**

## 1.4 Soil Moisture and Global Hydrologic Cycle

Although soil moisture constitutes only 0.005% of the total water reservoir of the Earth (see Table 1), it controls other major components of the global hydrologic cycle as well as the interaction between land and atmosphere through the exchange of water and energy fluxes, since it provides the lower boundary for the atmosphere. Equation 1 implies that a change in soil moisture is a response to changes in one or more of the elements of the water cycle, since the mass of total water is conserved at all times. Therefore, soil moisture plays a crucial role in global hydrologic cycle because it exerts an essential control on water and energy balances, regulates the rates of other pieces of the hydrologic cycle such as precipitation, evapotranspiration, surface runoff and groundwater runoff (percolation), and provides an aggregate measure of water availability. The impact of soil moisture on the hydrologic cycle is examined on the basis of Equation 1 such that the effect of soil moisture on each term is investigated individually.

### 1.4.1 Soil Moisture and Precipitation

Of particular interest is the interaction between soil moisture and precipitation, and the possible existence of a strong feedback between these two components of the hydrologic cycle [26, 27]. In spite of an apparent soil moisture-precipitation mechanism, the critical details of this relationship are poorly understood in the real world [28], because the simple assumption that an increase in precipitation results *solely* from an increased local evapotranspiration has been shown to be invalid [29, 30]. In fact, the water vapor can reside in the atmosphere for about one week, which means it can travel a long distance before it falls on the Earth surface as precipitation. Furthermore, the connection from soil moisture to precipitation is complex, as it includes impacts of both surface energy and moisture fluxes, and is affected by the atmospheric boundary layer and general circulation [31].

Various observational and model-based investigations have been carried out in order to better understand the feedback between soil moisture and precipitation.

Koster et. al. [32] reported on several distinct ‘hot spots’, where the impact of soil moisture on precipitation is significant, by averaging the results of 12 circulation models to determine the coupling strength. These hot spots are seen in the central Great Plains (North

America), the Sahel (equatorial Africa), and India. Regions where the coupling strength is less intense are in South America, central Asia, and China. Another study by Koster et. al. [33] suggested that oceanic impacts on summer precipitation are small compared to soil moisture impacts in transitional regions (continental midlatitudes, between dry and wet climates). This is because soil moisture is not a limiting factor for evapotranspiration in a wet climate, and evapotranspiration is too scarce in a dry climate to influence precipitation. A confirming study by Zangvil et. al. [34] reported that the main source of atmospheric moisture for the daytime precipitation for a test area (1300 km x 750 km) in east central Illinois comes from the local evapotranspiration, which is highly dependent on the soil moisture availability. Rowntree and Bolton [35] revealed a strong sensitivity of precipitation with respect to initial soil moisture conditions over Europe such that soil moisture distribution has important implications for the summertime European precipitation distribution. Also, Schar et. al. [29] showed that summertime European precipitation climate in a belt about 1000 km wide between the wet Atlantic and the dry Mediterranean climate depends on the soil moisture content. Fast et. al. [36] indicated that horizontal heterogeneity of soil moisture might play a role in the spatial distribution and intensity of precipitation in the central US. Castelli et. al. [37] proposed that an increase in soil moisture content might increase local precipitation, while it might decrease precipitation at larger scales. Walker and Rowntree [38] demonstrated that positive anomalies of soil moisture, under certain conditions, interact with the atmosphere in such a way as to sustain themselves by enhancing evaporation, and therefore increasing precipitation rates and prolonging the initial soil wetness anomaly. Doublin et. al. [39] showed that soil moisture deficits in most southern US are strongly negatively correlated with precipitation. Gutowski et. al. [40] demonstrated by a simulation study that the insufficient soil moisture in the south-central US during fall caused a precipitation deficit in fall and winter of 1979-1988.

### 1.4.2 Soil Moisture and Evapotranspiration

Evapotranspiration is a significant component of the hydrologic cycle. At the global scale, it represents more than 60% of the total precipitation [41] and therefore conveys an important constraint on water availability on land surface.

The interaction between soil moisture and evapotranspiration is more straightforward than that of precipitation. If there is not sufficient soil moisture, then no evapotranspiration can occur and most of the incoming energy (net radiation) goes into sensible heat flux, thus strongly enhances air temperature. Conversely, if water is available in ample supply (moist surface or water body), then a large amount of energy will be used for evapotranspiration thus affecting a net cooling compared to dry surfaces. These effects are, however, only true for regions where soil moisture is the main controlling factor for evapotranspiration. In high latitudes, for example, evapotranspiration is limited by net radiation and the length of the growing season [26]. Several studies [36, 39, 42, 43, 44, 45, 46] confirm that negative (positive) anomalies of soil moisture decrease (increase) evapotranspiration rates and increase (decrease) surface temperature.

### 1.4.3 Soil Moisture and Surface Runoff

Soil moisture is the main source of natural water resources for agriculture and natural vegetation. It affects not only the vertical fluxes of energy and moisture, but also the horizontal fluxes of moisture, namely, runoff [47]. Several investigations for different regions of the globe address the significance of soil moisture on runoff, and runoff predictability.

Upon analiyzing the daily data of the Serein and Leaf rivers of Mississippi, and using an artificial neural network model to forecast streamflow, Anctil et. al. [48] revealed that only the soil moisture input is useful for one-day-ahead streamflow forecasting, with both the evapotranspiration and precipitation inputs failing to improve the model performance. Maurer [49] explored the importance of climatic indicators and the initial states of simulated snow and soil moisture fields for understanding the predictability of runoff. Their results demonstrate that the soil moisture initial state contributes significantly to runoff predictability at lead times of 1.5 months, except over portions of the Mississippi River basin dominated by snowmelt. Mahanama et. al. [50] examined the relative contribution of soil moisture initialization to the streamflow forecasts in several watersheds on the tropical island of Sri Lanka. Their results indicate that accurate soil moisture initialization can contribute to the generation of useful streamflow predictions that have a stronger impact on the prediction skill during inter-monsoon seasons. Berg and Mulroy [51] showed the correlation between the modeled soil moisture and gauge-measured streamflow in the Saskatchewan/Nelson River basin of the Canadian Prairies. Their results suggest that further predictability in streamflow is possible when an estimate of soil moisture initial state is given, Wei et. al. [52] investigated the effect of antecedent soil moisture on runoff by collecting soil moisture (at 10 cm before a rain event) and runoff measurements at a research site in southern China, which is characterized by a subtropical monsoon climate. Their experiment reveals that the antecedent soil moisture impacts runoff significantly through the control of runoff generation mechanisms. Castillo et. al. [53] suggested that antecedent soil moisture content is an important factor controlling runoff in semiarid regions during medium to low intensity storms, while runoff response is more uniform and independent of the initial soil moisture content during high intensity storms, after a model-based analysis for a Mediterranean river basin in southeast Spain. They also concluded that the exclusion of the initial soil moisture content from the modeling approach may result in substantial errors in runoff predictions for most recurrent rainstorms in semiarid environments. Koster [54] indicated that one factor that affects soil moisture persistence (memory) in climate models is the variation of runoff with soil moisture such that runoff acts to remove anomaly.

### 1.4.4 Soil Moisture and Percolation

Soil moisture can contribute to surface flow or percolate down to a deeper layer such as 1 m, or even become groundwater, depending on the porous properties of the ground [55]. Soils with large pore spaces, such as sandy soils, usually have a high percolation rate, while the soils with small pore spaces have low percolation rates.

Percolation theory, which is developed mathematically to deal with disordered media, where the disorder is defined by a random variation in the degree of connectivity, can be used to explain the percolation through the soil. The main concept of percolation theory is the existence of a percolation threshold, defined in the following way: Suppose p is a parameter that defines the average degree of connectivity between various sub-units of some arbitrary system. When $p = 0$, all sub-units are totally isolated from every other sub-unit. When $p = 1$, all sub-units are connected to some maximum number of neighboring sub- units. At this point, the system is connected from one side to the other, since there are paths that go completely across the system, linking one sub-unit to the next along the spanning cluster. Now suppose, starting at $p = 1$, connections are randomly broken, so that p, the measure of average connectivity, decreases. The percolation threshold is that value of p, usually denoted $p_c$, at which there is no longer an unbroken path from one side of the system to the other. Alternately, if we start out at $p = 0$, and randomly create connections, so that p increases, $p_c$ is defined as the point at which a spanning cluster first appears. For p less than $p_c$, only isolated, non-spanning clusters can exist. For p greater than $p_c$, there is always a spanning cluster, although some isolated, non-spanning clusters can still be present.

Several studies [56, 57] investigated how the soil moisture content affects the percolation through the soil, utilizing the percolation theory.

## 1.5 Global Change

The Earth' s climate has always been changing [58]. There is no doubt that the climate is growing warmer currently; indications of that change are all around us.

Average global temperatures have increased about 0.7°C since the late 1800s. This increase in temperature is largely responsible for average global sea levels that rise by 10 to 25 cm (4 to 10 inches) since 1900 [59]. The average surface temperature of the Earth has warmed since the late 1800s, by about 0.6°C [60]. The 1990s were not only the warmest decade of the 20th century but also the millennium [61].

Sea ice cover in the Arctic is a clear indicator of climate change and an important player for the interaction between the Arctic and the globe [26]. Records of increasing temperature, melting glaciers, reductions in thickness of sea ice, thawing permafrost, and rising sea level all provide strong evidence of recent warming in the Arctic. In Alaska and western Canada, winter temperatures have increased as much as 3-4 °C in the past 50 years. [62]. Figure 4 shows the 100,000 years of temperature variation in Greenland. The plot indicates a high variability in climate over the last 100,000 years. It also suggests that the climate has been unusually stable for the last 10,000 years (during which human civilization developed). There is concern that the rapid warming today might destabilize this condition.

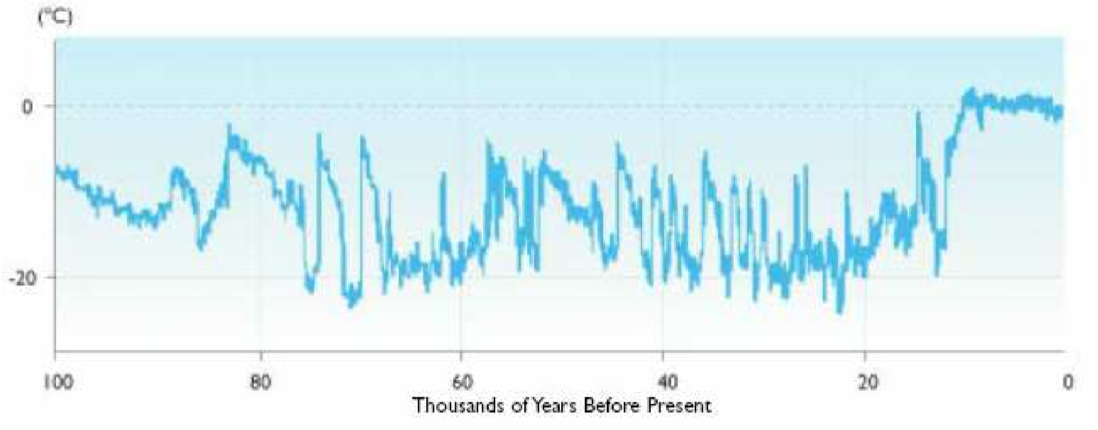

**Figure 4. 100,000 years of temperature variation in Greenland [62].**

This warming cannot be adequately explained by natural phenomena such as increased solar activity and volcanic eruptions [60]. Furthermore, the report of Working Group I of the International Panel on Climate Change (IPCC 2007) concludes that, very likely (probability >90%), human influence has contributed to a warming of the planet during the past 50 years and that it virtually certainly (>99%) will lead to an accelerated warming in the future [26].

The composition of atmosphere has changed markedly since pre-industrial times due to human activity (fossil fuel burning, land use changes, production and use of halocarbons etc.). Carbon dioxide ($CO_2$) levels in the atmosphere have risen from about 280 parts per million per volume (ppmv) in the pre-industrial period (defined as the average of several centuries before 1750) to around 360 ppmv in the late 1990s [58, 63, 64]. Human-induced (anthropogenic) increases in the concentration of greenhouse gases such as $CO_2$, water vapor, methane ($CH_4$), nitrous oxide ($N_2O$), and chlorofluorocarbons (abbreviated as CFC) are at least partially responsible for the current global warming [60], while $CO_2$ is the greenhouse gas that is thought to have contributed the most to global warming over the last 250 years [65]. Greenhouse gases enhances the greenhouse effect, in which the radiated infrared emission from the Earth’ s surface is trapped by the greenhouse gases and re-radiated back towards the Earth’ s surface causing a warming. This increase of the greenhouse effect heats the atmosphere and provokes a stronger evaporation at the ocean surface. As water vapor is one of the greenhouse gases, a positive feedback leads to an amplification of the atmospheric warming [66].

The results of the global warming could be devastating. Sea level rise, if not stopped in time, could totally submerge the Maldives and other small islands. The islands in the Indian and Pacific oceans are already being evacuated because of rising waters. In Bangladesh, 15 million people live less than a meter above the sea level. Climate change makes a drastic difference to the food supply: The poorest continent, Africa, is already suffering from food shortages made far worse by a series of droughts, believed to be at least partly caused by climate change [67]. The IPCC’ s Second Assessment Report noted that global circulation model (GCM) results suggest gradual increases in the frequency of intense precipitation events (heavy rainfall, snowfall) and, in some regions, increases in the probability of dry days and the length of the dry spells [59]. Floods and droughts projected for the 21st century show significant and large changes from those in the 20th century (i.e. from 1901-2000). The results indicate an increase in the frequency of floods in many regions of the globe, except regions including North America and central and western Eurasia. [68]. One study [69] suggested that severe drought (which occurs 5% of the time at present) will occur 50% of the time by 2050s. Higher temperatures will increase the potential evapotranspiration and possibly result in increased drought occurrence, although actual changes will be controlled by available moisture from precipitation and be modified by temperature impacts on snow [70]. Arctic sea ice might change abruptly in the future [71].

## 1.6 Soil Moisture and Global Change

### 1.6.1 Soil Moisture and Extreme Events

Immediate impacts of climate change are mainly caused by the extreme events, rather than the fluctuations in the mean conditions [72], as the early stages of a worldwide change will not be a problem because socio-economic factors such as diversity in agriculture, international trade, and planned water resources will act as a buffer to change [73]. The role of soil moisture and its anomalies in extreme events such as droughts and floods, prolonged heatwaves, and heavy rainfalls have been documented in different studies.

The US experienced several droughts and floods during the 20th century. The droughts of 1930s, 1950s and 1988, and the flood of 1993 have been among the most severe extremes [74]. These extreme events resulted in heavy financial losses for the agricultural community, and the flooding caused personal loss in many urban communities [75]. Atlas et. al. [76] used model simulations to investigate the effect of soil moisture anomalies on the 1988 summer drought. That study showed that the impact of using the 1988 soil moisture anomalies in the model simulations was larger and more consistent than the impact of sea surface temperature anomalies. The anomalous soil moisture resulted in a larger decrease in the precipitation over the Great Plains, which was accompanied by a correspondingly large increase in the mean surface temperature. Furthermore, the combined effect of soil moisture and sea surface temperature anomalies was very similar to the impact of soil moisture alone. Pan et. al. [75] suggested that the saturated surface, over the ‘flood-stricken’ region, was quite significant in contributing to the total rainfall during the flood of 1993. Lakshmi et. al [2] investigated the correlation between extreme events and a set of parameters in the Upper Mississippi Basin over 1950-1999 and suggested that deep (40-140cm) soil moisture content could be the best indicator for the extremes, which held true for the drought of 1988 and flood of 1993. Kunkel et. al. [77] pointed out that above-normal soil moisture levels in early June 1993 was one factor that contributed to the flood of 1993. Beljaars et. al. [78] indicated that the soil moisture anomaly affected the precipitation pattern during the flood of 1993, as their simulation of rainfall with an initial soil moisture content of 100% returned more realistic values than those of 25%. Koster et. al. [79] suggested that soil moisture feedback accounted for the two-thirds of the low-frequency (time scales longer than about 6 years) variability in precipitation during the droughts of 1930s and 1950s in the Great Plains, while sea surface temperature contributed to one-third of the variation. Schubert et. al. [80]

proposed that the drought of 1930s was caused by anomalous tropical sea surface temperatures, and soil moisture-precipitation feedback was responsible for its severity, since excluding this feedback mechanism in a simulation run for the period 1932-1938 resulted in a reduction of 50% in precipitation deficit.

The vegetation-albedo-precipitation mechanism, in which a reduction of vegetation with a consequent increase in albedo (reflectivity averaged out over all wavelengths), which also depends on soil moisture [81], results in a decrease in cloud formation and precipitation. Charney [82] proposed that such a mechanism is applicable to the semi-arid Sahel of west Africa. A confirming study by Charney et. al. [83] demonstrated through numerical simulation that appreciable increases in albedo significantly decreased the simulated precipitation in the Sahel and the Western Great Plains of North America, which might extend the period of droughts. Simmonds and Hope [84] mention that the same effect might be one factor (besides the ocean conditions and circulation anomalies) that contributes to the rainfall anomalies in Australia.

Another expression of the global warming is the observed increase in the occurrence of heatwaves [Schar ref 5,6]. Changes in the frequency of extreme high (or low) temperatures are of importance not only to agriculture but also, for example, energy demand and human mortality [wigley 1985]. Schar [85] suggested that the suppression of evapotranspiration due to the lack of soil moisture, and a soil moisture-precipitation feedback were linked to the abnormally hot European summer in 2003. Fischer et. al. [86] determined that soil moisture-temperature interactions increased the heatwave duration and accounted for typically 50-80% of the number of hot summer days during the same heatwave event in 2003. Lare et. al. [87]

suggested that the persistence of rainfall anomalies (positive and negative) in the Sahel might be due to land-atmosphere feedback, since they reported a parallel change in observed precipitation and simulated soil moisture (and evaporation) for both wet and dry years. The Kalahari, which has similar characteristics to the Sahel, does not experience such persistence, implying that the impact of the land surface changes might be less significant. Another study by Douville [88] showed that soil moisture anomalies influence the Sahelian monsoon, using a climate model to observe the effect of the simulated soil moisture on the simulated variability of the monsoon rainfall. Webster [89] postulated that surface hydrology and soil-moisture feedback might play a role in the repeated northward progression of the monsoon through India with about a 30 to 40-day period.

### 1.6.2 Soil Moisture and Climate Modeling

Global climate models (GCMs) have been developed to simulate the present climate and used to predict future climatic change [90]. These models require boundary conditions that are provided by land surface schemes (LSSs), which describe the energy, mass and momentum exchange at the Earth’ s continental surface. However, different GCMs employ very different land surface schemes (LSSs) and, as a result, their predictions of land surface quantities are often difficult to compare. Furthermore, the uncertainty in surface-atmosphere coupling has implications for the reliability of the simulated soil moisture-atmosphere feedback in the LSSs, which prohibits accurate verification and/or calibration of the parametrizations in the GCMs [28], narrows the predictive capability of GCMs [91], and toughens our interpretation of the response of the hydrologic cycle to simulated climate change. [26].

Maintaining an estimate of soil moisture is an essential task of the LSSs because the errors in the estimate of the either surface soil moisture or stored water contribute to errors in the estimates of latent energy flux and, finally to potentially significant errors in GCMs. [3,92]. It is well known that the improved observations of soil moisture may lead to dramatic improvements in the performance of LSSs and hence the GCMs [31, 93, 94]. One method for the measurement of soil moisture is microwave radiometry, which is described in the next section.

## 1.7 Microwave Radiometry

The term ‘microwave radiometry’ means the measurement of incoherent radiant electromagnetic energy in the microwave band of electromagnetic spectrum. All materials at a finite absolute temperature emit (radiate) electromagnetic energy.

The energy that is received by the Earth is the solar electromagnetic radiation. A part of the received energy is scattered and absorbed by the atmosphere, and the rest of the energy is transmitted to the Earth surface. The surface reflects and absorbs the incident energy. The absorption of the energy means a transformation into thermal energy with a rise in the thermometric temperature of the medium (surface). The reverse process is called the ‘thermal emission’, which is the study area of radiometry.

### 1.7.1 Planck’ s Law and Its Approximations

The theory of thermal radiation mechanism is described by Planck’ s blackbody radiation law, which was introduced in 1901. A *blackbody radiator* is an important concept in understanding the radiation process of the real materials. A blackbody radiator is defined as an idealized, perfectly opaque material that absorbs all the incident radiation at all frequencies, reflecting none [95]. A blackbody is also a perfect emitter. According to Planck' s law, a blackbody has a uniform radiation in all directions:

$$B_f = \frac{2hf^3}{c^2}\left(\frac{1}{e^{hf/kT}-1}\right) \tag{3}$$

where $B_f$ is the blackbody spectral brightness [W m$^{-2}$ sr$^{-1}$ Hz$^{-1}$], which is defined as the radiated power per unit area per unit solid angle per unit bandwidth for a blackbody, h=6.63x10$^{-34}$ [J s] is Planck' s constant, f is the frequency [Hz], k=1.38x10$^{-23}$ [J K$^{-1}$] is Boltzmann' s constant, T is the absolute temperature [K], c=3.00x10$^{8}$ [m sec$^{-1}$] is the velocity of light. The only variables in Equation (3) are $f$ and $T$.

For high frequencies, at typical Earth temperatures $hf/kT>>1$. Then,

$$\frac{1}{e^{hf/kT}-1} \approx \frac{1}{e^{hf/kT}} = e^{-hf/kT} \tag{4}$$

Equation (3) reduces to

$$B_f = \frac{2h}{c^2} f^3 e^{-hf/kT} \tag{5}$$

Equation (5) is called Wien Radiation Law.

For low frequencies, at typical Earth temperatures, we use the Taylor series approach such that

$$e^x - 1 = \left(1 + x + \frac{x^2}{2} + \ldots\right) - 1 \approx x \qquad \text{for } x<<1 \tag{6}$$

Then,

$$B_f = \frac{2f^2kT}{c^2} \tag{7}$$

Equation (7) is called Rayleigh-Jeans law. It is useful in the microwave region.

### 1.7.2 Brightness Temperature and Emissivity

A blackbody is an idealized material. Real materials, called *grey bodies*, emit less than a blackbody, and do not absorb all the energy incident on them. In the microwave region, the brightness (radiated power per unit area per unit solid angle) of a blackbody is

$$B_{bb} = B_f \Delta f \tag{8}$$

Using Equation (7) in Equation (8)

$$B_{bb} = \frac{2f^2kT}{c^2}\Delta f \tag{9}$$

for a bandwidth $\Delta f$. For a grey body with a direction-dependent brightness $B(\theta,\phi)$ and a physical temperature $T$, we can define a blackbody equivalent radiometric temperature so that $B(\theta,\phi)$ is similar to Equation (9). This temperature is called the *brightness temperature*, and given as

$$B(\theta,\phi) = \frac{2f^2k}{c^2}T_B(\theta,\phi)\Delta f \tag{10}$$

The ratio $B(\theta,\phi)/B_{bb}$ is called the *emissivity*, and

$$e(\theta,\phi) = \frac{B(\theta,\phi)}{B_{bb}} = \frac{T_B(\theta,\phi)}{T} \tag{11}$$

It is obvious that emissivity is the normalized brightness temperature and radiometrically, a body always looks cooler than its actual temperature since $0<e<1$. For dry surfaces emissivity is larger while it becomes smaller as the water content increases.

Theoretically, a perfectly conducting material, such as a metal object, has zero emissivity, thereby making it easier to differentiate from the Earth' s background (the emissivity for land surfaces is rarely <0.3 and is often >0.7). Although metal objects do not self emit, the observed brightness temperature is not identically zero because they reflect downward-emitted sky radiation.

### 1.7.3 Why L-Band?

Emissivity is determined by the dielectric properties of a transition layer at the surface of an object. It has been shown that at longer wavelengths the transition layer that the sensors see through is deeper which means a longer wavelength sensor provides information on thicker layer of soil than does a shorter wavelength. L-band covers a range of frequencies between 390MHz and 1.55GHz. The optimum wavelength for soil moisture measurements falls in the L-band at a wavelength of 21 cm ($\lambda \approx 21$ cm) operating at near-nadir look angles and horizontal polarization (horizontal polarization has higher sensitivity to soil moisture then does vertical polarization) [96, 97]. The transition layer at $\lambda \approx 21$ cm is about 5 cm while it is less than 1 cm for $\lambda \approx 2.25$ cm. The 21 cm wavelength at the 1.4 GHz radio astronomy window provides for significant penetration of vegetation and decreases the normalized surface roughness [98].

### 1.7.4 Effects on Radiometric Measurements: Vegetation Cover and Surface Roughness

Surface roughness and vegetation cover are two important effects that should be considered for application purposes.

Microwave emissivity from a soil surface is related to the reflectivity of the surface. The simplest situation is a smooth surface, where the variations in the surface are a fraction of the wavelength being used. Under these conditions, emissivity and reflectivity can be modeled.

Surface roughness causes an increase in emissivity compared to a smooth surface. The reason is that as the surface roughness increases, the soil surface area that interfaces with the air increases and more upwelling energy is transmitted. However, current models are considered insufficient since the geometry of soil surfaces and the details of radiation scattering from these surfaces are not well known.

The complexity of the vegetation cover, in terms of modeling, limits our understanding. However, deterministic approaches accounting for its effects have been successful and have shown that soil moisture can be determined under a wide range of canopy conditions. A vegetation canopy over the soil attenuates the radiation from the soil and adds its own emissions. Thus, vegetation cover acts like an absorber (and a scatterer). The level of absorption is dependent on plant shape, wavelength, incidence angle and vegetation water content. Instrument sensitivity is lost due to attenuation by vegetation canopies. However, at L-band there is less instrument sensitivity loss compared to that at shorter wavelengths.

## 1.8 Dissertation Format

The following second chapter focuses on the Iowa State University Direct Sampling L-band Digital Radiometer (DSDR). A general description of noise characterization that includes equivalent noise temperature and noise figure is given. Radiometer types such as total power radiometer and Dicke radiometer are summarized. Then the DSDR instrument description is covered: The components such as antenna, radio frequency (RF) chain, digitizer, digital back end, and thermal control are investigated.

The third chapter describes the radiative transfer models that are utilized throughout the study. Fresnel model, the incoherent model, the coherent model, the transmission line model are summarized. Modifications to the incoherent model and the coherent model are presented. Semi-infinite layer effect is included in the incoherent model, and the programming code for the coherent model is modified such that an air-water-soil test case, which is also given in chapter 3 to test the agreement between the radiative transfer models, can be simulated. A land surface model called ‘The Atmospheric and Land-surface Exchange model (ALEX)’, a dielectric mixing model, and a soil surface roughness model is also explained.

The fourth chapter illustrates the application of the radiative transfer models to a set of data that was collected in Michigan in 2001. An abrupt change in the brightness temperature variation is investigated, and verified that the abrupt change is caused by ponding of water. Fresnel model is shown to fail to model ponding. The transmission line model and the incoherent model are able to model ponding events. An error analysis is carried out in order to determine the relative error and the root mean square error between the measured and the modeled brightness temperatures. It is observed that the incoherent model returns a smaller root mean square error.

Finally, the fifth chapter concludes the study. An overall analysis of the dissertation is presented, and possible future work is illustrated.

## 1.9 Conclusion

We have examined the proposed study as well as a description of the global hydrologic cycle, land water and energy balances, soil moisture and hydrologic cycle interaction, global change, how soil moisture and global change are related, microwave radiometry, which describes Planck' s Law, brightness temperature and emissivity, the reason why L-band is preferred for radiometric soil moisture measurements, and the vegetation and surface roughness factors on microwave measurements. We have also included the format of the following chapters.

## BIBLIOGRAPHY

[1] Koster, R. D., Suarez, M. J., Higgins, R. W., Van den Dool, H. M. (2003). Observational evidence that soil moisture variations affect precipitation, *Geophysical Research Letters,* 30(5).

[2] Lakshmi, V., Piechota, T., Narayan, U., Tang, C. (2004). Soil moisture as an indicator of weather extremes, *Geophysical Research Letters*, 31.

[3] Alvala, R. C. S., Gielow, R., Da Rocha, H. R., Freitas, H. C., Lopes, J. M., Manzi, A. O., Von Randow, C., Dias, M. A. F. S., Cabral, O. M. R.,Waterloo, M. J. (2002). Intradiurnal and seasonal variability of soil temperature, heat flux, soil moisture content, and thermal properties under forest and pasture in Rondonia, *Journal of Geophysical Research,* 107(D20). pp. 1-20.

[4] Prigent, C., Aires, F., Rossow, W. B., Robock, A. (2005). Sensitivity of satellite microwave and infrared observations to soil moisture at a global scale: relationship of satellite observations to in situ soil moisture measurements, *Journal of Geophysical Research* 110(D07110).

[5] Jackson, T. J., Schmugge, T. J. (1989). Passive microwave remote sensing system for soil moisture: some supporting research, *IEEE Trans. Geosci. Remote Sensing*, 27(2), 225-234.

[6] Jackson, T. J., O' Neill, P. E., Swift, C. T. (1997). Passive microwave observations of diurnal surface soil moisture, *IEEE Trans. on Geoscience and Remote Sensing*, 35(5), 1210-1222.

[7] Kerr, Y. H., Waldteufel, P., Wigneron, J. P., Martinuzzi, J. M., Font, J., Berger, M. (2001). Soil moisture retrieval from space: the soil moisture and ocean salinity (SMOS) mission, *IEEE Transactions on Geoscience and Remote Sensing*, 39(8), 1729-1735.

[8] Hornbuckle, B. K., England, A. W. (2005). Diurnal variation of vertical temperature gradients within a field of maize: implications for satellite microwave radiometry, *IEEE Geoscience and Remote Sensing Letters*, 2(1), 74-77.

[9] Leopold, L. B. (1997). *Water, Rivers and Creeks*. California: University Science Books.

[10] Raschke, E. (1996). *Radiation and Water in the Climate System: Remote Measurements.* Berlin: Springer-Verlag.

[11] Weight, W. D., Sonderegger, J. L. (2000). *Manual of Applied Field Hydrogeology*. New York: McGraw-Hill.

[12] Soliman, M. M., LaMoreaux, P. E., Memon B. A., Assaad, F. A., LaMoreaux, J. W. (1997). *Environmental Hydrogeology*. New York: Lewis Publishers.

[13] Furon, R. (1963). *The Problem of Water: A World Study*. New York: Elsevier

[14] http://www.physicalgeography.net/fundamentals/8b.html

[15] Berner, E. K., Berner, R. A. (1987). *The Global Water Cycle: Geochemistry and Environment*. New Jersey: Prentice-Hall.

[16] Wilson, E. M. (1974). *Engineering Hydrology*. Great Britain: Macmillan.

[17] Jury, W. A., Horton, R. (2004). *Soil Physics*. New Jersey: John Wiley & Sons.

[18] Scott, D. (2000). *Soil Physics*. Ames: Iowa State University Press.

[19] Lal, R., Shukla, M. K. (2004). *Principles of Soil Physics* New York: CRC Press.

[20] Ward, A. D., Elliot, W. J. (1995). *Environmental Hydrology*. New York: CRC Press.

[21] Wild, A. (1993). *Soils and the Environment: An Introduction*. New York: Cambridge University Press.

[22] Guymon, G. L. (1994). *Unsaturated Zone Hydrology*. New Jersey: Prentice-Hall.

[23] Waltham, T. (2002). *Foundations of Engineering Geology*. London: Spon Press.

[24] Cocannouer, J. A. (1958). *Water and the Cycle of Life*. New York: The Devin-Adair Company.

[25] Todd, D. K., Mays, L. W. (2005). *Groundwater Hydrology*. New Jersey: John Wiley & Sons.

[26] Bronnimann, S., Luterbacher, J., Ewen, T., Diaz, H. F., Stolarski, R. S., Neu, U. (2008). *Climate Variability and Extremes during the Past 100 Years*. Zurich: Springer.

[27] Koster, R. D. et. al. (2002). Comparing the degree of land-atmosphere interaction in four atmospheric general circulation models. *Journal of Hydrometeorology.* 3. pp. 363-375.

[28] Meehl, G. A., Washington, W. M. (1987). A comparison of soil-moisture sensitivity in two global climate models. *Journal of the Atmospheric Sciences.* 45(9). pp. 1476-1492.

[29] Schar, S., Luthi, D., Beyerle, U. (1998). The soil-precipitation feedback: a process study with a regional climate model. *Journal of Climate.* 12. pp. 722-741.

[30] McDonald, J. E. (1962). *The evapotranspiration-precipitation fallacy.* Weather. 17. pp. 168-177.

[31] Dirmeyer, D. A. (1999). Using a global soil wetness dataset to improve seasonal climate simulation. *Journal of Climate.* 13. pp. 2900-2922.

[32] Koster, R. D. et. al. (2004). Regions of strong coupling between soil moisture and precipitation. *Science.* 305. pp. 1138-1140.

[33] Koster, R. D., Suarez, M. J., Heiser, M. (1999). Variance and predictability of precipitation at seasonal-to-interannual timescales. *Journal of Hydrometeorology.* 1. pp. 26-46.

[34] Zangvil, A., Portis, D. H., Lamb, P. J. (1993). Diurnal variations in the water vapor budget components over the Midwestern United States in summer 1979. *Geophysical Monograph.* 15. pp. 53-63.

[35] Rowntree, P. R., Bolton, J. A. (1983). Simulations of the atmospheric response to soil moisture anomalies over Europe. *Quarterly Journal of the Royal Meteorological Society*. 109(461). pp. 501-526.

[36] Fast, J. D., McCorcle, M. D. (1991). The effect of heterogeneous soil moisture on a summer baroclinic circulation in the central United States. *Monthly Weather Review.* 119(9). pp. 2140-2167.

[37] Castelli, F., Rodriguez-Iturbe, I., Entekhabi, D. (1996). An analytical framework for the modeling of the spatial interaction between soil moisture and the atmosphere. *Journal of Hydrology*. 184. pp. 19-34.

[38] Walker, J. M., Rowntree, P. R. (1977). The effect of soil moisture on circulation and rainfall in a tropical model. *Quarterly Journal of the Royal Meteorological Society.* 103(435). pp. 29-46.

[39] Doublin, J. K., Grundstein, A. J. (2008). Warm-season soil-moisture deficits in the southern United States. *Physical Geography*. 29(1). pp. 3-18.

[40] Gutowski, W. J., Otieno, F. O., Arritt, R. W., Takle, E. S., Pan, Z. (2003). Diagnosis and attribution of a seasonal precipitation deficit in a US regional climate simulation. *Journal of Hydrometeorology*. 5. pp. 230-242.

[41] Korzoun, V. I., Sokolov, A. A., Budyko, M. I., Voskresensky, K. P., Kalinin, G. P., Konoplyantsev, A. A., Korotkevich, E. S., Lvovich, M. I. (1978). *Atlas of World Water Balance*. UNESCO: Paris.

[42] Shukla, J., Mintz, Y. (1982). Influence of land-surface evapotranspiration on the Earth’ s climate. *Science.* 215(4539). pp. 1498-1501.

[43] Laio, F., Porporato, A., Ridolfi, L., Rodriguez-Iturbe, I. (2001). Plants in water-controllede ecosystems: active role in hydrologic process and response to water stress II. Probabilistic soil moisture dynamics. *Advances in Water Resources.* 24. pp. 707-723.

[44] Chen, X., Rubin, Y., Ma, S., Baldocchi, D. (2008). Observations of stochastic modeling of soil moisture control on evapotranspiration in a Californian oak savanna. *Water Resources Resources.* 44(W08409). pp. 1-13.

[45] Irmak, S., Istanbulluoglu, E., Irmak, A. (2008). An evaluation of evapotranspiration model complexity against performance in comparison with Bowen ratio energy balance measurements. *Transactions of the ASABE.* 51(4). pp. 1295-1310.

[46] Gollan, T., Turner, N. C., Schulze, E. D. (1985). The responses of stomata and leaf gas exchange to vapour pressure deficits and soil water content. *Oecologia.* 65(3). Pp.356-362.

[47] Robock, A. et. al. (2000). The global soil moisture data bank. *Bulletin of the American Meteorological Society*. 81(6). Pp. 1281-1299.

[48] Anctil, F., Michel, C., Perrin, C., Andreassian, V. (2004). A soil moisture index as an auxiliary ANN input for stream flow forecasting. *Journal of Hydrology*. 286. pp. 155-167.

[49] Maurer, E. P., Lettenmaier, D. P. (2003). Predictability of seasonal runoff in the Mississippi river basin. *Journal of Geophysical Research-Atmospheres.* 108(D16).

[50] Mahanama, S. P. P., Koster, R. D., Reichle, R. H., Zubair, L. (2008). The role of soil moisture initialization in subseasonal and seasonal streamflow prediction-a case study in Sri Lanka. *Advances in Water Resources.* 31. pp. 1333-1343.

[51] Berg, A. A., Mulroy, K. A. (2006). Streamflow predictability in the Saskatchewan/Nelson River basin given macroscales estimates of the initial soil moisture status. *Hydrological Sciences*. 51(4). Pp. 642-654.

[52] Wei, L., Zhang, B., Wang, M. (2007). Effects of antedecent soil moisture on runoff and soil erosion in alley cropping systems. *Agricultural Water Management*. 94. pp. 54-62.

[53] Castillo, V. M., Gomez-Plaza, A., Martinez-Mena, M. (2003). The role of antecedent soil water content in the runoff response of semiarid catchments: a simulation approach. *Journal of Hydrology*. 284. pp. 114-130.

[54] Seneviratne, S. I. et. al. (2006). Soil moisture memory in AGCM simulations: analysis of global land-atmosphere coupling experiment (GLACE) data. *Journal of Hydrometeorology*. 7(5). pp. 1090-1112.

[55] Washington, W. M., Parkinson, C. L. (2005). An Introduction to Three-Dimensional Climate Modeling. New York: University Science Books.

[56] Nieber, J. L. (1983). Relationship between soil moisture storage and deep percolation and subsurface return flow. *Report.* Texas Water Resources Institute. pp. 1-88.

[57] Di Domenico, A., Laguardia, G., Fiorentino, M. (2007). Capturing critical behaviour in soil moisture spatio-temporal dynamics. *Advances in Water Resources*. 30. pp. 543-554.

[58] Burroughs, W. J. (2001). *Climate Change: A Multidisciplinary Approach*. New York: Cambridge University Press.

[59] Claussen, E. (2001). *Climate Change: Science, Strategies, & Solutions*. Leiden: Brill.

[60] Wigley, T. M. L. (1999). *The Science of Climate Change: Global and US Perspectives.* Arlington: Pew Center on Global Climate Change.

[61] IPCC (2001). *Climate Change: 2001: The Scientific Basis*. Cambridge: Cambridge University Press.

[62] Hassol, S. (2004). *Impacts of a warming Arctic: Arctic Climate Impact Assessment*. Cambridge. Cambridge University Press.

[63] Wilson, C. A., Mitchell, J. F.B. (1987). *Simulated* $CO_2$ *induced climate change over western Europe*. Clim. Change, 10. pp. 11-42.

[64] Schlesinger, M. E., Zhao, Z. C. (1989). *Seasonal climate changes induced by doubled* $CO_2$ *as simulated by OSU atmospheric GCM mixed layer ocean model.* J. Glaciol. 2. pp. 459-495.

[65] Griffin, J. M. (2003) *Global Climate Change.* Great Britain: Edward Elgar Publishing.

[66] Etchevers, P., Golaz, C., Habets, F., Noilhan, J. (2002). *Impact of a climate change on the Rhone river catchment hydrology*. Journal of Geophysical Research. 107(D16). pp. 1-18.

[67] Brown, P. (2006). *Global Warning: The Last Chance for Change.* Lomdon: Dakini Books.

[68] Hirabayashi, Y., Kanae, S., Emori, S., Oki, T., Kimoto, M. (2008). Global projections of changing risks of floods and droughts in a changing climate. *Hydrological Sciences*. 53(4). pp. 754-772.

[69] Rind D., Goldberg, R., Hansen J., Rosenzweig, C., Ruedy, R. (1990). *Potential evapotranspiration and the likelihood of future drought.* Journal of Geophysical Research. 95(07). pp. 9983-10004.

[70] Sheffield, J., Wood, E. F. (2008). Global trends and variability in soil moisture and drought characteristics, 1950-2000, from observation-driven simulations of the terrestrial hydrologic cycle. *Journal of Climate.* 21. pp. 432-458.

[71] Holland, M. M., Bitz, C. M., Tremblay, B. (2006). Future abrupt transitions in the summer Arctic sea ice. *Geophysical Research Letters*. 33(L23503).

[72] Sillmann, J., Roeckner, E. (2008). Indices for extreme events in projections of anthropogenic climate change. *Climatic Change.* 86. pp. 83-104.

[73] Wigley, T. M. L. (1985). Impact of extreme events. *Nature.* 316. pp. 106-107.

[74] Giorgi, F., Mearns, L. O., Shields, C., Mayer, L. (1996). A regional model study of the importance of local versus remote controls of the 1988 drought and 1993 flood over the central United States. *Journal of Climate.* 9. pp. 1150-1162.

[75] Pan, Z., Segal, M., Turner, R., Takle, E. (1995). Notes and correspondence: model simulation of impacts of transient surface wetness on summer rainfall in the United States Midwest during drought and flood years. *Monthly Weather Review.* 123. pp. 1575-1581.

[76]  Atlas, R., Wolfson, N., Terry, J. (1993). The effect of SST and soil moisture anomlies on GLA model simulations of the 1988 US summer drought. *Journal of Climate.* 6. pp. 2034-2048.

[77] Kunkel, K. E., Changnon, S. A., Angel, J. R. (1994). Climatic aspects of the 1993 Mississippi River Basin flood. *Bulletin of the American Meteorological Society.* 75(5). pp. 811-822.

[78] Beljaars, A. C. M., Viterbo, P., Miller, M. J. (1996). The anomalous rainfall over the United States during July 1993: sensitivity to land surface parametrization and soil moisture anomalies. *Monthly Weather Review.* 124. pp. 362-383.

[79] Schubert, S. D., Suarez, M. J., Pegion, P. J., Koster, R. D., Bacmeister, J. T. (2004). Causes of long-term drought in the US Great Plains. *Journal of Climate.* 17. pp. 485-503.

[80] Schubert, S. D., Suarez, M. J., Pegion, P. J., Koster, R. D., Bacmeister, J. T. (2004). On the cause of the 1930s dust bowl. *Science.* 303. pp. 1855-1859.

[81] Shukla, J., Mintz, Y. (1982). Influence of land-surface evapotranspiration on the Earth’ s climate. *Science.* 215(4539). pp. 1498-1501.

[82] Charney J. G. (1975). *Dynamics of deserts and drought in the Sahel.* The Quarterly Journal of the Royal Meteorological Society. 101(428). pp. 193-202.

[83] Charney, J., Quirk, W. J., Chow, S., Kornfield, J. (1977). A comparative study of the effects of albedo change on drought in semi-arid regions. *Journal of the Atmospheric Sciences.* 34. pp. 1366-1385.

[84] Simmonds, I., Hope, P. (1997). Persistence characteristics of Australian rainfall anomalies. *International Journal of Climatology*. 17. pp. 597-613.

[85] Schar, C., Vidale, P. L., Luthi, D., Frei, C., Haberli, C., Liniger, M. A., Appenzeller, C. (2004). The role of increasing temperature variability in European summer heatwaves. *Nature*. 427. pp. 332-336.

[86] Fischer, E. M., Seneviratne, S. I., Vidale, P. L., Luthi, D., Schar, C. (2007). Soil moisture-atmosphere interactions during the 2003 European summer heat wave. *Journal of Climate*. 20. pp. 5081-5099.

[87] Lare, A. R., Nicholson, S. E. (1994). Contrasting conditions of surface water balance in wet years dry years as a possible land surface-atmosphere feedback mechanism in the west African Sahel. *Journal of Climate*. 7. pp. 653-668.

[88] Douville, H. (2002). Influence of soil moisture on the Asian and African monsoons. Part II: interannual availability. *Journal of Climate*. 15. pp. 701-720.

[89] Webster, P. J. (1983). *Mechanisms of monsoon low-frequency variability:surface hydrological effects*. Journal of the Atmospheric Sciences. 40(9). pp.2110-2124.

[90] Arora, M., Singh, P., Goel, N. K., Singh, R. D. (2008). Climate variability influences on hydrological responses of a large Himalayan basin. *Water Resour Manage*. 22. pp. 1461-1475.

[91] Handerson-Sellers, A. (1996). Soil moisture: A critical focus for global change studies. *Global and Planetary Change*. 13. pp. 3-9.

[92] Liou, Y., Galantowicz, J. F., England, A. W. (1999). *A land surface process/radiobrightness model with coupled heat and moisture transport for prairie grassland.* IEEE Transactions on Geoscience and Remote Sensing. 37(4). pp. 1848-1858.

[93] Miller, G. R., Baldocchi, D. D., Law, B. E., Meyers, T. (2007). An analysis of soil moisture dynamics using multi-year data from a network of micrometeorological observation sites. *Advances in Water Resources.* 30. pp. 1065-1081.

[94] Basara, J.B. , Crawford, K.C. Linear relationships between root-zone soil moisture and atmospheric processes in the planetary boundary layer. *Journal of Geophysical Research.* 107. pp. 4274.

[95] Ulaby, F. T., Moore, R. K., Fung, A. K. (1981). *Microwave remote sensing: Active and passive*. 1. Addison Wesley.

[96] Shi. J. et. al. (2002). *A parametrized surface reflectivity model and estimation of bare-surface soil moisture with L-band radiometer.* IEEE Transactions on Geoscience and Remote Sensing. 40(12). pp. 2674-2686.

[97] De Roo, R. D., England, A. W., Munn, J. (2004). *Circular polarization for L-band radiometric soil moisture retrieval.* . IEEE Transactions on Geoscience and Remote Sensing. pp. 1-9.

[98] Njoku, E. G. et. al. (2002). *Observations of soil moisture using a passive and actlive low-frequency microwave airborne sensor during SGP99.* IEEE Transactions on Geoscience and Remote Sensing. 40(12). pp. 2659-2673.

# CHAPTER 2. THE IOWA STATE UNIVERSITY DIRECT SAMPLING L-BAND DIGITAL RADIOMETER

This chapter describes a polarimetric-capable L-band radiometer that has been built for Iowa State University (ISU) by The University of Michigan. It is a ‘Direct Sampling Digital Radiometer’ (DSDR), in which most of the operations are performed digitally and mixer stages are eliminated. The system is to be used for soil moisture retrieval studies. It could provide supportive data for future L-band satellite missions and is reconfigurable for radio frequency interference (RFI) mitigation purposes.

## 2.1 Introduction

Recent advances in remote sensing have shown that microwave radiometry is a suitable approach to assess soil moisture [1, 2, 3]. Radiometry holds great promise for global measurement of soil moisture since it is possible to make continuous observations over a large area and the primary property that affects the measurements is directly dependent on the liquid water present. Furthermore, at low microwave frequencies, signals are not affected by clouds, which makes data collection possible in all-weather conditions; solar radiation does not influence the measurements, which enables day-and-night observations; and vegetation cover is transparent to microwave emission [4]. L-band is accepted to be optimum for soil moisture retrieval [5,6]. There has not been a dedicated spaceborne mission at this frequency band due to the high cost and mechanical challenges associated with the need for large antenna apertures to produce a useful spatial resolution. The first spaceborne mission, the Soil Moisture and Ocean Salinity (SMOS) mission [7] by the European Space Agency

(ESA) will be launched in 2009. One promising development is the direct RF sampling receiver architecture where the RF signal is sampled and digitized through analog-to-digital converters (ADCs) after the front-end amplification and filtering stages so that all subsequent processing is performed digitally. Hence, the gain fluctuations and noise sources due to analog mixers and local oscillators that are used in a conventional receiver are eliminated. A simplified hardware and digital processing allows the integration onto a multi-chip module (or eventually onto a single chip monolithic microwave integrated circuit) and lowers the cost, weight and packaging.

In this study, the Direct Sampling Digital Radiometer, which has been built for ISU by the University of Michigan, is introduced after a brief discussion of noise characterization, and other radiometer types. System description as well as antenna performance, RF receiver components, analog to digital converter and digital back end sections are explained. The FPGA firmware and microcontroller operations are emphasized. Thermal control and monitoring mechanism of the system is examined.

## 2.2 Noise Characterization

A radiometer is a highly sensitive receiver that measures thermal electromagnetic emission of a given object to determine its brightness temperature. The emitted power is captured by an antenna. The output power of the antenna is sent to a receiver that produces an output voltage that is related to the brightness temperature of the object.

Since a radiometer measures the thermal noise power that is emitted by lossy materials [8], the noise characteristics of the radiometer become significant. To model the radiometer receiver and antenna in order to determine the performance and noise characteristics of the overall system, it is useful to review the noise characterization of individual and cascaded devices. Two characterizations, equivalent noise temperature and noise figure, are covered to describe noisy components.

### 2.2.1 Noise Power and Equivalent Noise Temperature

Consider a resistor at a temperature $T$ K. The electrons in the resistor are in random motion that produces small, random voltage fluctuations $v_n$ across the resistor terminals. This voltage has a zero mean but a nonzero root mean square (rms) value that is shown by Nyquist:

$$v_{rms} = \langle v_n(t) \rangle = \sqrt{4RkTB} \tag{1}$$

where $k$=1.38x10$^{-23}$ J/K is Boltzmann' s constant, $R$ is the resistance in ohms, and $B$ is the noise bandwidth in Hz, which is the bandwidth of a rectangular filter. The Thevenin equivalent of the noisy resistor $R$ at temperature $T$ K that delivers maximum power to a load resistor $R$ through an ideal bandpass filter, and its equivalent circuit are shown in Figure 1. The equivalent circuit consists of a noiseless source resistor with a voltage generator $v_n$, and a load resistor $R$ for maximum power transfer.

Hence, the maximum available noise power from a noisy resistor at temperature $T$ is

$$P_n = \left( \frac{v_{rms}}{2R} \right)^2 R = \frac{v_{rms}^2}{4R} = kTB \tag{2}$$

Equation (2.2) is a fundamental result for microwave radiometry because it states a direct linear relationship between power and temperature, and the interchangeable use of the two parameters. Note that the noise power is independent of frequency such that the power spectral density is a constant. Such noise sources are called ‘white noise sources’ and their

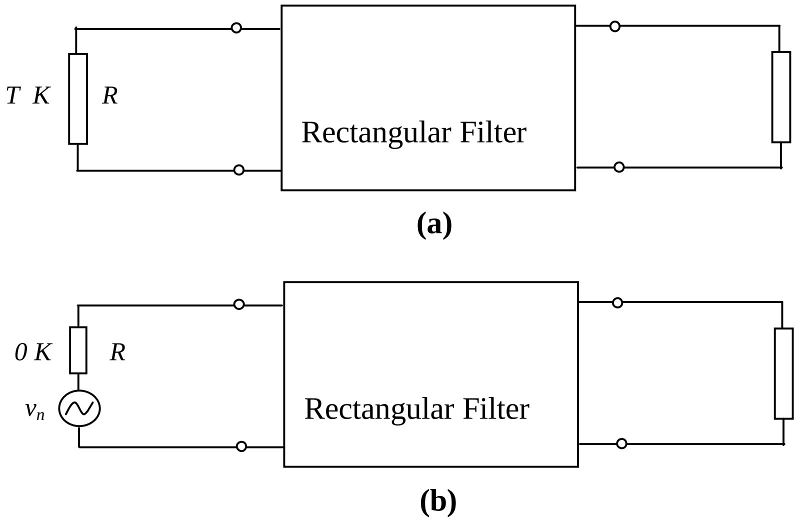

**Figure 1. Noisy resistor delivering maximum power to a load resistor (a) and its equivalent circuit (b).**

noise powers (variances) are additive. $P_n$ is directly proportional to the bandwidth $B$, which is usually the bandwidth of the microwave system.

If a noise source is white, it can be represented as an equivalent thermal noise source that is characterized by an equivalent noise temperature $T_e$, and a device or a system is said to have an equivalent noise temperature of $T_e$ that is a function of the parameters of the device or the system only. $T_e$ is defined through the equivalence of the two networks that are given in Figure 2. If the source resistor $R$ of a noisy device is at a hypothetical temperature of 0 K, then the noise power $P_o$ delivered to the matched load $R$ is due to the noise that is generated by the device itself since the source resistor is noise-free. $T_e$ is the temperature of a source resistor connected to the input terminals of an equivalent noise-free device that produces the same output power $P_o$ and is given by

$$T_e = \frac{P_o}{GkB} \tag{3}$$

where $G$ is the power gain of the device. $T_e$ of a cascaded system that consists of $N$ components is [9]

$$T_e = T_{e1} + \frac{T_{e2}}{G_1} + \frac{T_{e3}}{G_1 G_2} + ....... + \frac{T_{eN}}{G_1 G_2 ... G_{N-1}} \tag{4}$$

where $T_{ei}$ ($i$=1,2,…$N$) and $G_j$ ($j$=1,2,…$N$-1) denote the equivalent noise temperature and gain of each component, respectively.

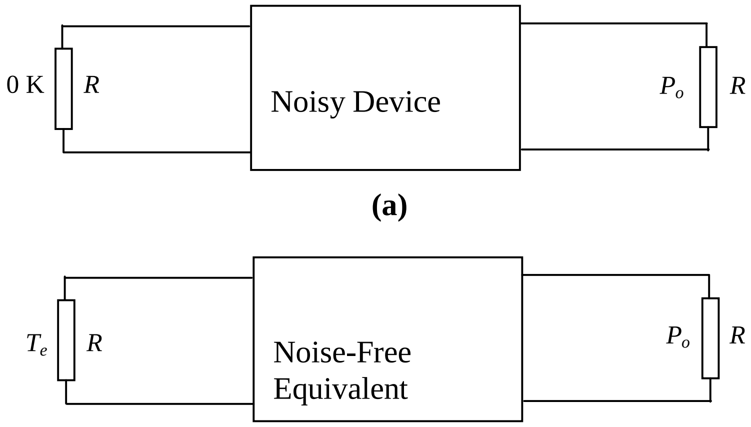

**(a)**

**(b)**

**Figure 2. Noisy device (a) and its equivalent noise-free representation (b) in terms of equivalent noise temperature Te.**

### 2.2.2 Noise Figure

An alternative representation of the noise performance of a device is noise figure, which is a measure of degradation in the signal-to-noise ratio between the input and output of the device due to the noise addition by the device:

$$F = \frac{P_{si} / P_{ni}}{P_{so} / P_{no}} \tag{5}$$

where $F$ is the noise figure, $P_{si}$ and $P_{ni}$ are the input signal and noise powers, and $P_{so}$ and $P_{no}$ are the output signal and noise powers, respectively. By definition, $F$ is evaluated for a certain noise power $P_{ni} = kT_0B$ that is generated by a matched resistor at the input port of the component whose temperature is $T_0$=290 K. The input signal power $P_{si}$ is amplified by the power gain $G$, so $P_{so}=GP_{si}$. The input noise power $P_{ni}$ is also amplified, however the noise power generated by the device itself is added to the output power as well:

$$P_{no}=G\,P_{ni}+GkT_eB \tag{6}$$

Equation (2.5) can be rewritten as

$$F = \frac{P_{si} / P_{ni}}{P_{so} / P_{no}} = \frac{P_{si}}{P_{so}}\frac{P_{no}}{P_{ni}} = \frac{P_{si}}{GP_{si}}\frac{GkT_0B + GkT_eB}{kT_0B} = \frac{1}{G}\frac{GkB(T_0 + T_e)}{kT_0B} = \frac{T_0 + T_e}{T_0} = 1 + \frac{T_e}{T_0} \tag{7}$$

Solving for $T_e$ yields

$$T_e = (F - 1)T_0 \tag{8}$$

Hence, $F$ and $T_e$ are interchangeable quantities, and $F$ is always greater than 1. For an ideal device, $T_e$=0 and $F$=1.

A noisy device (or system) can be modeled by its noise-free equivalent, and the noise generated within the device can be added to the input noise $P_{ni}$, if the input noise is affected by the noise figure of the component. The input noise power for an ideal noise-free condition is

$$P_{ni}^{'} = P_{ni} + \frac{GkT_eB}{G} = P_{ni} + kT_eB = kT_0B + k[(F-1)T_0]B = FkT_0B \qquad (9)$$

which leads to an equivalent noise temperature of $FT_0$. The noisy component and its noise-free equivalent is given in Figure 3.

A cascaded system of $N$ subsystems has a noise figure of [9]

$$F = F_1 + \frac{F_2 - 1}{G_1} + \frac{F_3 - 1}{G_1G_2} + .......+ \frac{F_N - 1}{G_1G_2...G_{N-1}} \qquad (10)$$

where $F_i$ ($i$=1,2,…$N$) and $G_j$ ($j$=1,2,…$N$-1) are the noise figure and gain of each subsystem, respectively. Equation10 implies that the first subsystem has the largest impact on the noise figure, if its gain is much larger than 1.

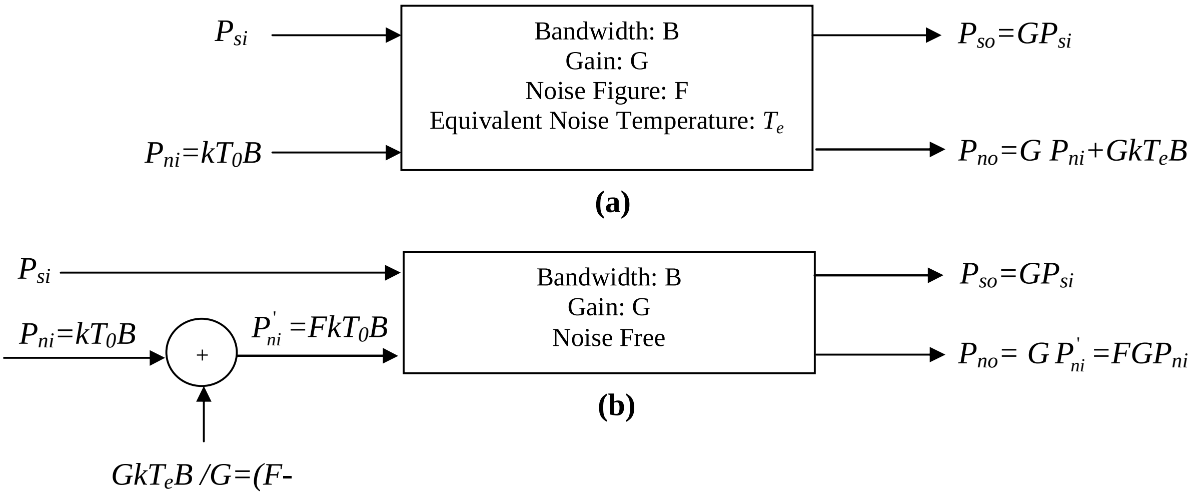

**Figure 3. Noisy device (a) and its noise-free equivalent (b). Input and output noise powers are represented in terms of noise figure $F$.**

## 2.3 Radiometer Types

### 2.3.1 Total Power Radiometer

A total power radiometer measures the time-averaged power of its input signal within a radio-frequency (RF) range. The block diagram of the system is shown in Figure 4.

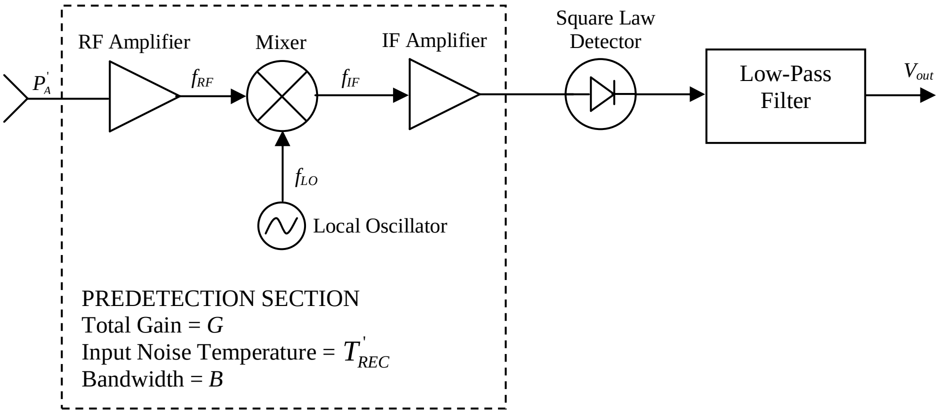

**Figure 4. Total power radiometer block diagram. Redrawn from [10].**

The antenna is connected to a superheterodyne receiver, in which the RF amplifier is followed by a mixer that multiplies the amplifier output with a sine wave that is generated by a local oscillator (LO). The RF amplifier filters the input signal by amplifying the frequency components centered at a frequency $f_{RF}$ within a bandwidth B. The LO produces a sine wave of frequency $f_{LO}$. The resulting frequencies after the mixing stage is

$$\begin{aligned} f_1 &= f_{RF} + f_{LO} \\ f_2 &= f_{RF} - f_{LO} = f_{IF} \end{aligned} \tag{11}$$

where the latter frequency $f_2$ is called the intermediate frequency ( $f_{IF}$ ) at which further amplification and detection schemes are performed. The $f_{IF}$ is usually between 10 MHz and 100 MHz [11]. $f_1$ is eliminated through the bandwidth associated with the IF amplification, which is a part of the superheterodyne receiver, after the mixing process. The system bandwidth $B$ is determined by the IF amplifier because the RF amplifier usually has a wider bandwidth than that of the IF amplifier [10].

The advantages of the superheterodyne receiver include doing most of the amplification at lower frequencies, and precise control of the frequency range for any device connected after the receiver, since it is sufficient to tune only the LO frequency to change the range of operation.

The signal that is amplified and RF-to-IF converted within the superheterodyne receiver is inputted to the square-law detector, whose output voltage is proportional to its input power (hence the input temperature) [12]. The square-law detector is followed by a low-pass filter (integrator) that reduces the signal fluctuations by averaging the detector output over an integration time τ, and produces the output voltage $V_{out}$ .

The receiver can be modeled by a noise-free equivalent that is shown in Figure 5, with an input noise power of $P_{REC}^{'} = kT_{REC}^{'}B$, where $T_{REC}^{'}$ is the equivalent input noise temperature of the receiver (transmission line between the antenna and the receiver is taken into account also). Likewise, the antenna can be represented by a noise source with an output power of $P_A^{'} = kT_A^{'}B$, which is the noise power delivered by the antenna to the receiver. $T_A^{'}$ is called the antenna radiometric temperature.

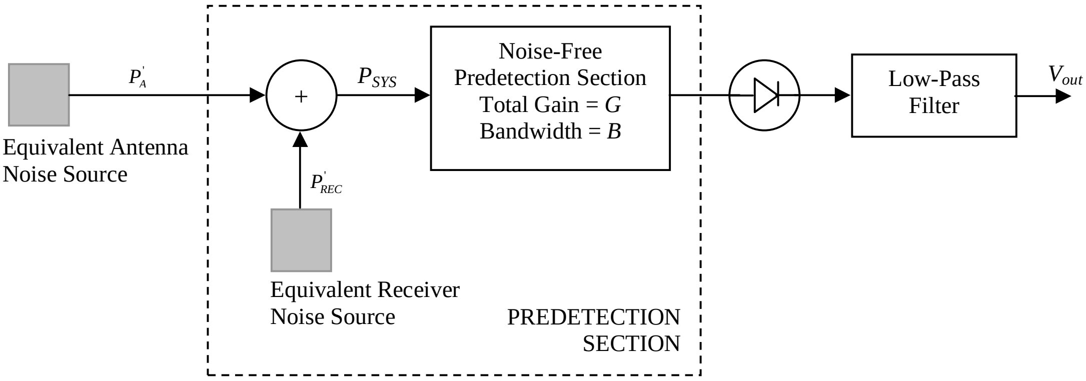

**Figure 5. Noise-free equivalent of the receiver. Redrawn from [10].**

Since the antenna and the receiver are white noise sources and their noise signals (and powers) are independent, the total system noise power at the input of the noise-free equivalent is the superposition of $P_A'$ and $P_{REC}'$:

$$P_{SYS} = P_A' + P_{REC}' = kT_A'B + kT_{REC}'B = k\left(T_A' + T_{REC}'\right)B = kT_{SYS}B \tag{12}$$

where $T_{SYS} = T_A' + T_{REC}'$ is called the system input noise temperature.

The sensitivity of an ideal total power radiometer ($\Delta T$), which is the minimum change in $T_{SYS}$ that can produce a detectible change at the radiometer output, is

$$\Delta T = \Delta T_{SYS} = \frac{T_{SYS}}{\sqrt{B\tau}} = \frac{T_A' + T_{REC}'}{\sqrt{B\tau}} \tag{13}$$

Equation (2.13) takes into account only the uncertainty due to noise fluctuations and does not include receiver gain variations. Although the slow changes in gain can be handled by frequent calibration, fast changes that occur within the intervals smaller than the period between successive calibrations cannot be eliminated. One solution to the gain variation problem is presented in the following section.

### 2.3.2 Dicke Radiometer

A Dicke radiometer uses modulation techniques to resolve the gain fluctuation issue. It is a total power radiometer that has a switch at the receiver input that modulates the input signal, and a synchronous demodulator that is placed in between the square-law detector and the low-pass filter. The modulation includes switching the receiver input between the antenna and a constant reference source at a switching rate that is higher than the highest spectral component in the gain variation spectrum, which means the system gain is effectively constant and is the same for the antenna and the reference source half-cycles. The block diagram of the Dicke radiometer is given in Figure 6.

The radiometric sensitivity $\Delta T$ of the Dicke radiometer consists of the contribution of the three statistically independent $\Delta T$ s:

$$\Delta T = \left[ (\Delta T_G)^2 + (\Delta T_{ANT})^2 + (\Delta T_{REF})^2 \right]^{1/2} \tag{14}$$

where $\Delta T_G$, $\Delta T_{ANT}$ and $\Delta T_{REF}$ are the uncertainties of the gain, antenna and the reference source, respectively, that are given as

$$\Delta T_G = \left( T_A^{'} - T_{REF} \right) \left( \frac{\Delta G_S}{G_S} \right) \tag{15}$$

$$\Delta T_{ANT} = \frac{T_A^{'} + T_{REC}^{'}}{\sqrt{B\tau / 2}} \tag{16}$$

$$\Delta T_{REF} = \frac{T_{REF} + T_{REC}^{'}}{\sqrt{B\tau / 2}} \tag{17}$$

where $T_{REF}$ is the equivalent noise temperature of the reference source. Plugging Equations 15, 16, 17 into Equation 14 yields

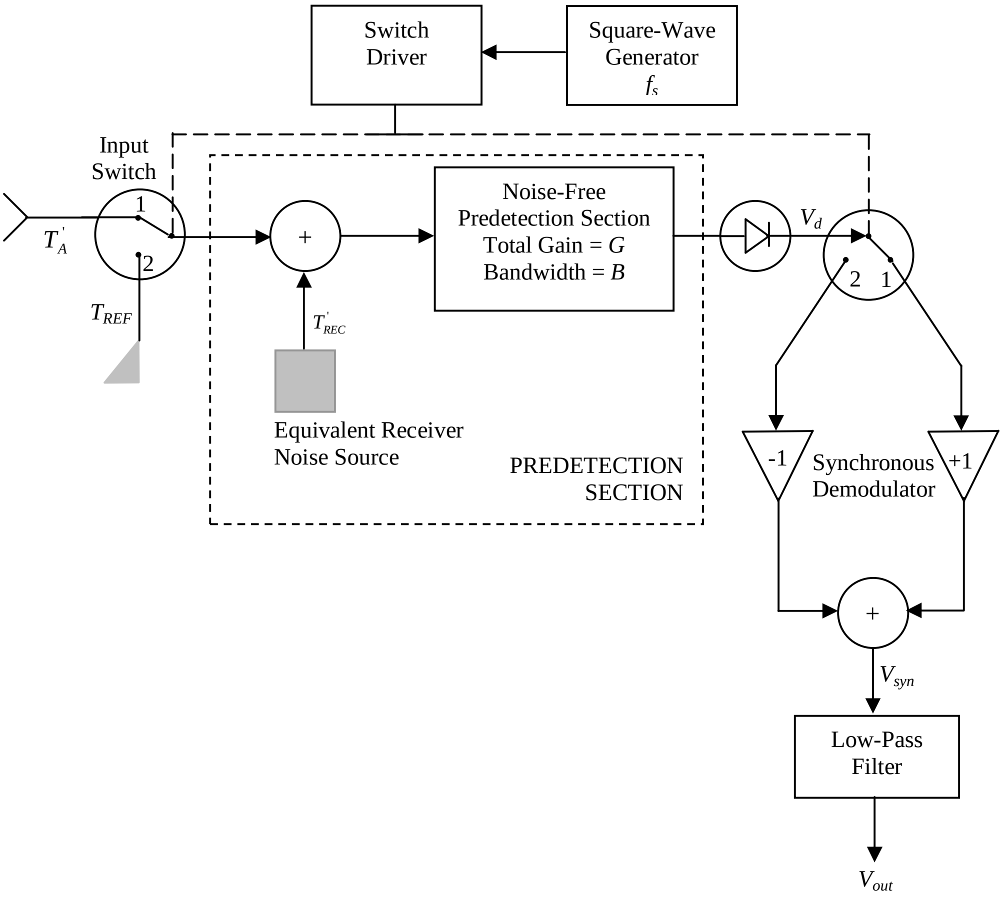

**Figure 6. Functional block diagram of a Dicke radiometer. Receiver input is switched between the antenna at a radiometric temperature of $T_A^{'}$, and the reference source at a noise temperature of $T_{ref}$, through a switching rate of $f_s$. $V_d$, $V_{syn}$ and $V_{out}$ are the the square-law detector output voltage, synchronous demodulator output voltage, and the output voltage of the Dicke radiometer, respectively. Redrawn from [10].**

where $T_{REF}$ is the equivalent noise temperature of the reference source. Plugging Equations (2.15), (2.16),(2.17) into Equation (2.14) yields

$$\Delta T = \left[ \frac{2\left(T_A^{'} + T_{REC}^{'}\right)^2 + 2\left(T_{REF} + T_{REC}\right)^2}{B\tau} + \left(\frac{\Delta G_S}{G_S}\right)^2 \left(T_A^{'} - T_{REF}\right)^2 \right]^{1/2} \tag{18}$$

The radiometric sensitivity of the Dicke radiometer is superior to that of the total-power radiometer.

## 2.4 DSDR: Instrument Description

The system is an L-band dual-polarization radiometer that operates between 1400-1427 MHz (1413.5 MHz center frequency), with capability for polarimetric operation. It is designed as a total power radiometer. Brightness incident upon the antenna is amplified until it is at a power level that can be detected. Since power is proportional not only to brightness but to bandwidth (P=kTB), filters are employed within the system to carefully define system bandwidth (RF bandwidth).

The radiometer uses a Direct Sampling detection scheme. The radiometric signal, after appropriate amplification and filtering, is digitized for further processing [13]. This further processing occurs in a Field Programmable Gate Array (FPGA) for both receivers (H-pol and V-pol). In addition to quantifying the power in each channel, it is possible to cross-correlate the signals between the channels for polarimetric operation. Also, FPGA processing allows for limited RFI mitigation (in both time and frequency domains) and for special operations such as spectrometry (within the limited bandwidth of the system).

The radiometer is designed to be autonomous. That is, the radiometer is equipped with a microcontroller that has responsibility for taking measurements, monitoring the thermal environment, and storing data until the user requests a download. The user can configure the radiometer to maintain a particular thermal set point, and make periodic measurements of the brightness at both polarizations and the reference load on its own. The master computer, which provides the user interface, does not need to be in continuous communication with the radiometer for the radiometer to be operating as intended. The master computer running the user interface communicates with the radiometer through a Radiometer Control Language, or RadiCL. The data collected by the radiometer is not calibrated within the instrument, since calibration errors could corrupt an otherwise useful dataset. Calibration, using measurements of the sky and an absorber at a measured temperature, should be done in post-processing.

The instrument uses a thermoelectric cooler (TEC) for thermal control of the RF stages. This system uses a state-of-the-art in thermal controller, with 0.01°C resolution. The controller is bipolar (it can drive the TEC in reverse, for heating as well as cooling) and uses a PID (proportional-integral-derivative) control algorithm. The aluminum interior plate to which all the RF components are attached is chosen to have sufficient thermal mass to eliminate short term thermal drifts. All components attached to this thermal plate, including the TEC, use thermal paste to minimize thermal gradients across junctions. The interior plate (top and bottom) is shown in Figure 7.

In order to distribute the mass and heat generation of the system, the electronics are enclosed in two environmental enclosures. To maintain environmental integrity, the aluminum cases used are penetrated with only a minimum of needed holes. These penetrations of the case are, on the receiver module, the bulkheads for RF signal input, DC power input, data connection and heat sinks for exhausting internally generated heat.

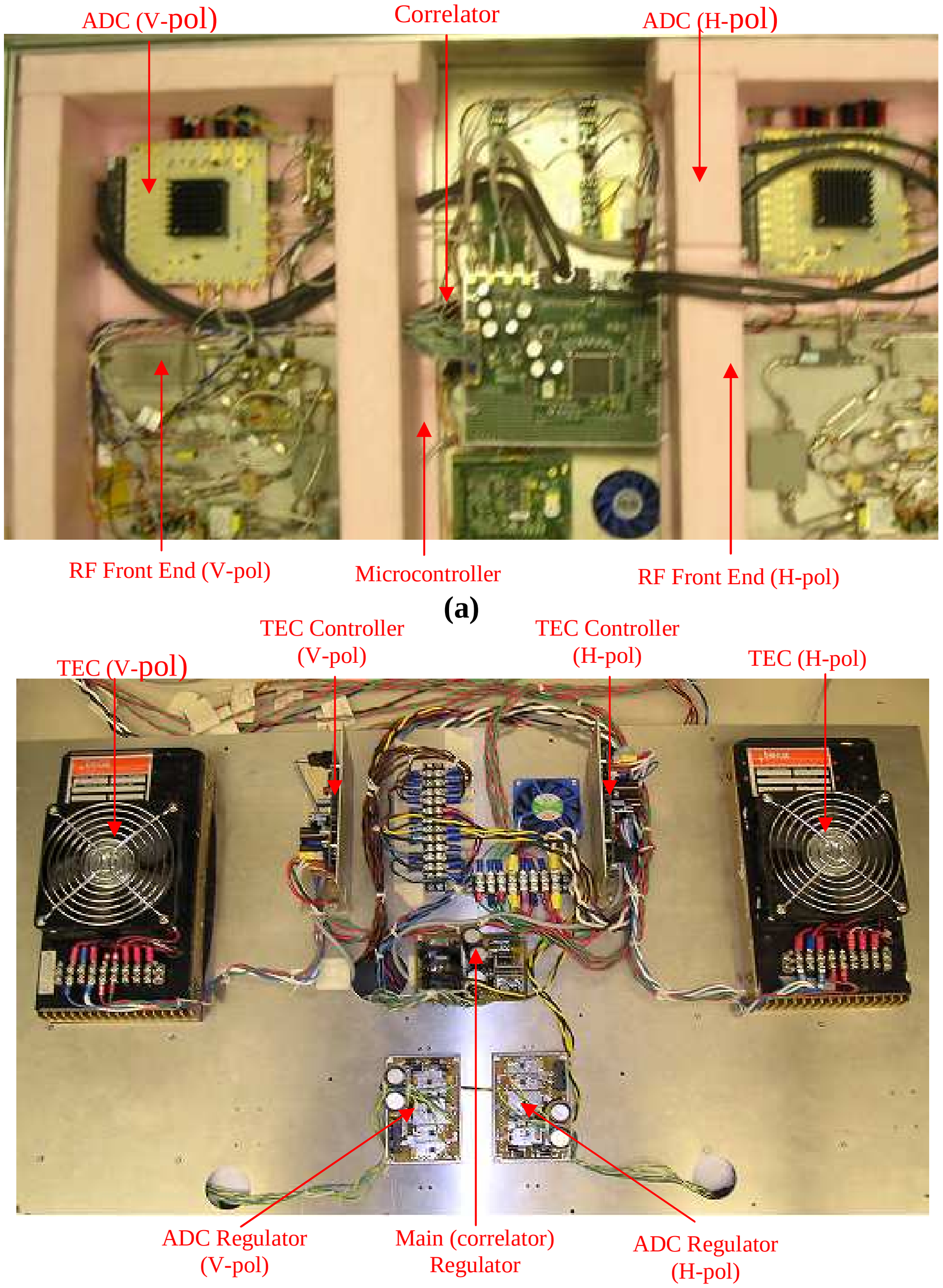

(a)

(b)

**Figure 7. Interior plate with the circuitry attached: Top side (a) and bottom.**

On the power supply module, the penetrations consist of the AC power input socket and DC power leads to the RF module. The radiometer and its block diagram are shown in Figure 8 and Figure 9, respectively.

**Figure 8. ISU radiometer on a lifter. Receiver and power supplies are contained in two separate boxes mounted on the sides of antenna orthomode**

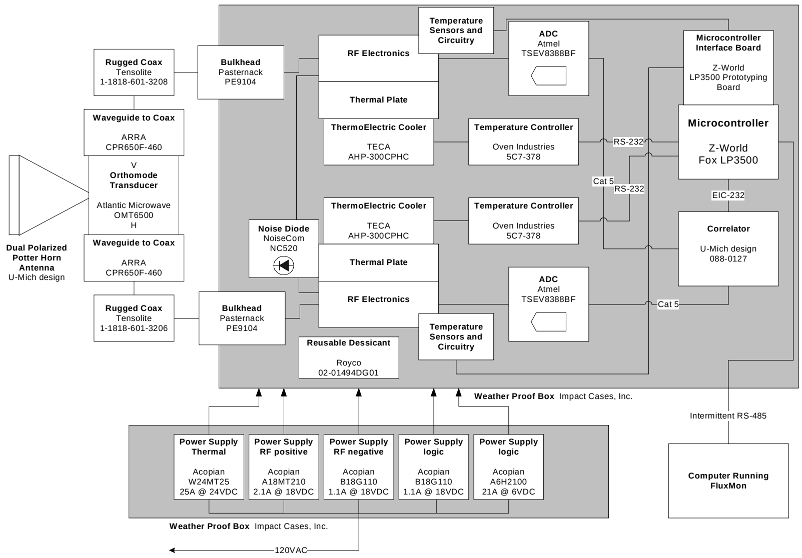

**Figure 9. System block diagram. Contents of the receiver and power supply boxes are outlined in gray.**

### 2.4.1 Antenna

The ISU L-band antenna for the ISU L-band radiometer is a dual polarized square Potter horn [14] employing a custom designed Potter horn, a commercial off-the-shelf (COTS) orthomode transducer, and a pair of COTS waveguide to coax transitions. The RF terminals are N-type female coaxial connectors. The antenna system is tuned for operation in the radio astronomy hydrogen line band of 1400-1427MHz. The aperture is 730mm square (3.44$\lambda$ at 1413.5MHz). The overall size of the antenna itself is 32" x 32" x 54" tall. The antenna itself weighs 85lbs. All of the components in the system are made from aluminum and all parts have been alodyned (gold chromate finished) to prevent corrosion. No radome has been installed on the antenna since prior experience indicates that this tends to trap moisture inside the antenna, possibly adversely affecting the radiometer sensitivity to the microwave brightness of the scene. However, the aperture is equipped with a flange to allow for a future installation of a radome if desired. The antenna is shown in Figure 10.

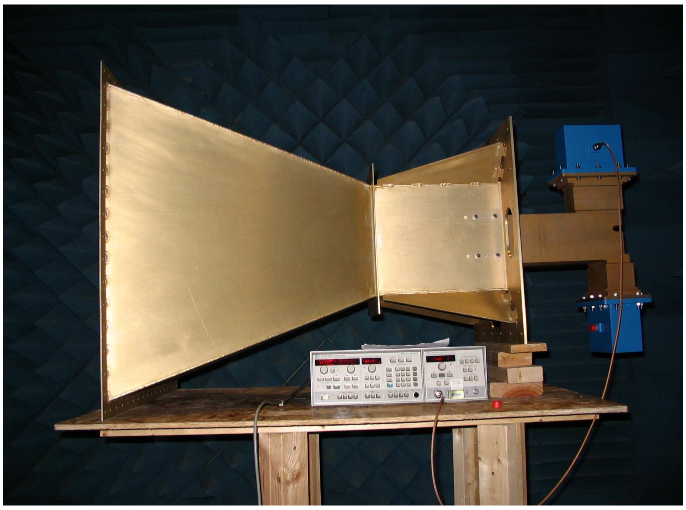

**Figure 10. L-band Potter antenna. Photo taken during the antenna pattern measurements in anechoic chamber.**

Antenna pattern measurements have been performed in the Radiation Laboratory in The University of Michigan. The ISU antenna was fed with a signal generator and the radiated power was received by a small L-band horn antenna connected to a spectrum analyzer. The operational frequency was 1413.5 MHz, which is the center frequency of the available band. Data wass electronically recorded. The antenna was rotated from –90° to +90° in azimuth (with respect to boresight) under different transmitter/receiver orientations and orthomode port excitations. Figure 11 shows two of the antenna patterns. The orientations of the ISU antenna and the receive antenna are horizontal and vertical, respectively. For the H-port excitation, it represents a copolarization while it is a cross-polarization for the E-port excitation. Note that no distinct sidelobes exist.

The measured 3dB beamwidths for horizontal and vertical polarizations were 20.3° (elevation) x 17.9° (azimuth) and 18.4° (elevation) x 20.4° (azimuth), respectively. Highest sidelobe level was measured to be 26.8 dB down from boresight, which occured at 41° from boresight in H-pol azimuth.

Largest return loss (RL) was measured as -17 dB at 1427 MHz. The estimated polarization coherency was 98%. The polarization coherency ρ was calculated through the following equation [15]:

$$\rho = \frac{\left|\iint E_H E_V^* d\Omega\right|}{\iint |E_H||E_V| d\Omega} \tag{19}$$

which is the normalized cross-correlation between the horizontal and vertical components of the electric field ($E_H$ and $E_V$) where

$$d\Omega = \sin\theta d\theta d\phi \tag{20}$$

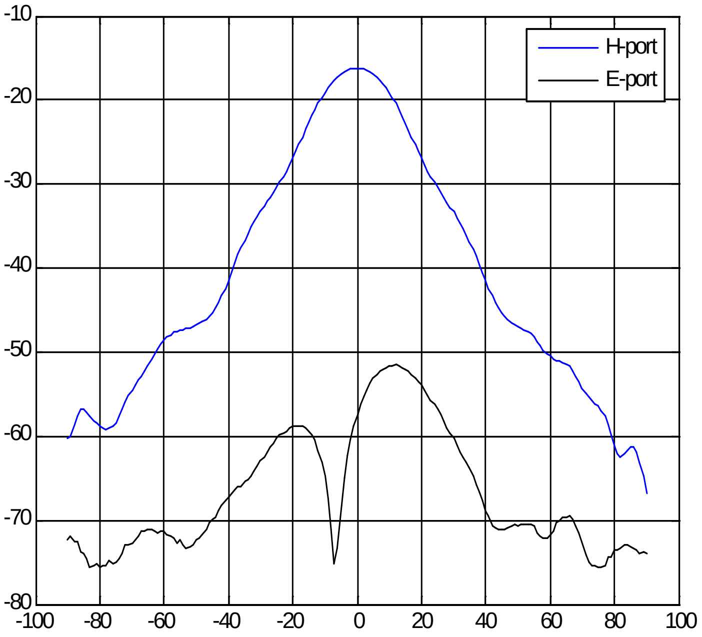

**Figure 11. Antenna patterns. Co-polarization (blue) and cross-polarization (black).**

### 2.4.2 RF Chain

The signal received by the antenna needs to be amplified and filtered before it is digitized. The RF chain block diagram is given in Figure 12.

The majority of the gain in the system is provided by a gain and filtering block consisting of connectorized components. The main advantage of the choice of connectorized components is the fact that very little crosstalk is expected between even physically close components, an important feature when a system has nearly 100dB of gain at a single frequency. This gain block is designed for a radiometer working at the radio astronomy

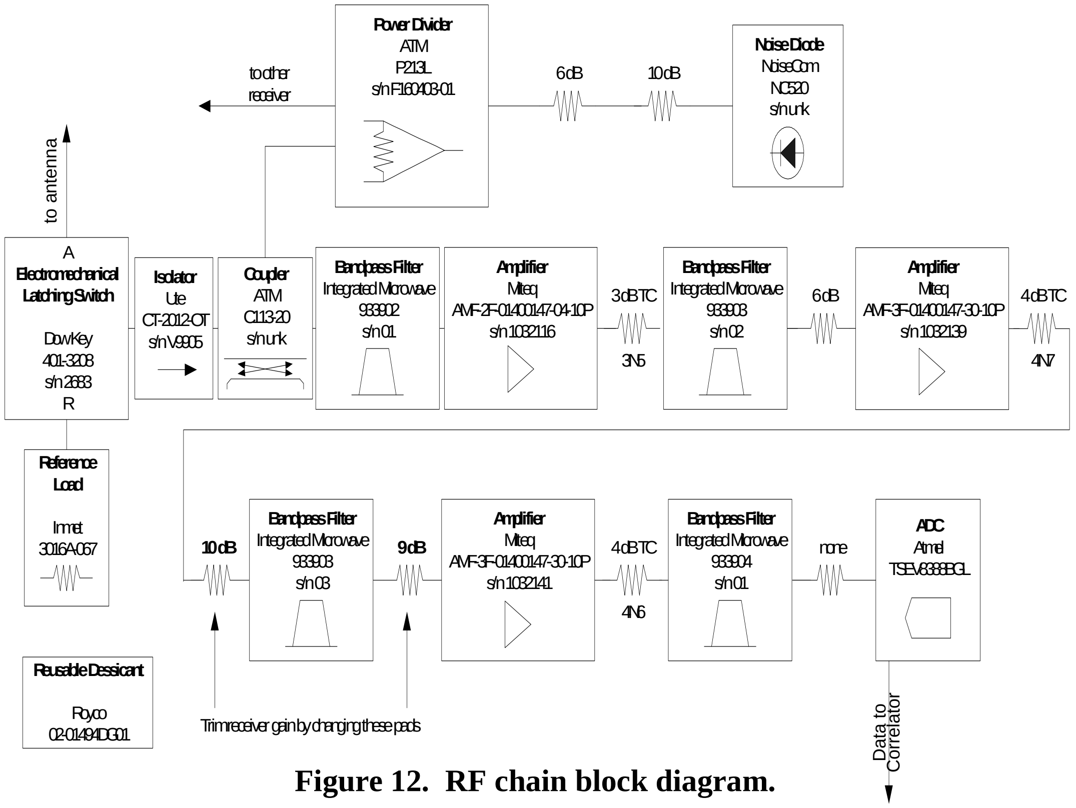

Figure 12. RF chain block diagram.

window of 1400 to 1427 MHz. In order to minimize the receiver noise figure, an L-band low-noise amplifier (LNA) is used prior to the majority of filtering and gain. At the very front end of the receiver, before the LNA, the part count and part insertion losses are critical, because the sum of all insertion losses of these parts contribute directly to the receiver noise figure. In particular, the front end parts include:

1. a microwave switch for reference load comparisons
2. an isolator for stabilizing the subsequent components' overall gain, which can otherwise vary due to different amounts and phase of reflection when looking from the receiver through the switch at the different load (reference or antenna)

3. a directional coupler, for injection of correlated noise into both receivers for calibration purpose
4. a very low insertion loss ceramic filter (0.7dB) for performing the majority of interference rejection prior to the LNA.

These components increase the H-pol and V-pol receiver temperatures to 167.2K and 153.9K, respectively. The remaining components in the receiver function to:

1. amplify the signal to a level that can be detected by ADC (about –35dBm).
2. filter out-of-band interference
3. provide matches between amplifiers and filters to keep the amplifiers stable, and prevent distortion of the filter passbands.

One important consideration is the receiver linearity. Linearity is important because calibration is achieved at only a few points, with the brightnesses between determined by assuming a linear receiver response. The generation of non-linearity is the same mechanism that eventually results in saturation when interference gets through the filters. Figure 13 shows the result of an experiment in which the liquid nitrogen and the reference load are used as cold load and warm load, respectively. Two attenuators at values of 1.2dB and 3dB are connected to the output of the cold load in order to generate different brightness temperatures. The noise diode is used to cover a larger range of brightness temperatures (it adds 130K). The RF chain output power varies linearly with the input brightness temperature, which confirms the receiver linearity.

The amplification in the receiver is large (71.4 dB [16]) and a small change in gain of the system will incorrectly appear at the output as a change of the brightness. The amplifiers are the devices that cause most of the change in gain of the system, and this is due to their sensitivity to their supply voltage and their ambient temperature. The supply voltage is stabilized by using regulators near the amplifiers and by using other standard electrical noise reduction techniques such as using twisted pair supply and return lines. Amplifiers were stabilized by cycling operating temperature while powered (10 times) and soaking at 45°C for 24 hours (Figure 14).

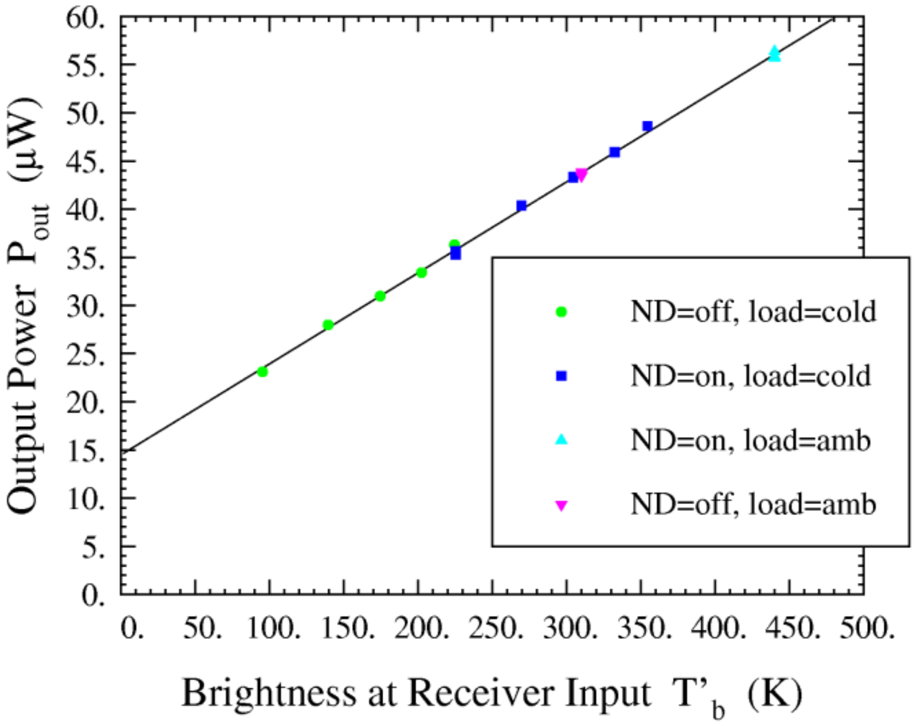

**Figure 13. RF chain output power versus input brightness temperature.**

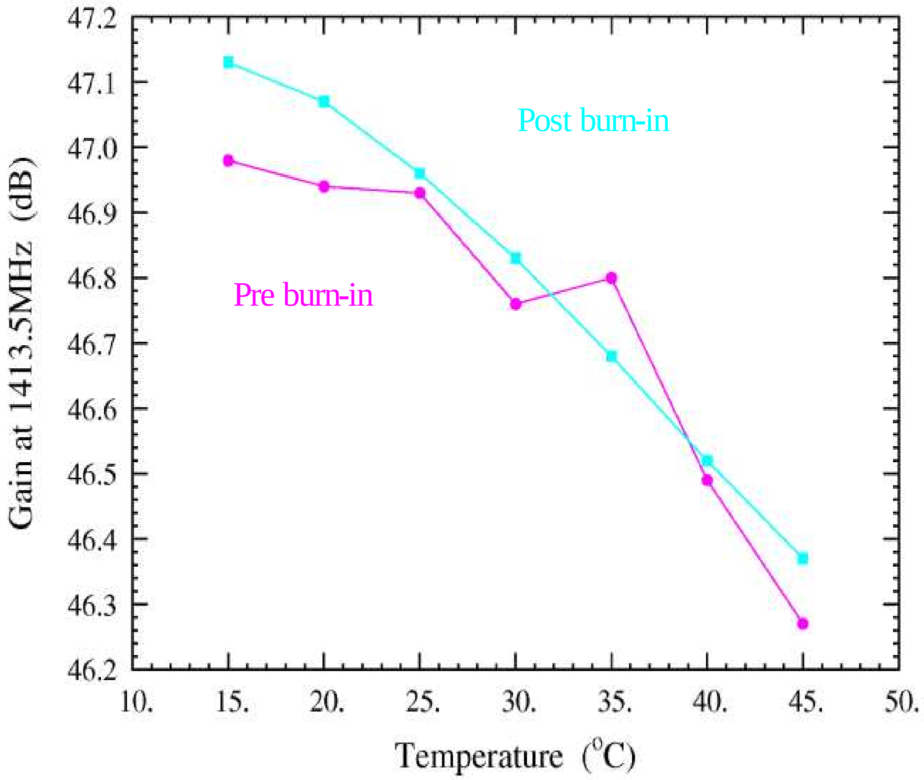

**Figure 14. Amplifier stabilization.**

### 2.4.3 Digitizer

The choice of Analog to Digital Converter (ADC) is important. Few ADCs are commercially available which can directly digitize signals at 1.4GHz (as of 2005-time of manufacturing). The Atmel 8388 family of ADCs is chosen for the system, as it has a number of advantages over other ADCs available. While several ADCs have an input bandwidth covering the radiometer operational frequency of 1.4GHz, no ADC is commercially available that is capable of digitizing at the full Nyquist rate (2.8 GSamples/sec). Fortunately, the Nyquist criterion is strictly applicable only to the bandwidth of the signal to be digitized. As such, the digitizer performs the downconversion operation instead of a mixer and LO. The system has two digitizers (ADCs) for H-pol and V-pol signal digitization. The two digitizers are identical and the sampling rate is 102.8 MSamples/sec. The input bandwidth is 1.8GHz while the minimum RF power level is -20 dBm. Figure 15 shows the ADC (right) and the current source (left) circuits for one polarization. The current source is used to monitor the ADC temperature through the measurement of a diode voltage, which is converted into temperature readings by the microcontroller.

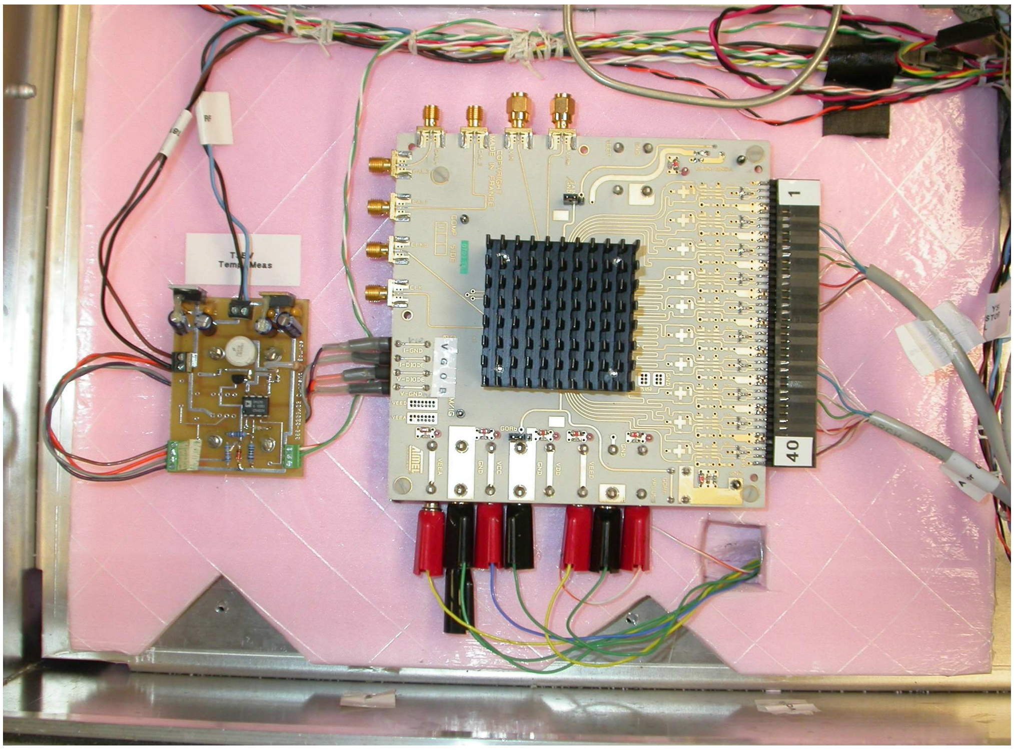

**Figure 15. Analog-to-digital converter (right) and current source (left). 8-bit low voltage differential signal (LVDS) outputs are attached on the right side of the ADC. ADC is surrounded by insulation and is a part of the thermally controlled environment to minimize its gain fluctuations.**

### 2.4.4 Digital Back End

The digital back end consists of the correlator and the microcontroller. The correlator generates a clock signal of 102.8MHz for the ADCs and the FPGA. The FPGA is a critical portion of the correlator where several complex mathematical operations such as gray-to-binary conversion, 8-bit to-3-bit mapping, filtering, quadrature demodulation, decimation, autocorrelation, crosscorrelation and histogram generation are performed on the digitized signals from H-pol and V-pol receivers. The microcontroller is the ‘brain’ of the radiometer whose responsibilities include temperature monitoring and control, analog to digital conversion control, data logging and storage, serial communication and management of the noise diode and RF switches. Xilinx VirtexE and Z-world LP3500 familes are chosen for the FPGA and the microcontroller, respectively. The correlator-centric view of the radiometer system is given in Figure 16.

The FPGA is programmed in VHDL using Xilinx Foundation development software. The firmware design is for basic operation of the radiometer with polarimetric capability, which is reconfigurable even after the radiometer is complete. All eight bits of the digitized signal from both ADCs are piped into the FPGA, where the first operation is a Gray code to binary conversion since the ADC outputs the data in Gray code. Then, a mapping from 8 bits to 3 bits is performed using a look-up table. The next stage is a Finite Impulse Response (FIR) digital filter that supplements the filters in the RF gain chain. A major advantage of the onboard filtering is the fact that it is digital, and therefore can be used to define the noise bandwidth with significantly reduced sensitivity to the temperature of the RF electronics. The filter uses an architecture that is very compact. The I/Q demodulation involves demultiplexing into an I and Q channel and a delay on I channel to keep the data aligned between the I and Q channels.  At this point, the data may be decimated by a factor of two without loss of information.  The final stage of the data processing stream is the correlator. In the correlator, each of the four channels is summed in an accumulator.  The data in each of the four channels is also squared (via a look-up table) and summed in an accumulator for autocorrelation.  This data is proportional to the product of the integration time and the system temperature on each channel.  Measurements proportional solely to the system temperatures are accomplished by dividing the accumulated values by the number of clock cycles used. This division is performed in the microcontroller.  Finally, the correlator also calculates the cross correlations (products) between channels and accumulates the results.

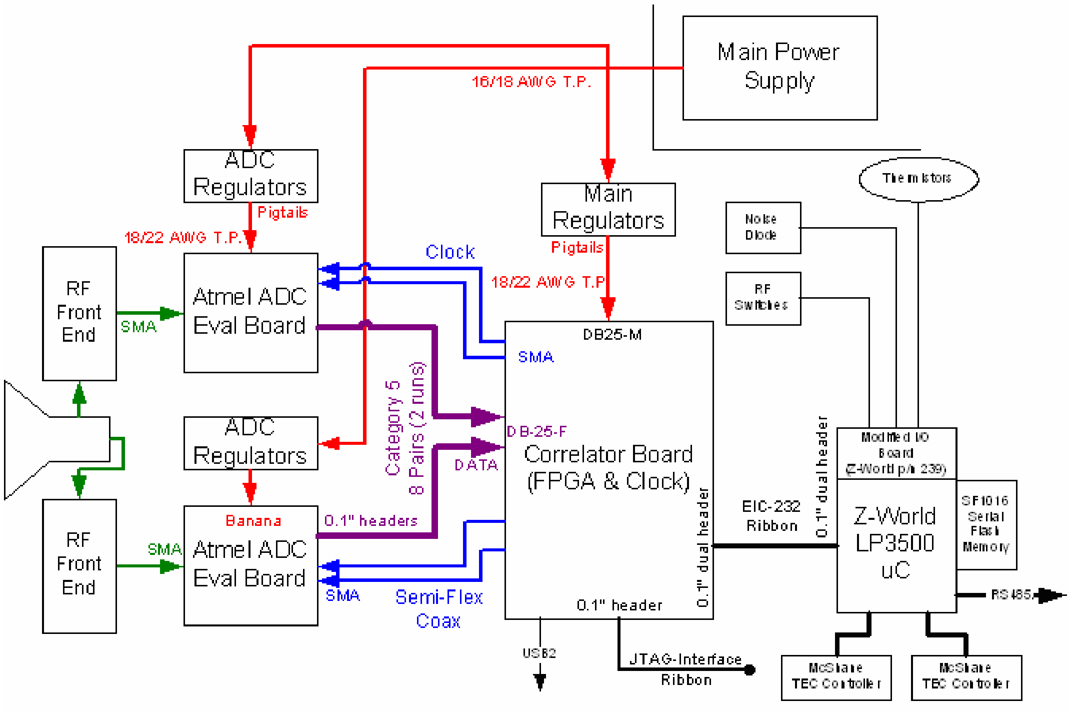

**Figure 16.  Correlator-centric system block diagram.**

The cross correlations between I and Q of a single polarization are not collected, since they are expected to be zero from theory. The firmware description is shown in Figure 17.

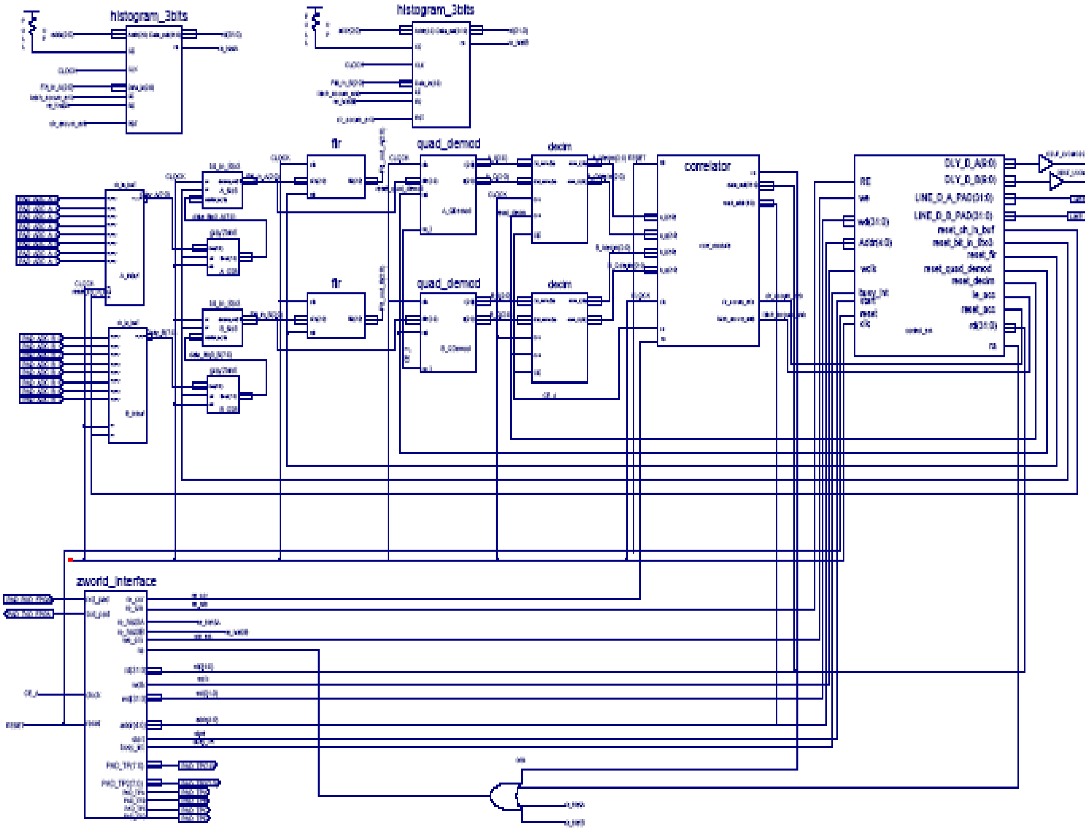

**Figure 17. Firmware. Histograms (top), input latch, Gray-to-binary conversion, 8 to 3 bit mapping, FIR filtering, I/Q demodulation, decimation, correlation, state machine and serial interface (bottom left).**

The remaining portions of the correlator deal with communication with the outside world. From the point of view of the microcontroller, the operations needed are the ability to read and write registers in the FPGA. Examples of registers for reading are the accumulators in the correlator, and registers in the totalizer, which calculate histograms of the data at different stages in the processing scheme. All of these registers can be written to for the purpose of initializing. Other registers include the clock delays for the ADCs, the values of which should be determined in the process of polarimetric calibration.

The microcontroller performs several tasks in order for the radiometer to operate properly. The tasks fall into four main categories: serial communication, temperature control, data logging and FPGA control. The overall efficiency of the system can be improved if the microcontroller can perform these tasks in a parallel manner. Although in reality a microprocessor can only execute one task at a time, it can appear to execute several of them in parallel by utilizing the inherent delays within each task. That is the processor can carryout the work for one task while others wait for an event. The microprocessor cycles through the tasks completing parts of each task. In this way the tasks can execute almost in parallel.

The microcontroller communicates serially with the FPGA. It communicates with the two thermoelectric cooler controllers and the PC through RadiCL, which is is an ASCII based communication protocol used for microwave radiometry. RadiCL utilizes two serial communiation standards, one is called RS-232 and the other is RS-485. RS-232 is bidirectional, that is it can send and receive information at the same time while RS-485, on the other hand, allows only one device to send information at a time. RS-232 uses one wire for transmitting data, one wire for receiving data, and one wire is reference ground. RS-485 utilizes differential signaling, that is two wires are used for transmission one wire is positive going signal and the other is its complement, it also uses a third wire as reference ground.

The devices that utilize the RS-232 standard are the FPGA and the two thermoelectric cooler controllers. There is a message format specific to each device in the system. For example the message standard used to communicate with the thermoelectric cooler controllers is different from that for the FPGA which is in turn different from used for the PC communication. Therefore, RadiCL contains separate communication functions that will allow the microcontroller to exchange information with each device.

### 2.4.5 Thermal Control

The temperature inside the radiometer needs to be carefully monitored and controlled at all times during operation. The thermal control of the RF electronics is critical since a temperature unstability may result in gain fluctuations within the analog parts. Two ThermoElectric Coolers (TECs), which operate at 24VDC and 6A maximum, are used for fine thermal control of the H-pol and V-pol RF sections. The TEC is bidirectional. That is, while a positive voltage applied to the TEC terminals results in heat flow from the TEC cold plate to exhaust side (physically located in the lower chamber), a negative voltage applied to the TEC terminals moves heat from the lower chamber to the cold plate. The efficiencies of these two modes are asymmetric, however. Resistive heating within the TEC is the same regardless of the sign of the current flowing through the TEC. As a result, using the TEC as a heater (negative voltage applied) requires about 50% of the effort as it does for cooling. For illustration, while the TEC is capable of 24VDC @ 6A = 144W of power consumption (either full power heating or full power cooling), only about 96W is available for heat pumping. The other 48W is dissipated as heat in either heating or cooling modes. Thus, a given number of watts of heating require less effort than the same number of watts of cooling. This is a fundamental limitation of TEC materials. Thermal control via TECs within the receiver box (side view) is given in Figure 18.

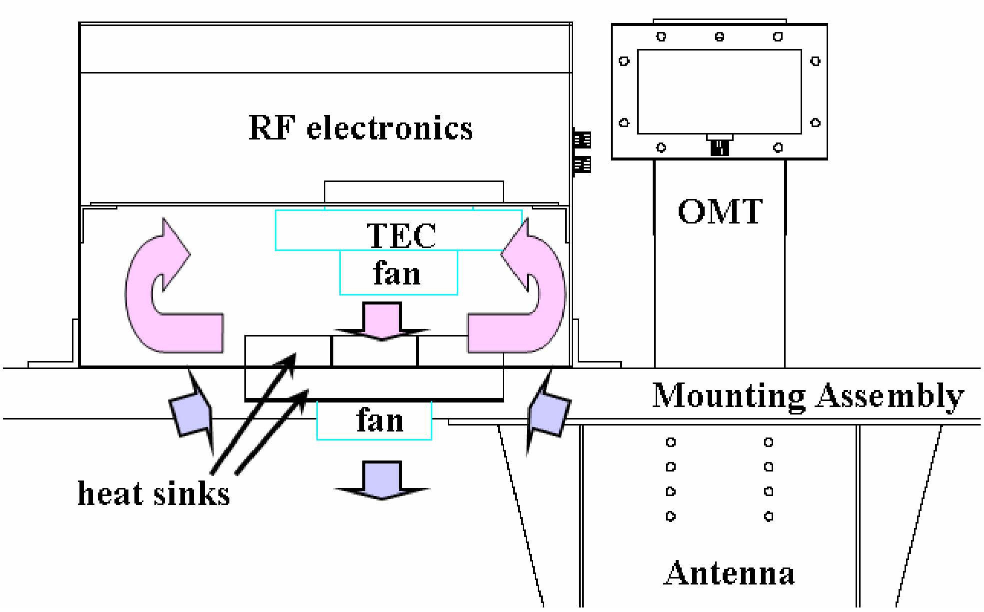

**Figure 18. Thermal control (receiver side view). TEC is located in lower chamber. When positive (negative) voltage is applied to TEC, it cools (heats) the air in lower chamber which in turn cools (heats) the RF plate in upper chamber. Heatsinks, internal and external fans accelerate the process.**

The TEC is controlled by a commercially available thermal controller manufactured by Oven Industries, Inc. and marketed as the “McShane” thermal controller. The McShane controller can handle up to 24VDC and 10A, and provides bidirectional control of a TEC via a MOSFET H-bridge circuit. It requires its own thermistor for control feedback. The McShane thermal resolution is 0.01C, and can achieve nearly this level of control if the control algorithm is properly tuned. There are two McShanes in the system which are located in the lower chamber, isolated from the RF loads by the interior plate, because they switch large currents as a means of controlling the TEC.

A total of ten thermistors are installed within the radiometer in order to control the system temperature. These thermistors are located at Two McShane thermistors are used to control H-pol and V-pol RF plate temperatures while two other thermistors are used for temperature monitoring. Hence, a total of ten temperature measurements are performed continuously.

There are a total of ten locations within the radiometer where temperature data is collected continuously. These locations include the antenna, case, H-pol and V-pol reference loads, H-pol and V-pol RF plates, and H-pol and V-pol ADCs. H-pol and V-pol RF plates have four thermistors installed: Two McShane thermistors for temperature control, and two other thermistors for temperature monitoring purposes. All other locations include one thermistor each, and except for the ADCs, they all have been populated by precision thermistors. A thermistor is a resistor made of semiconductors having resistance that varies rapidly and predictably with temperature. The voltage across each thermistor, except those connected to the McShanes is fed into the ADC inputs on the microcontroller where it is sampled several times, averaged and converted to a temperature in Kelvin. The ADCs, on the other hand, have a built in temperature diode whose junction voltage varies in direct proportion to the temperature inside the ADC chip. This voltage is also fed to the ADC on the microcontroller and converted to temperature in Kelvin. Each temperature diode requires a constant current source of 3mA in order to operate as expected. The McShanes are needed to operate the TECs which in turn maintain the RF plate at a constant temperature. The temperature measured by the McShane thermistor is retrieved via the RS-232 serial link.

## 2.5 Conclusion

The ISU direct sampling L-band digital radiometer is introduced along with an overview of noise characterization of devices, and other types of radiometers. Components of the DSDR such as the Potter antenna, RF stage, analog to digital converter, and digital back end are described. Furthermore, the thermal control, which is especially important for the RF section, is highlighted. The radiometer is capable of performing autocorrelation and crosscorrelation operations, which enables the polarimetric applications.

## bibliography

[1] Schmugge, T., Gloersen, P., Wilheit, T., Geiger, F. (1974). Remote sensing of soil moisture with microwave radiometers. *Journal of Geophysical Research.* 79(2). pp. 317-323.

[2] Jackson, T. J., O’Neill, P. E. (1990). Attenuation of microwave emission by corn and soybeans at 1.4 and 5 GHz. *IEEE Transactions on Geoscience and Remote Sensing*. 28(5). pp. 978-980.

[3] Jackson, T. J. (1993). Measuring of soil moisture using passive microwave remote sensing. *Hydrological Processes.* 7(2). pp. 139-152.

[4] Schneeberger, K., Schwank, M., Stamm, Ch., De Rosnay, P., Matzler, Ch., Fluhler, H. (2004). Topsoil structure influencing soil water retrieval by microwave radiometry. *Vadose Zone Journal.* 3. 1169-1179.

[5] Jackson, T. J., Schmugge, T. J. (1989). Passive microwave remote sensing system for soil moisture: some supporting research. *IEEE Transactions on Geoscience and Remote Sensing*, 27(2), 225-235.

[6] Schneeberger, K., Stamm, C., Matzler, C., Fluhler, H. Ground-based dual frequency radiometry of bare soil at high temporal resolution. *IEEE Transactions on Geoscience and Remote Sensing.* 42(3). pp. 588-595.

[7] Kerr, Y. H., Waldteufel, P., Wigneron, J. P., Martinuzzi, J. M., Font, J., Berger, M. (2001). Soil moisture retrieval from space: the soil moisture and ocean salinity (SMOS) mission, *IEEE Transactions on Geoscience and Remote Sensing*, 39(8), 1729-1735.

[8] Ridaoui, K., Mamouni, A., Ait-Abdelmalek, R., Bocquet, B., Leroy, Y. (1995). Near field weighting functions for microwave radiometric signals. *IEEE Transactions on Magnetics*, 31(3), 2166-2169.

[9] Misra, D. K. (2004). *Radio-Frequency and Microwave Communication Circuits.* John Wiley & Sons.

[10] Ulaby, F. T., Moore, R. K., Fung A. K. (1981). *Microwave Remote Sensing: Active and Passive*. Reading: Addison-Wesley.

[11] Pozar, D. M. (1998). *Microwave Engineering*. New York: John Wiley & Sons.

[12] Skou N. (1989). *Microwave Radiometer Systems-Design and Analysis*. Artech House.

[13] Fischman, M. A. (2001). Development of a Direct-Sampling Digital Correlation Radiometer for Earth Remote Sensing Applications. *Ph.D. dissertation*. The University of Michigan: Ann Arbor.

[14] Potter, P. D. (1963). A new horn antenna with suppressed sidelobes and equal beamwidhs. *The Microwave Journal*, 6, 71-78.

[15] De Roo,R. (2005). ISU L-band antenna report. *Report*. The University of Michigan: Ann Arbor.

[16] De Roo,R. (2005). ISU L-band link and noise budget. *Report*. The University of Michigan: Ann Arbor.

# CHAPTER 3. MODELS

This chapter describes the numerical radiative transfer models that are utilized in this study. A land surface model called 'The atmospheric and land exchange model (ALEX)', and a soil surface roughness model are explained. In order to verify the agreement between the radiative transfer models, a test case is considered , and the reflectivity (1 – emissivity) for each model is computed.

The system geometries that are investigated are shown in Figure 1. The simplest geometry is an air soil system with an observation angle θ. A more complicated system consists of air, and soil that is divided by a number of finite distinct boundaries. The distance between two consecutive boundaries that has a finite thickness is called a *layer*. The thicknesses of the layers through the soil are not necessarily the same. The angle θ is the observation angle.

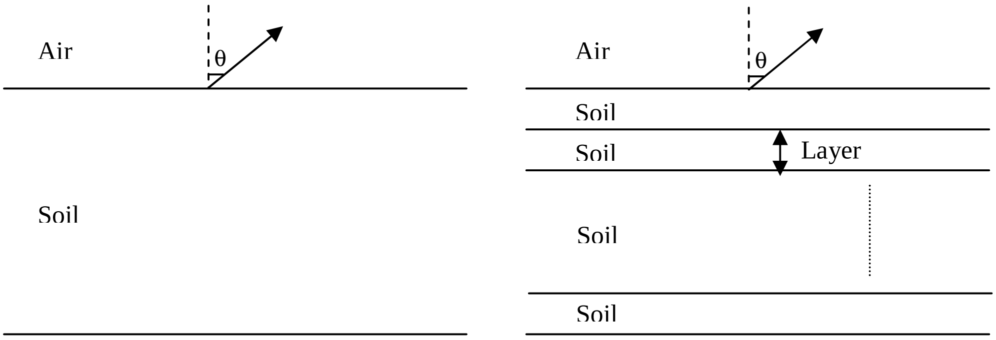

**Figure 1. System geometries: Simplest geometry that consists of air, and one layer soil (left). A more complicated geometry that consists of air, and soil that has a finite number of layers (right).**

Layer(s) of the soil is (are) assumed to have horizontally homogeneous moisture and temperature values. For multiple number of soil layers (>1) these values constitute the soil moisture and soil temperature profiles, which vary with depth only. For a one-layer soil system, the soil moisture and soil temperature profiles are said to be uniform.

## 3.1. Introduction

Verification of the agreement/disagreement between the radiative transfer models is an important step before we apply these models to the field data, and carry out the error analysis. In order to make sure the models return meaningful results, and there are no technical problems such as coding issues, we evaluate the results of radiative transfer models that are capable of characterizing wetting fronts and models that cannot characterize discontinuities in the soil moisture profile through the use of a test case, which is an air-soil-soil system.

The models that are used in this study are described before the test case is illustrated. The radiative transfer models are the Fresnel model, the incoherent model, the coherent model, and the transmission line model. A land-surface scheme called ‘Atmospheric and Land-Surface EXchange Model (ALEX)’ is introduced. This model produces the soil temperature and soil moisture profiles that are two inputs to the radiative transfer models. A dielectric mixing model, which reproduces the soil dielectric profile, is explained. A soil surface roughness model is also summarized.

The order of the usage of the above models is as follows: The soil temperature and soil moisture profiles that are the outputs of the ALEX model are inputted to the radiative transfer models. Within the radiative transfer models, the soil dielectric constant profile is generated first. Then the models produce the brightness temperatures for a smooth surface. The soil surface roughness model returns the brightness temperatures for a rough surface.

The test case is a three layer air-soil-soil system. The reflectivities that are computed through the radiative transfer models are plotted and compared. The Fresnel model is not taken into account for the test case analysis because the Fresnel model is not able to characterize the discontinuities in the soil moisture profile since the soil is assumed to be uniform in terms of soil moisture and soil temperature.

## 3.2 Radiative Transfer Models

### 3.2.1 Fresnel Model

The Fresnel model has long been used due to its simplicity and accuracy. It would be an appropriate model to implement in a satellite algorithm because it requires less inputs compared to the other radiative transfer models, which is appropriate for a large-scale application. The Fresnel model is a single-layer model based on the Fresnel reflectivity equations. Application of the reflectivity equation requires assumptions that the dielectric and temperature profiles of the soil are uniform throughout the emitting layer, that emissivity is related principally to the dielectric constant [1].

In the model, the reflection coefficient is computed through the Fresnel reflectivity equations, which are defined for two media that are divided by a boundary. Figure 2 shows the two medium and the transmission through a boundary. Equation (1) and Equation (2) illustrates the Fresnel reflectivity equations.

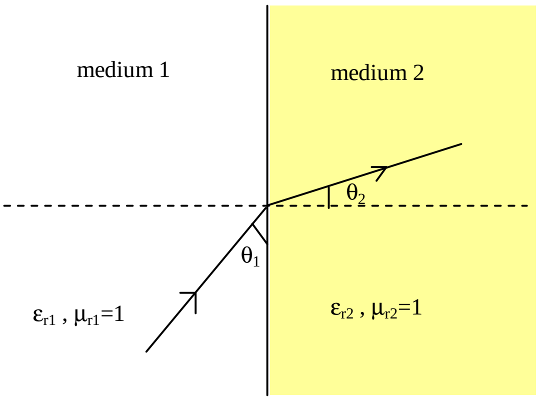

**Figure 2. Transmission between medium 1 and medium 2.**

$$\Gamma_h = \frac{n_1\mu_1 - n_2\mu_2}{n_1\mu_1 + n_2\mu_2} \tag{1}$$

$$\Gamma_v = \frac{n_1\mu_2 - n_2\mu_1}{n_1\mu_2 + n_2\mu_1} \tag{2}$$

where $\Gamma_h$ and $\Gamma_v$ are the reflection coefficients for h-pol and v-pol, respectively. Likewise, $n_1$ and $n_2$ are the index of refraction for medium 1 and medium 2, respectively. $\mu_1$ is the direction of cosine for medium 1, and $\mu_2$ is the direction of cosine for medium 2. These parameters are defined as

$$n_1 = \sqrt{\mathrm{Re}(\varepsilon_{r1})} \tag{3}$$

$$n_2 = \sqrt{\mathrm{Re}(\varepsilon_{r2})} \tag{4}$$

$$\mu_1 = \cos\theta_1 \tag{5}$$

$$\mu_2 = \cos\theta_2 = \sqrt{1 - \left(\frac{n_1}{n_2}\right)^2 (\sin\theta_1)^2} \quad (6)$$

where $\varepsilon_{r1}$ and $\varepsilon_{r2}$ are the dielectric constant of medium 1 and medium 2, respectively. $\theta_1$ is the incidence angle for medium 1, and $\theta_2$ is the incidence angle for medium 2.

Note that Equation (6) is derived from Snell' s Law, which is given as

$$\sin\theta_2 = \frac{n_1}{n_2}\sin\theta_2 \quad (7)$$

Using the trigonometric identity

$$\cos\theta_2 = \sqrt{1 - \sin^2\theta_2} \quad (8)$$

and Equation (7), Equation (6) is obtained.

The reflectivities for h-pol and v-pol are

$$R_h = |\Gamma_h|^2 \quad (9)$$

$$R_v = |\Gamma_v|^2 \quad (10)$$

Finally, the brightness temperatures for h-pol and v-pol are (for bare soil) computed as

$$T_{\mathbf{B}h} = (1 - R_h)T_{soil} \quad (11)$$

$$T_{Bv} = (1 - R_v)T_{soil} \quad (12)$$

where $T_{soil}$ is the physical temperature of the soil.

### 3.2.2 The Incoherent Model

The incoherent model makes the following assumptions:

- The radiation is incoherent, in which the phase effect is avoided.

- Soil moisture and soil temperature are functions of depth only.
- Soil dielectric and thermal properties are constant across layers of finite thickness.

The system geometry for a one-layer and two-layer systems are illustrated in Figure 3 and Figure 4, respectively. The observation angle is denoted as θ. The depth varies across z direction. For a number of N layers, there are N+1 boundaries. The thicknesses of the layers are $\Delta z_1$ and $\Delta z_2$.

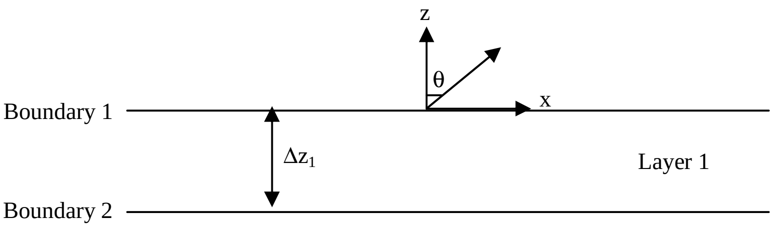

**Figure 3. Soil layer, boundaries of the layer, layer thickness, and the incidence angle for a one-layer system.**

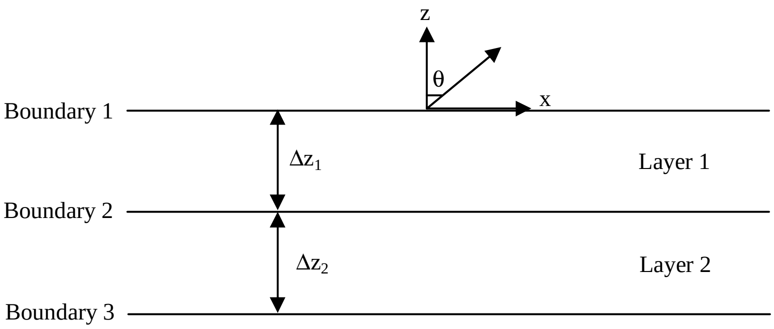

**Figure 4. Soil layers, boundaries between layers, layer thicknesses, and the incidence angle for a two-layer system.**

For a one-layer system, the radiation emitted from the soil, which is represented by $T_B$ is

$$T_B\left(1^+,\theta\right)=T_1\left(1-\frac{1}{L_1}\right)\left(1+\frac{R_2}{L_1}\right)\left(1-R_1\right) \tag{13}$$

where $T_1$ and $R_i$ $i=1,2$ are the soil temperature of layer 1, and the reflectivities for boundary 2 and boundary 2, respectively, and

$$L_1=e^{2\alpha_1\Delta z_1/\mu_1} \tag{14}$$

is the power loss factor, where $\mu_1$ is the direction cosine for layer 1, and $\alpha_1$ is the attenuation constant of layer 1, which is defined as

$$\alpha_1=\left(\frac{2\pi}{\lambda_0}\right)\left|\mathrm{Im}\left(\sqrt{\varepsilon_{r1}}\right)\right| \tag{15}$$

where $\lambda_0$ is the free-space wavelength and $\varepsilon_{r1}$ is the relative dielectric constant of layer 1. $T_B(1^+,\theta)$ denotes the brightness temperature above the first boundary between air and soil at an incidence angle of $\theta$.

For a two-layer system, the radiation emitted from the soil, which is represented by $T_B$ is

$$T_B\left(1^+,\theta\right)=T_1\left(1-\frac{1}{L_1}\right)\left(1+\frac{R_2}{L_1}\right)\left(1-R_1\right)+T_2\left(1-\frac{1}{L_2}\right)\left(1+\frac{R_3}{L_2}\right)\left(\frac{\left(1-R_1\right)\left(1-R_2\right)}{L_1}\right) \tag{16}$$

For an N-layer system, the system is shown in Figure 5.

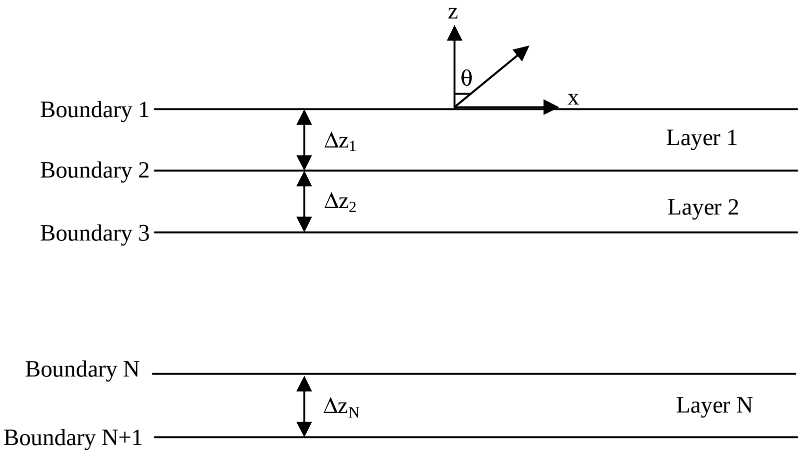

**Figure 5. Soil layers, boundaries between layers, layer thicknesses, and the incidence angle for an N-layer system.**

The radiation emitted from the soil for an N-layer system is

$$T_B\left(1^+,\theta\right)=T_1\left(1-\frac{1}{L_1}\right)\left(1+\frac{R_2}{L_1}\right)\left(1-R_1\right)+T_2\left(1-\frac{1}{L_2}\right)\left(1+\frac{R_3}{L_2}\right)\left(\frac{\left(1-R_1\right)\left(1-R_2\right)}{L_1}\right)+\ldots\ldots\ldots\ldots\ldots\ldots$$
$$+T_N\left(1-\frac{1}{L_N}\right)\left(1+\frac{R_{N+1}}{L_N}\right)\left(\frac{\left(1-R_1\right)\left(1-R_2\right)\ldots\ldots\left(1-R_N\right)}{L_1L_2\ldots\ldots L_{N-1}}\right) \tag{17}$$

### 3.2.3 Modification to the Incoherent Model

In the original work that was developed by Burke [2] , semi-infinite layer contribution is not taken into account. A modification has been made in order to illustrate the semi-infinite layer effect.

For $N$=1, the semi-infinite layer (layer 3) contribution is

$$T_{Bsemi-\inf}\left(N=1\right)=\frac{T_2\left(1-R_1\right)\left(1-R_2\right)}{L_1} \tag{18}$$

For $N$=2, the semi-infinite layer (layer 3) contribution is (see Appendix A)

$$T_{Bsemi-\inf}(N=2)=\frac{T_3(1-R_1)(1-R_2)(1-R_3)}{L_1L_2} \tag{19}$$

For $N$=3, the semi-infinite layer (layer 4) contribution is

$$T_{Bsemi-\inf}(N=3)=T_4\frac{(1-R_1)(1-R_2)(1-R_3)(1-R_4)}{L_1L_2L_3} \tag{20}$$

For $N$=$N$, the semi-infinite layer (layer $N$+1) contribution is

$$T_{Bsemi-\inf}(N=N)=T_{N+1}\frac{(1-R_1)(1-R_2)(1-R_3)(1-R_4)\ldots\ldots(1-R_N)}{L_1L_2L_3\ldots\ldots L_{N-1}}\frac{(1-R_{N+1})}{L_N} \tag{21}$$

For $N$=1, Figure 6 illustrates the impact of the semi-infinite layer effect for the air-pure water-soil test case that is given in Section 3.6. In Figure 6, reflectivities for the configuration with the semi-infinite layer and without semi-infinite layer versus water depth are plotted. Soil temperature profile is uniform. The results are presented for h-pol with an observation angle of 35°. It is observed that as the water depth decreases, the impact of the semi-infinite layer increases. Note that when water depth is zero, the reflectivity for the configuration without the semi-infinite layer effect is 1, which means the corresponding emissivity is zero. This is because all the emissivity is supposed to contribute from the semi-infinite layer since there is no water layer when water depth is zero. However, the semi-infite layer is excluded in that plot and the resulting emissivity is zero.

For $N$=1, Ulaby et. al [3] developed an equation that includes the semi-infinite layer effect. Neglecting multiple reflections between layers, the equation is

$$T_B(1^+,\theta)=T_1\left(1-\frac{1}{L_1}\right)\left(1+\frac{R_2}{L_1}\right)(1-R_1)+\frac{T_2(1-R_1)(1-R_2)}{L_1} \tag{22}$$

which consists of the single layer contribution and the semi-infinite layer contribution, which is presented here. In this study, the brightness temperature equation including the semi-infinite layer effect is generalized for *N* layers using Burke' s approach.

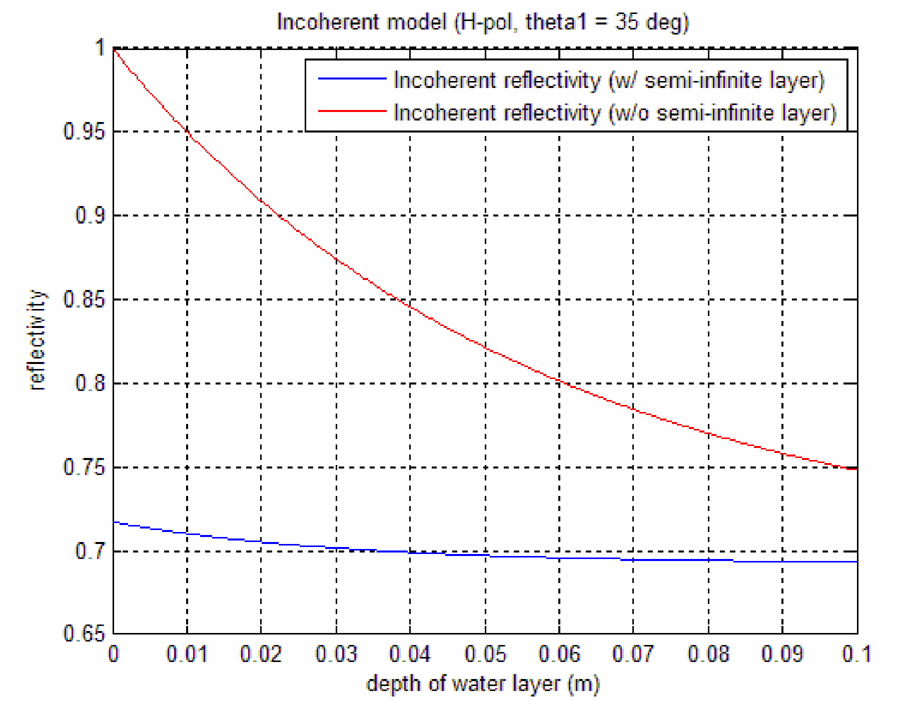

**Figure 6. Incoherent reflectivity for a uniform soil temperature profile: Incoherent model result with and without the semi-infinite layer effect.**

### 3.2.4 The Coherent Model

Njoku and Kong [4] developed a coherent model that assumes that the soil consists of layers, the soil is horizontally homogeneous, and soil moisture and soil temperature vary with depth. The approach is considered coherent because the amplitudes and phases of the reflections in the medium are both taken into account.

$$T_{Bh}(\theta)=\frac{k}{\cos\theta}\int_{-\infty}^{0}dzT(z)\varepsilon_r^{''}(z)\left|\Psi(z)\right|^2 \tag{23}$$

$$T_{Bv}(\theta)=\frac{k}{\cos\theta}\int_{-\infty}^{0}dzT(z)\varepsilon_r^{''}(z)\left(\left|\frac{1}{\varepsilon_r(z)}\frac{d\phi(z)}{dz}\right|^2+\left|\frac{k_x\phi(z)}{\varepsilon_r(z)}\right|^2\right) \tag{24}$$

where $\varepsilon_r(z)=\varepsilon_r^{'}(z)+\varepsilon_r^{''}(z)$ is the relative dielectric constant, $k$ is the free-space wave number, $\theta$ is the incidence angle, and $k_x=k\sin\theta$, and $T(z)$ is the vertical soil temperature profile. $\Psi(z)$ and $\phi(z)$ are governed by the following equations.

$$\frac{d^2\Psi(z)}{dz^2}+\left[\varepsilon_r(z)k^2-k_x^2\right]\Psi(z)=0 \tag{25}$$

$$\varepsilon_r(z)\frac{d}{dz}\left(\frac{1}{\varepsilon_r(z)}\frac{d\phi(z)}{dz}\right)+\left[\varepsilon_r(z)k^2-k_x^2\right]\phi(z)=0 \tag{26}$$

$$\left[\frac{d\Psi(z)}{dz}+jk\cos\theta\left(2-\Psi(z)\right)\right]_{z=0}=0 \tag{27}$$

$$\left[\frac{d\phi(z)}{dz}+j\varepsilon_r(z)k\cos\theta\left(2-\phi(z)\right)\right]_{z=0}=0 \tag{28}$$

Equation (17) and Equation (18) can be reformulated in terms of a stratified medium that consists of a large number of horizontally homogeneous layers, each with a uniform temperature and dielectric constant characteristics. The integrals of Equation (17) and Equation (18) can be replaced by summations. The resultant expressions are

$$T_{Bh}(\theta)=\frac{k}{\cos\theta}\sum_{l=1}^{N}\frac{\varepsilon_l''T_l}{\varepsilon_0}\begin{pmatrix}\dfrac{\left|A_l e^{-jk_{lz}d_l}\right|^2}{2k_{lz}''}\left(1-e^{2k_{lz}''(d_{l-1}-d_l)}\right)-\dfrac{\left|B_l e^{jk_{lz}d_l}\right|^2}{2k_{lz}''}\left(1-e^{-2k_{lz}''(d_{l-1}-d_l)}\right)- \\ \dfrac{\left(A_l e^{-jk_{lz}d_l}\right)\left(B_l e^{jk_{lz}d_l}\right)^*}{2jk_{lz}'}\left(1-e^{-j2k_{lz}'(d_{l-1}-d_l)}\right)+ \\ \dfrac{\left(A_l e^{-jk_{lz}d_l}\right)^*\left(B_l e^{jk_{lz}d_l}\right)}{2jk_{lz}'}\left(1-e^{j2k_{lz}'(d_{l-1}-d_l)}\right)\end{pmatrix} \tag{29}$$

$$+\frac{k}{\cos\theta}\frac{\varepsilon_l''T_l}{\varepsilon_0}\frac{\left|T_h\right|^2e^{-2k_{lz}''d_n}}{2k_{lz}''}$$

$$T_{Bv}(\theta)=\frac{k}{\cos\theta}\sum_{l=1}^{N}\frac{\varepsilon_l''T_l}{\varepsilon_0\left|k_l\right|^2}\left(\left|k_{lz}\right|^2+k_x^2\right)\begin{pmatrix}\dfrac{\left|C_l e^{-jk_{lz}d_l}\right|^2}{2k_{lz}''}\left(1-e^{-2k_{lz}''(d_{l-1}-d_l)}\right)-\dfrac{\left|D_l e^{jk_{lz}d_l}\right|^2}{2k_{lz}''}\left(1-e^{2k_{lz}''(d_{l-1}-d_l)}\right)+ \\ \dfrac{\left|k_{lz}\right|^2-k_x^2}{\left|k_{lz}\right|^2+k_x^2}\begin{pmatrix}\left(\dfrac{C_l e^{-jk_{lz}d_l}\left(D_l e^{-jk_{lz}d_l}\right)^*}{2jk_{lz}'}\right)\left(1-e^{j2k_{lz}'(d_{l-1}-d_l)}\right)- \\ \dfrac{\left(C_l e^{-jk_{lz}d_l}\right)^*\left(D_l e^{jk_{lz}d_l}\right)}{2jk_{lz}'}\left(1-e^{-j2k_{lz}'(d_{l-1}-d_l)}\right)\end{pmatrix}\end{pmatrix}+ \tag{30}$$

$$\frac{k}{\cos\theta}\frac{\varepsilon_l''\left(\left|k_{lz}\right|^2+k_x^2\right)T_t}{\varepsilon_0\left|k_l^2\right|}\frac{\left|T_v\right|^2e^{-2k_{lz}''d_n}}{2k_{lz}''}$$

The subscript *l* refers to the quantities in the $l^{th}$ layer of the medium, and $d_l$ is the depth below the surface of the interface between the $l^{th}$ and $(l+1)^{th}$ layer. The $A_l$, $B_l$, $C_l$, $D_l$, $T_h$, and $T_v$ are the wave amplitudes and are related to one another by propagation matrices [5].

### 3.2.5 Modification to the Coherent Model

The programming code of the coherent model has been modified in order to model a three layer air-pure water-soil test case that is described in section 3.6, and ponding effect for a set of data that was collected in Michigan in 2001.

For the air-pure water-soil test case, a variable ‘water_depth’, which represents the thickness of the layer for pure water, has been added as an input variable to the Fortran subroutine. The water_depth can cover a range so that the reflectivity can be evaluated as a function of changing water_depth.

For the first layer, the relative dielectric constant is 1, which means the first layer is air. For all other layers, the relative dielectric constant is set to that of pure water first, which is $\varepsilon_{rwater}$=80+j5. Then the soil_depth variable is taken into account: If the depth is greater than the water_ depth, the soil layer relative dielectric constant is set to $\varepsilon_{rsoil}$=25+j3.

This condition is shown in the Fortran subroutine as

```
do i=1,nzz1
     if(ddz(i) .gt. water_depth) then
       epss(i)=cmplx(25,3)
      end if
 end do
```

where nzz1 is the total number of layers, ddz is a variable for the depth in z direction, epss is the relative dielectric constant of the layers. Note that using a negative number as the imaginary part returns errors in the code, therefore, positive imaginary parts are preferred. This choice returns meaningful results when compared to those of the negative imaginary parts that are used in MATLAB.

For the ponding case, the soil surface roughness parameter has been changed for a rain event, because the soil becomes smoother after precipitation. Hence, there are two regions in the dataset: In the first region (before the rain event), the standard deviation of surface height is larger. In the second region (after the rain event), that parameter is smaller. For a set of data that was collected in Michigan in 2001 (including two ponding events), the transmission line model is applied instead of the coherent model, because of the interpolation issues that are considered in the programming code that is related to the coherent model. The linear interpolation in the Fortran subroutine does not allow the user to implement a layer of water on top of the soil layer. As an alternative, the transmission line model is used in order to compute the brightness temperatures for two timesteps where the ponding occurs. The transmission line model assumes that the soil temperature profile is uniform. For that reason, the average temperature of the first 10 cm of soil is used as the uniform temperature in the transmission line model, which returns meaningful results.

Note that a layer of water stands on top of a soil layer both in the test case and the ponding case for the Michigan data. However, the implementation of the test case is possible using the coherent model, while the programming code for the coherent model does not return accurate results for the Michigan data due to the structure of the code. In the programming code, there is a main program that calls a subroutine, which returns user-defined outpus such as brightness temperatures, relative dielectric constant profile, reflection coefficient profile etc. The number of soil layers in the main program represents the soil moisture and soil temperature measurement depths. Using the soil moisture profile and another set of inputs, relative dielectric constant profile is evaluated for the soil moisture measurement depths in the subroutine. Then the subroutine interpolates the relative dielectric constant profile (for the measurement depths) to the model layers, whose quantity (number of layers) is user-defined. Hence, the number of layers (and the depth through the soil) in the main program, and the number of layers (and the depth through the soil) in the subroutine could be different. In the test case, the relative dielectric constant of water and soil are set by the user after an interpolated relative dielectric constant profile, which could be random because it is overwritten by the water and soil relative dielectric constants, is produced by the program. Hence, the interpolation errors are excluded, and a sharp transition between different media is achieved (linear interpolation tends to smoothen the relative dielectric constant transitions). However, in the Michigan data case, applying a water layer on top of a non-interpolated relative dielectric constant profile causes errors. If the water layer is located on a non-interpolated relative dielectric constant profile, and then interpolation is performed, the programming code returns a smooth, linearly-interpolated profile between and including the top layer (water) and the bottom (soil) layer. If the water layer is located on an interpolated relative dielectric constant profile, the result will be erroneous again because the relative dielectric constant of the first soil layer will change due to the interpolation, and the transition between the water and the soil will be different, which results in a non-neglectable error.

### 3.2.6 Transmission Line Model

Transmission line model is a coherent approach that utilizes the analogy between transmission lines and the soil dielectric properties. It assumes that the soil consists of layers and is horizontally homogeneous, that is the dielectric constant is a function of depth only (it does not change across the xy plane). It is also based on the assumption that the soil temperature is uniform in all directions [3].

For a three layer air-soil-soil case, in which layer 1 is air, layer 2 extends from z=0 to z=d, and layer 3 extends from z=*d* to z=∝, the coherent reflectivity $R(\theta_1;p)$ can be calculated. System geometry and its transmission line equivalent is illustrated in Figure 7.

Using the transmission line parameters, the reflection coefficient for boundary 2 is computed as

$$\Gamma_2 = (-1)^n \left( \frac{Z_3 - Z_2}{Z_3 + Z_2} \right) \tag{31}$$

where

$$Z_i = \begin{cases} \eta_i cos\,\theta_i & \text{for v-pol} \\ \eta_i sec\,\theta_i & \text{for h-pol} \end{cases} \qquad i=2,3 \tag{32}$$

$$\eta_i = \frac{1}{\sqrt{\varepsilon_i}} \qquad i=2,3 \tag{33}$$

The input impedance seen at z=0 is

$$Z_{in} = Z_2 \left( \frac{1 + (R_2 / L_2) e^{-j2\beta_2' d}}{1 - (R_2 / L_2) e^{-j2\beta_2' d}} \right) \tag{34}$$

where

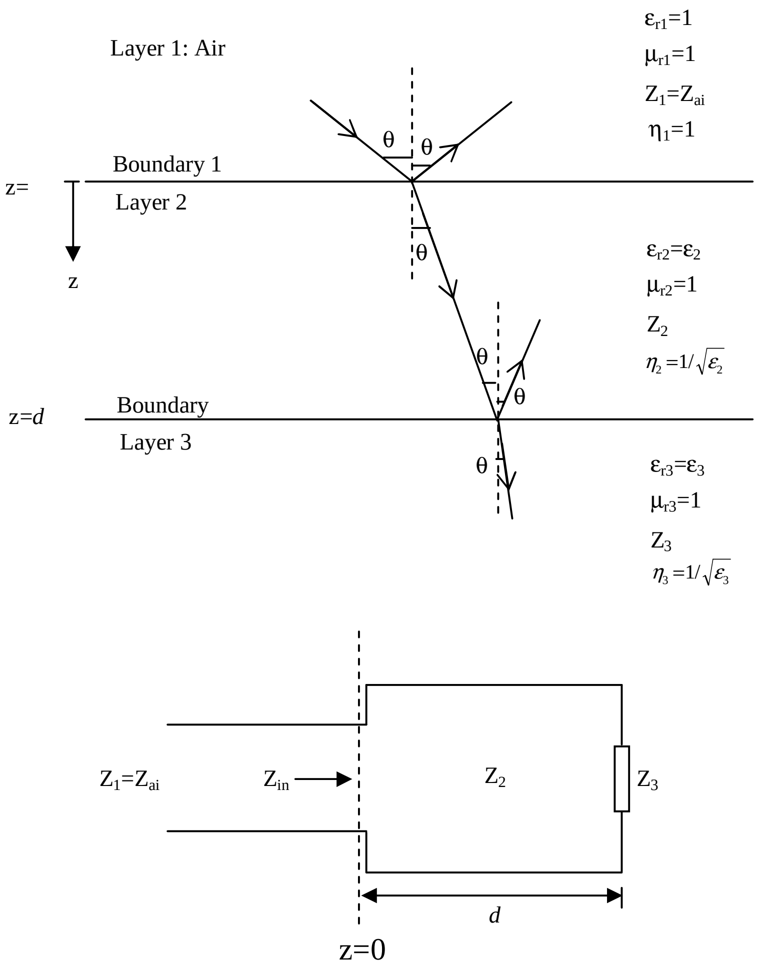

**Figure 7. System geometry and its transmission line equivalent.**

$$\beta_2^{'} = \beta_2 \sec\theta_2 \tag{35}$$

$$\beta_2 = \frac{2\pi}{\lambda_0} \mathrm{Re}\left(\sqrt{\varepsilon_2}\right) \tag{36}$$

and

$$L_2 = e^{2\alpha_2 d \sec\theta_2} \tag{37}$$

$$\alpha_2 = \frac{2\pi}{\lambda_0} \left|\mathrm{Im}\left(\sqrt{\varepsilon_2}\right)\right| \tag{38}$$

The reflection coefficient for boundary 1 is

$$\Gamma_1 = (-1)^n \left( \frac{Z_{in} - Z_1}{Z_{in} + Z_1} \right) \qquad n = \begin{cases} 0 \text{ for h-pol} \\ 1 \text{ for v-pol} \end{cases} \tag{39}$$

Using Equation (30) in Equation (35), we obtain

$$\Gamma_1 = \frac{R_1 + \dfrac{R_2}{L_2} e^{-j2\beta_2' d}}{1 + \dfrac{R_1 R_2 e^{-j2\beta_2' d}}{L_2}} \tag{40}$$

The coherent reflectivity is

$$R_c = \left| \Gamma_1 \right|^2 = \frac{R_1 + \dfrac{R_2}{L_2^2} + \dfrac{2\sqrt{R_1 R_2}}{L_2} \cos\left(2\beta_2' d + \phi_1 - \phi_1\right)}{R_1 + \dfrac{R_1 R_2}{L_2^2} + \dfrac{2\sqrt{R_1 R_2}}{L_2} \cos\left(2\beta_2' d + \phi_1 - \phi_1\right)} \tag{41}$$

where

$$R_1 = \left| \Gamma_1 \right|^2 \tag{42}$$

$$R_2 = \left| \Gamma_2 \right|^2 \tag{43}$$

and $\phi_1$ and $\phi_2$ are the phase angles of $\Gamma_1$ and $\Gamma_2$.

$$\Gamma_1 = \left| \Gamma_1 \right| e^{j\phi_1} \tag{44}$$

$$\Gamma_2 = \left| \Gamma_2 \right| e^{j\phi_2} \tag{45}$$

## 3.3 The Atmospheric and Land-Surface Exchange Model (ALEX)

The ALEX model is a land surface model that describes the transport of heat, water vapor, carbon and momentum within the soil-plant-atmosphere system [6] It is a simplified version of another land surface model called ‘Cupid’. ALEX requires less input parameters than Cupid and its computation time is lower. The empirical relationships are minimal in ALEX: Application to various types of crops is possible and a limited set of environmental conditions is not a restriction. ALEX uses the Richard’ s equation, and parameters such as root uptake, drainage and soil evaporation to evaluate the time-dependent soil moisture profile. In our case, the medium is bare soil, hence, vegetation parameters are not needed. The soil is considered as a layered medium and the depth of the each layer is user-defined.

The usage of a model such as ALEX to determine the moisture and temperature variations within the soil is important since it is not possible to sample at all depths in an experimental site. Actual field measurements often provide an insufficient number of inputs to a radiative transfer model, which might result in an inaccurate brightness temperature calculation.

By using various parameters of the land and the atmosphere that are commonly available, such as air temperature, wind speed, relative humidity, and solar radiation, it is possible to predict soil moisture and temperature values at different depths through the use of a land surface model like ALEX.

## 3.4 The Dielectric Mixing Model

Dobson et. al. [7] developed semiempirical model that evaluates the microwave dielectric behavior of soil-water mixtures. The model assumes that the soil-water mixture consists of four components: dry soil, air, free water, bound water. The modeled relative dielectric constant is calculated as

$$\varepsilon^{\alpha} = \sum_i V_i \varepsilon_i^{\alpha} \tag{46}$$

$$\varepsilon = \left(\varepsilon^{\alpha}\right)^{1/\alpha} \tag{47}$$

where α is a constant shape factor, $V_i$ and $\varepsilon_i$ are the volume and the relative dielectric constant of each component, respectively. More explicitly

$$\varepsilon^{\alpha} = V_s \varepsilon_s^{\alpha} + V_a \varepsilon_a^{\alpha} + V_{fw} \varepsilon_{fw}^{\alpha} + V_{bw} \varepsilon_{bw}^{\alpha} \tag{48}$$

The subscripts *s*, *a*, *fw* and *bw* denote soil, air, free water, and bound water, respectively, where

$$\varepsilon_s = (1.01 + 0.44\rho_s)^2 - 0.062 \tag{49}$$

$\rho_s$ denotes the particle density of dry soil. The relative dielectric constant of free water $\varepsilon_{fw} = \varepsilon'_{fw} + j\varepsilon''_{fw}$ is expressed as

$$\varepsilon'_{fw} = \varepsilon_{w\infty} + \frac{\varepsilon_{w0} - \varepsilon_{w\infty}}{1 + (2\pi f \tau_w)^2} \tag{50}$$

$$\varepsilon''_{fw} = 5 \tag{51}$$

where $\varepsilon_{w\infty}$ is the high-frequency limit of $\varepsilon_{fw}$, $\varepsilon_{w0}$ is the static dielectric constant of free water, f is the frequency in Hertz, and $\tau_w$ is the relaxation time of free water. In our case, the imaginary part of the relative dielectric constant of free water is a constant. Likewise, $\varepsilon_{bw}$ is chosen to be a constant.

$$\varepsilon_{bw} = 35 + j14.5 \tag{52}$$

The volume of the dry soil is

$$V_s = \frac{\rho_b}{\rho_s} \tag{53}$$

where $\rho_b$ is the bulk density of the soil. Also,

$$1 - V_s = V_a + V_{fw} + V_{bw} \tag{54}$$

It is possible to extract $V_a$ through Equation (50) assuming that $V_{fw}$ and $V_{bw}$ are known. Note that all radiative transfer models, which are the Fresnel model, the incoherent model, the coherent model, and the transmission line model, that are used for the analysis of a dataset that was collected in Michigan in 2001 use Dobson mixing model to convert soil moisture to dielectric constant.

## 3.5 The Soil Surface Roughness Model

Choudhury et. al. [8] developed a soil surface roughness model that is based on standard deviation of surface height $\sigma$. If the scattering surface is statistically rough such that there is no correlation between the amplitudes of the waves scattered by two points on the surface, and the surface height distribution is represented by a Gaussian distribution with a zero mean and a standard deviation $\sigma$, then a roughness parameter $h$ can be defined.

$$h = 4\sigma^2 \left( \frac{2\pi}{\lambda} \right)^2 \tag{55}$$

where $\lambda$ is the wavelength in free space. Assuming that the reflectivity of a specular surface $R_{specular}$ is known

$$R_{rough}(\theta) = R_{specular}(\theta) e^{-h\cos^2\theta} \tag{56}$$

where $R_{\mathrm{rough}}$ is the reflectivity of a rough surface, and θ is the observation angle. Then the emissivity of a rough surface $E_{rough}$ is

$$E_{rough}(\theta)=1-R_{rough}(\theta) \tag{57}$$

## 3.6 Comparison of the Radiative Transfer Models

In order to verify the agreement between the radiative transfer models, an air-pure water-wet soil test case that is illustrated in Figure 8 is considered. The models that are used for the test case are the incoherent model, the coherent model, and the transmission line model. Fresnel model cannot be used in this analysis because it assumes that the soil moisture profile is uniform throughout the soil, which is not applicable to the test case, because the soil moisture profile directly affects the dielectric constant profile of the soil. Note that the soil temperature profile is uniform in this system.

Reflectivity as a function of pure water depth, which varies between 0-10 cm, is plotted for h-pol and the observation angles $\theta_1=0°$ and $\theta_1=35°$, which are shown in Figure 9 and Figure 10, respectively. Figure 11 illustrates reflectivity versus pure water depth for v-pol with an observation angle of $\theta_1=35°$. Relative dielectric constants of air, pure water, and wet soil are $\varepsilon_{\mathrm{rair}}=1$, $\varepsilon_{\mathrm{rwater}}=80-j5$ [5], $\varepsilon_{\mathrm{rsoil}}=25-j3$, respectively. Note that emissivity=1-reflectivity for a uniform soil temperature profile.

Upon analyzing Figure 9 and Figure 10, an agreement between the models is observed. The transmission line model and the coherent model show oscillations while the incoherent model does not. This is because the coherent models take into account the phases adding up and subtracting, while the incoherent model does not include the phase effects.

Another point is the usage of different observation angles. $\theta_1$=0° returns lower reflectivity (higher emissivity) and $\theta_1$=35° returns higher reflectivity (lower emissivity). This is due to the shorter (longer) path length at $\theta_1$=0° ($\theta_1$=35°), which means there is more pure water on the path length when $\theta_1$=35° that results in more attenuation and less emission.

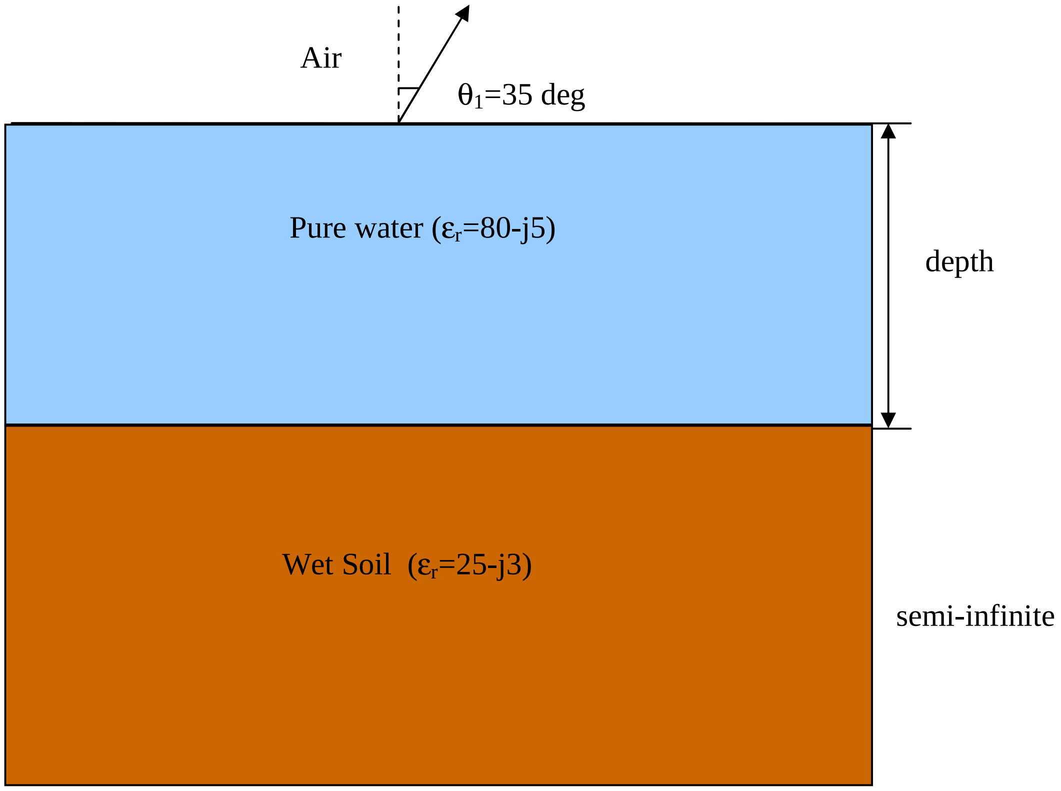

**Figure 8. Test case geometry: Air-pure water-soil system.**

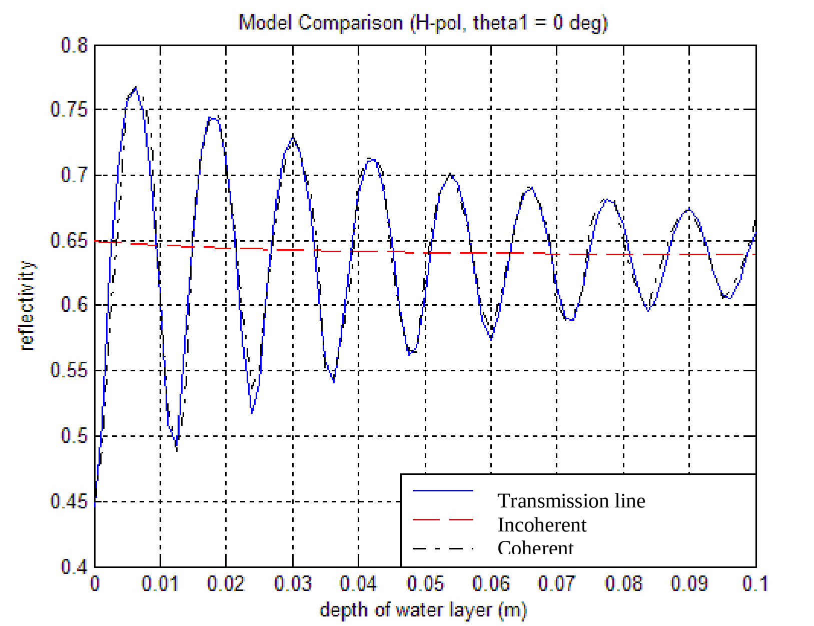

**Figure 9. Reflectivity versus depth of pure water layer (h-pol). Transmission line model, incoherent model, and coherent model results are presented for $\theta_1$=0°.**

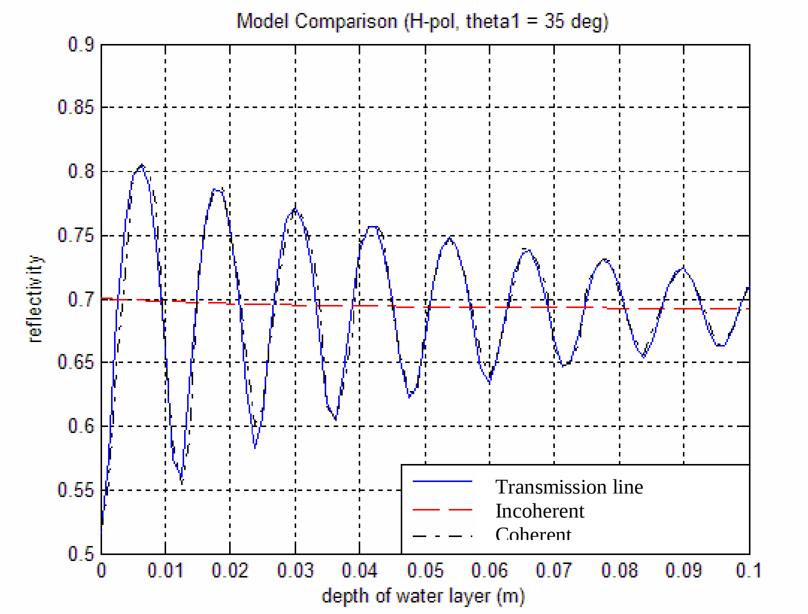

**Figure 10. Reflectivity versus depth of pure water layer (h-pol). Transmission line model, incoherent model, and coherent model results are presented for $\theta_1$=35°.**

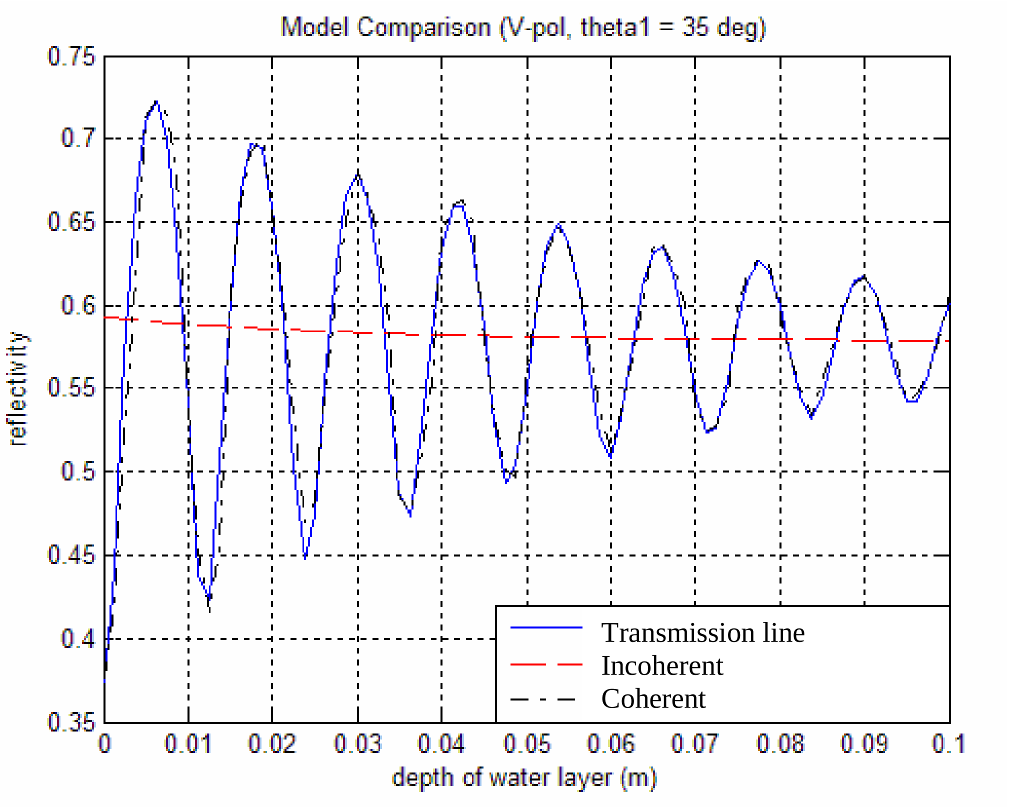

**Figure 11. Reflectivity versus depth of pure water layer (v-pol). Transmission line model, incoherent model, and coherent model results are presented for $\theta_1$=35°.**

## 3.7 Conclusion

Radiative transfer models along with a land surface model called ALEX, a dielectric mixing model, and a soil surface roughness model are introduced. Modifications to two of the radiative transfer models, which are the incoherent model and the incoherent model, are given. An air-pure water-wet soil test case is illustrated in order to verify the agreement between the radiative transfer models. Reflectivities that are produced by these models are plotted as a function of the pure water depth for two observation angles. Analysis of the resulting plots is presented.

# BIBLIOGRAPHY

[1] Wigneron, J. P. Chanzy, A., Calvet, J. C., Bruguier, N. (1995). A simple algorithm to retrieve soil moisture and vegetation biomass using passive microwave measurements over crop fields. *Remote Sens. Environ.* 51. pp. 331-341.

[2] Burke, W. J., Schmugge, T., Paris, J. F. (1979). Comparison of 2.8- and 21-cm microwave radiometer observations over soils with emission model calculations. *Journal of Geophysical Research.* 84(C1). pp. 287-294.

[3] Ulaby, F. T., Moore, R. K., Fung A. K. (1981). *Microwave Remote Sensing: Active and Passive*. Reading: Addison-Wesley.

[4] Njoku, E. G., Kong, J. A. (1977). Theory for passive microwave remote sensing of near-surface soil moisture. *Journal of Geophysical Research.* 82(20). pp. 3108-3118.

[5] Kong, J. A. (1975). *Theory of Electromagnetic Waves*. New York: Interscience.

[6] Anderson M. C., Norman, J. M., Meyers, T. P., Diak, G. R. (2000). An analytical model for estimating crop canopy transpiration and carbon assimilation fluxes based on canopy light-use efficiency. *Agricultural and Forest Meteorology*. 101. pp. 265-289.

[7] Dobson, M. C., Ulaby, F. T., Hallikainen, M. T., El-Rayes, M. A. (1985). Microwave dielectric behavior of wet soil-Part II: Dielectric mixing models. *IEEE Transactions on Geoscience and Remote Sensing.* GE-23(1). pp. 35-46.

[8] Choudhury, B. J. et. al. (1979). Effect of surface roughness on the microwave emission from soils. *Journal of Geophysical Research.* 84(NC9). pp. 5699-5706.

# CHAPTER 4. A NONLINEAR RELATIONSHIP BETWEEN TERRESTRIAL MICROWAVE EMISSION AT 1.4 GHZ AND SOIL MOISTURE CAUSED BY PONDING OF WATER

There is a strong, nearly linear relationship between terrestrial microwave emission at 1.4 GHz and soil water content. However, under certain conditions the relationship between microwave emission and soil moisture can be highly nonlinear. We present an example of such a nonlinear relationship. The 1.4 GHz brightness temperature record of a bare agricultural field exhibited strong variations (a large decrease, followed by a large increase and another decrease) during a rain event despite a steady increase in soil water content.We show that these variations were caused by water that ponded on the soil surface. Although extreme conditions such as these are not common, they do occur and the assumption of the normal linear relationship between microwave emission and soil water content would produce inaccurate estimates soil moisture.

## 4.1 Introduction

Terrestrial microwave emission is sensitive to soil moisture [1]. Soil moisture is an important yet unobserved reservoir of the hydrologic cycle linked to precipitation variability [2]. Remote sensing satellites that observe terrestrial microwave emission have the potential to map the spatial and temporal variability of soil moisture on a global basis. This year in 2009, the European Space Agency’s Soil Moisture and Ocean Salinity (SMOS) mission will begin to provide the first set of global soil moisture data [3]. This satellite will measure terrestrial microwave emission at 1.4 GHz, the optimal frequency for soil moisture remote sensing [4]. At 1.4 GHz, low levels of vegetation up to and including mature row crops are semi–transparent [5]. The emitting depth within the soil surface is also relatively large such that the 1.4 GHz brightness temperature is sensitive to the water content of the first few centimeters of the soil surface [6]. The relationship between the brightness temperature at 1.4 GHz and soil water content is nearly linear. As soil moisture increases, the microwave emissivity of a soil surface decreases. Assuming little or no change in the temperature of the soil, a decrease in emissivity results in a substantial decrease in the 1.4 GHz brightness temperature.

There are, however, certain conditions that can produce a nonlinear relationship between soil moisture and terrestrial microwave emission. We observed such a nonlinear relationship during an experiment conducted in a bare agricultural field. We observed strong variations in the horizontally–polarized brightness temperature at 1.4 GHz (a large decrease, followed by a large increase and another decrease) during a precipitation event despite the fact that there was a steady increase in the water content of the soil through the emitting depth. See Figure 1. We show in this paper that this nonlinear relationship was caused by the transient ponding of water on the soil surface. This case study demonstrates that although extreme conditions like these are uncommon, they do occur. Estimates of soil moisture retrieved from the 1.4 GHz brightness temperature under these situations will not be accurate if the normal linear relationship between soil moisture and brightness temperature is assumed.

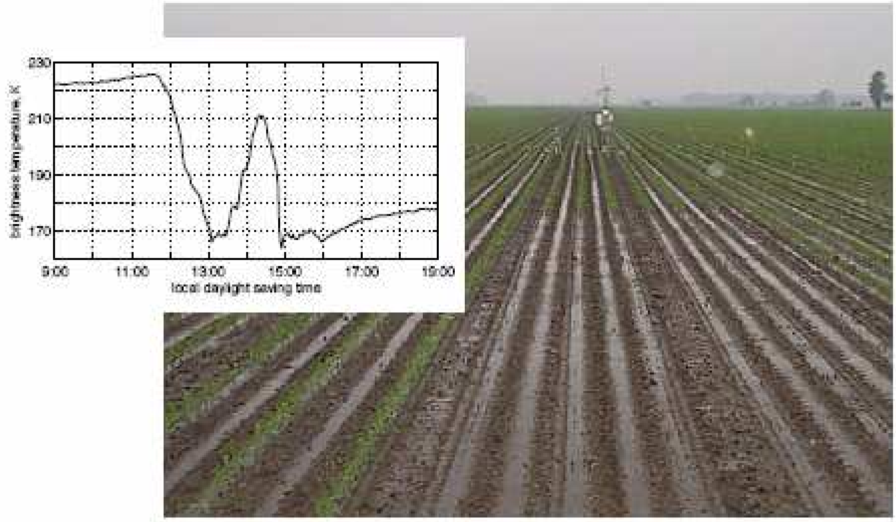

**Figure 1. The horizontally-polarized brightness temperature of bare soil at 1.4 GHz during a rain event and a picture of ponded water in an agricultural field. Note the large variation in brightness temperature of more than 40 K over a short period of time.**

## 4.2 Measurements

We collected measurements of soil moisture, vegetation and soil temperatures, precipitation, and horizontally–polarized brightness temperature at 1.4 GHz in an agricultural field in southeastern Michigan, USA, from May until October in 2001. These data were collected with micrometeorological instruments and a truck–mounted radiometer system. Measurements of soil moisture, soil and vegetation temperatures, and micrometeorology were 20–minute averages of data sampled every 10 seconds. We used single–frequency impedance probes, time–domain reflectometry (TDR) sensors, and gravimetric sampling to measure soil moisture [5]. Instantaneous measurements of brightness temperature were made every 2 minutes. The precision of the brightness temperature measurements was 0.4 to 0.5 K. The incidence angle of the antenna of the 1.4 GHz radiometer was 35◦, and the antenna was oriented 60◦ relative to row direction. Rows were planted in the east–west direction. Other details of the experiment, can be found in several papers [5], [7], [8]. Figure 2 illustrates the measurements of precipitation , 0-3 cm average volumetric soil moisture for low and high areas in the field, and the amount of ponding for day 144.

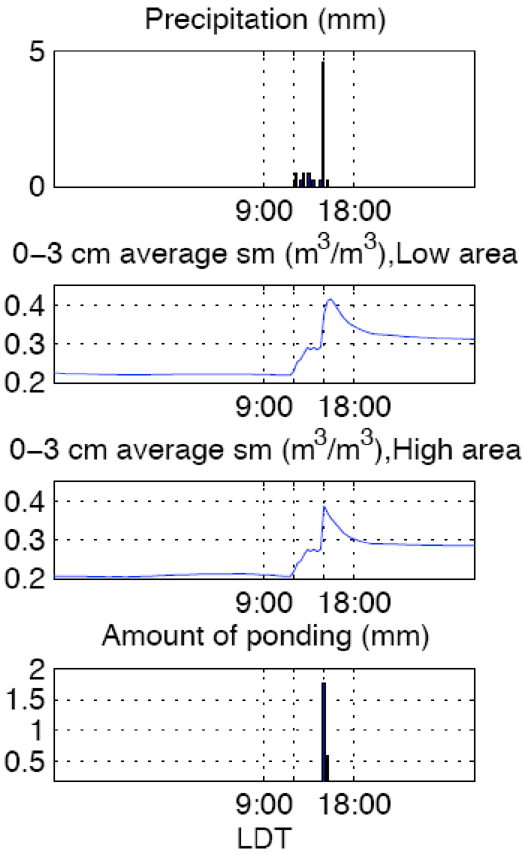

**Figure 2. Measurements of precipitation, 0-3 cm average volumetric soil moisture for low and high areas in the field, and the amount of ponding.**

## 4.3 Modeling a Ponding Event through Radiative Transfer Models

When water deposited by rain cannot infiltrate into the soil faster than the rate of precipitation (and if the water cannot move laterally to another area), the water will begin to collect, or *pond*, on the soil surface. Ponding of water can occur for several reasons. For example, if the precipitation rate is high, water cannot infiltrate fast enough into the soil. If the water content of the soil is initially high, the precipitation rate that will cause ponding will be considerable lower. Reduced infiltration rates caused by ice clogging soil pores can also produce ponding, particularly in the early spring. Normally ponding is a transient phenomenon lasting anywhere from minutes to hours. During periods of extreme wetness, or in areas of low topography, ponding can last for days.

Ponded water on top of a soil surface will change the emissivity of the surface. When a layer of water lies on top of a soil surface, there will be a sharp change in electrical properties at the boundary between the soil surface and the ponded water and at the boundary between the ponded water and the atmosphere. If the upper and lower boundaries of the layer of water has sufficient lateral extent (a significant fraction of the field of view of the remote sensing instrument), then the layer of water will add coherency to the radiation detected by a microwave radiometer. In this case, a microwave emission model that considers the coherent nature of electromagnetic radiation must be used to correctly model the emissivity of the soil and ponded water system.

Agricultural practices can also cause ponding. Tillage and planting can produce small alternating high and low areas in the soil surface. An illustration of this effect is shown in Figure 3. Since the low areas can collect water from both precipitation and runoff from the surrounding high areas, ponding often occurs in the low areas. This ponding can be exacerbated by lower rates of water infiltration in the low areas due to the compaction of the soil as the agricultural machinery responsible for the tillage or planting moved through the field.

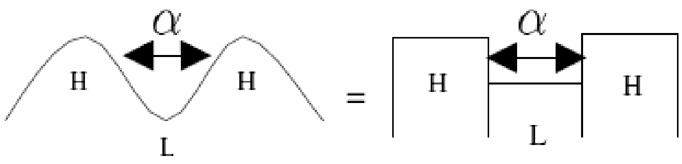

$$T_B = \alpha\, T_{B,L} + (1 - \alpha)\, T_{B,H}$$

**Figure 3. Agricultural practices can produce small, alternating high (H) and low (L) areas in the soil surface. We use α to represent the fraction of low areas.**

We hypothesize that ponding of water is responsible for the strong variations in the 1.4 GHz brightness temperature shown in Figure 1. We believe that ponding occured in the low areas of the tilled agricultural field during a rain event, and that this ponding was enhanced by soil compaction in the low areas due to the movement of agricultural machinery through the field.

The field has a certain row structure since there are periodic high and low areas. The high areas are the undisturbed areas that do not allow ponding, while the low areas are the compacted soils where ponding occurs. The bulk densities of the high and low areas are 1.09 g cm$^{-3}$ and 1.21 g cm$^{-3}$, respectively. In our approach, we run ALEX with the "all high" and "all low" conditions. High areas are represented by Ksat = $4 \times 10^{-5}$ kg s m$^{-3}$, which is a typical value for the silty clay loam. In order to determine the Ksat for the lower areas, the high area Ksat is lowered until ALEX produces ponding. The first Ksat that reproduces ponding is $5\times10^{-6}$ kg s $m^{-3}$. We use this value as the low area Ksat. The measured Ksats are not available. ALEX returns the soil moisture and temperature profiles for both cases. Then we run our radiative transfer model for the two cases through the use of these two distinct soil moisture and temperature profile sets as inputs, and produce two brightness temperature variations as a function of time. We combine the “all high” and “all low” brightness temperatures through a linear combination that is defined by a fraction $\alpha$, which represents the percentage of the ponded area (low area) in the field. See Figure 3.

In order to reproduce the brightness temperature variation as a function of time, we initially use the Fresnel model to show that Fresnel model is not capable of modeling a ponding event because it assumes that the soil moisture profile is uniform throughout the soil, which inhibits the inclusion of a water layer on top of the soil surface. The Fresnel model result without the ponding event is shown in Figure 4. Average soil moisture of 0-3 cm of soil is used as the uniform soil moisture profile for each time step. Soil temperature profile is also assumed to be uniform and is equal to the soil temperature at 1.5 cm depth for each time step.

We then use a coherent model that was developed by Njoku and Kong. However, in the case of a ponding event, inclusion of a water layer on top of a soil system introduces some interpolation issues that might affect the accuracy of the results, as described in chapter 3, section 3.2.5. The usage of the transmission line model resolves that problem. The transmission line model assumes that the soil temperature is uniform. We use the average temperature of the first 10 cm of the soil as an input to the model for each time step to produce the brightness temperature as a function of time.

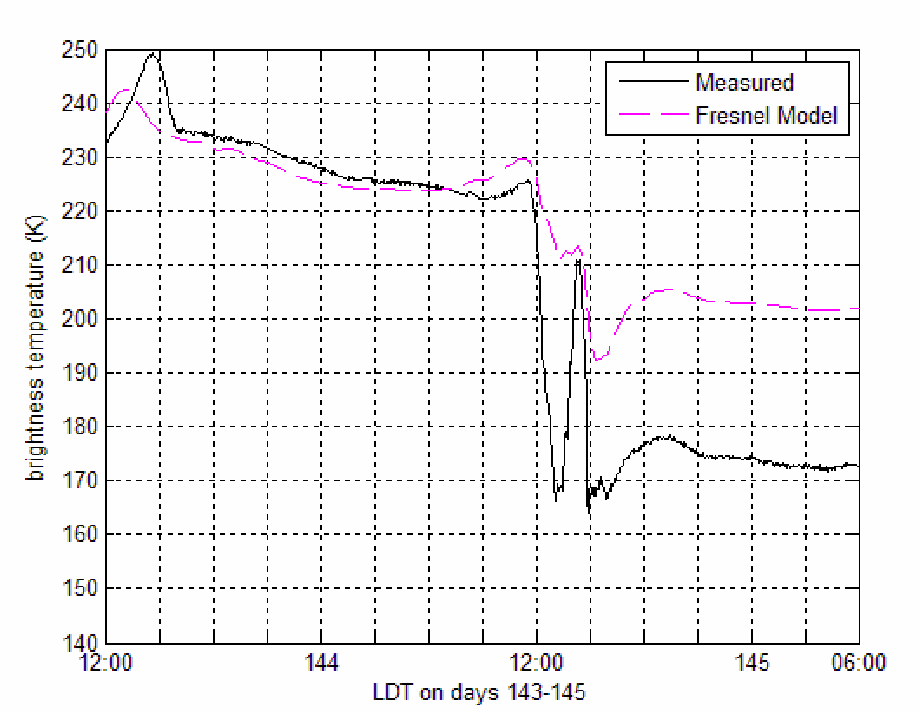

**Figure 4. Fresnel model result without including the ponding event.**

Before we apply the average soil temperature to the transmission line model, it is necessary to verify the agreement between the soil temperature profile and the average temperature of the first 10 cm of the soil, which are both produced by ALEX, in terms of the reproduced brightness temperature: We run the Njoku-Kong model for both temperature inputs when ponding effect is not included. Figure 5 shows the measured and the modeled brightness temperatures for $K_{sat}$=5x$10^{-6}$ kg s $m^{-3}$ with a standard deviation of surface height of 1.5 cm. Both inputs return close brightness temperature values and the error between the two results is negligible for day 144, where the ponding effect is of interest. The large difference between the measured and the modeled brightness temperatures after 15:00 pm on day 144 is because a roughness correction is not yet performed after the rain events.

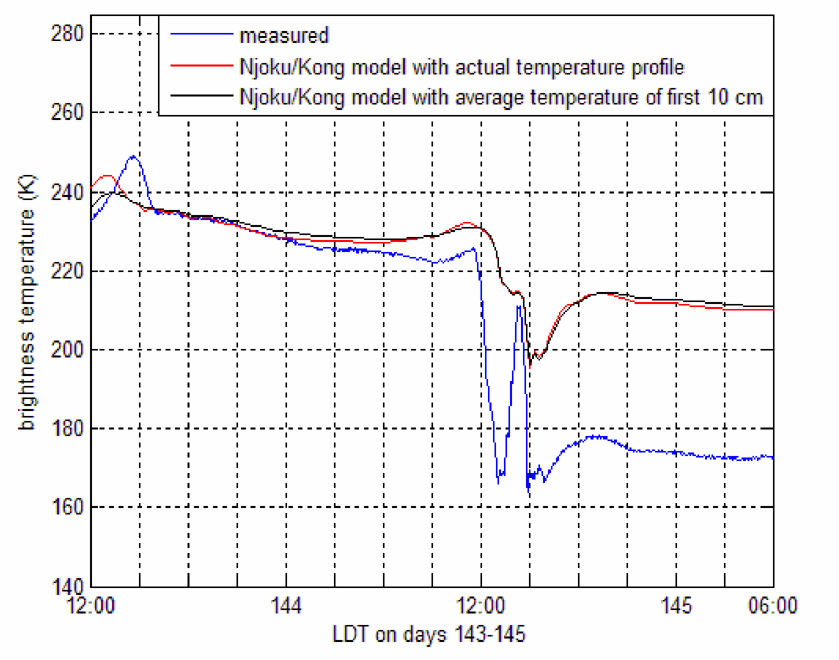

**Figure 5. Measurede and the modeled brightness temperatures: Modeling is performed by Njoku-Kong model with the average temperature of the first 10 cm of soil, and with the actual temperature profile. No ponding and roughness correction are included.**

We include a water thickness of 0.33 cm and 0.50 cm between air and soil to model the ponding effect for 13:21 pm and 15:00 pm on day 144 respectively, where two local minimums occur after two large decreases in the brightness temperature. 13:21 pm is the last time of a set of rain events before the largest amount of precipitation (4.57 mm) is recorded at 15:00 pm. The water layer depths are hypothetical values that are determined by investigating the precipitation pattern, soil properties, and the amount of decrease in the brightness temperature.

To compute the coherent emissivity for each air-water-soil case, the coherent emissivity of each air-soil system without the ponding effect is first calculated. The reflection coefficient for the air-soil boundary is computed. An ‘effective’ relative dielectric constant for the soil is extracted through the real angle of refraction equations since the soil is lossy, and is used as the relative soil permittivity in the three layer air-water-soil system. The equations to extract the effective relative dielectric constant of soil are

$$\Gamma = \frac{n_1\mu_1 - n_2\mu_2}{n_1\mu_1 + n_2\mu_2} \tag{1}$$

$$\tan \mathrm{X} = \frac{2\alpha\beta}{\beta^2 - \alpha^2 - k_1^2 \sin^2\theta_1} \tag{2}$$

where Γ is the reflection coefficient, *n* is the refraction index, μ is the direction cosine, X is the real angle of refraction for soil medium, $\beta$ is the phase constant for soil medium, $\alpha$ is the attenuation constant for soil medium, $k_1$ is the propagation constant for air medium, and $\theta_1$ is the incidence angle for air medium.

The coherent emissivity and the brightness temperature of the three-layer configuration is then computed. Figure 6 illustrates the modeled brightness temperature versus water layer depth for 15:00 pm on day 144. The incidence angle is 35° and the relative dielectric constant of the water is 79.6−j3.1, simulating the properties of water with a salinity of 2 ppt [10]. Note how the emissivity changes significantly as the depth of the water layer increases. This effect is caused by the coherent nature of the emitted radiation. The depths at which the emissivity changes are related to the wavelength of the 1.4 GHz radiation in water such that the distance between two successive maxima (or minima) is equal to $\lambda_2/2$, where $\lambda_2$ is the wavelength in water, which is related to the free-space wavelength $\lambda_0$ as

$$\lambda_2 = \frac{\lambda_0}{\sqrt{\mathrm{Re}\,al(\varepsilon_{rwater})}} \tag{3}$$

where $\varepsilon_{rwater}$ is the relative dielectric constant of water. In our case $\lambda_0$=21 cm. and

$$\lambda_2 = \frac{21}{\sqrt{79}} = 2.36 \text{ cm} \tag{4}$$

Hence, the distance between two successive maxima (or minima) is 2.36/2=1.18 cm.

Table 1 lists the depth ($d_{water}$) of 2 ppt water, average temperature of the first 10 cm of soil ($T_s$), efficient relative permittivity of soil, and the brightness temperature that is produced by the transmission line model ($T_b$) for the two time steps that take into account the ponding event. For all other time steps, the ponding effect is not included. The standard deviation of surface height is 1.5 cm until and including 15:00 pm on day 144, then it is lowered to 0.8 cm since the soil becomes smoother after the rain event. Figure 67, Figure 8, and Figure 9 show the measured and the modeled brightness temperatures for $\alpha$=0.6, $\alpha$=0.7 and $\alpha$=0.8, respectively.

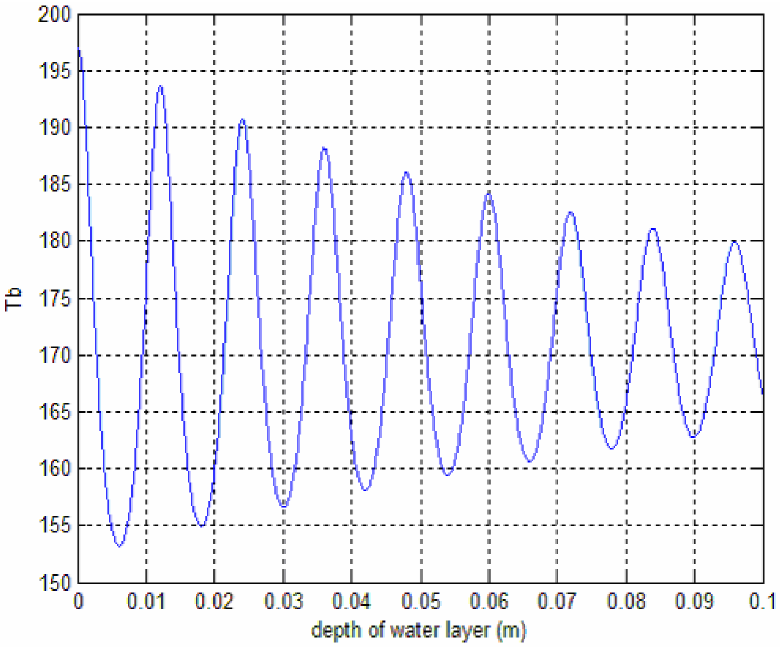

**Figure 6. Modeled brightness temperature through the transmission line model as a function of water depth for 15:00 pm on day 144.**

**Table 1. Parameters used in the transmission line model to model ponding: Water depth ($d_{water}$) , efficient relative dielectric constant of soil ($\varepsilon_r$), average temperature of the first 10 cm of soil ($T_s$), and modeled brightness temperature ($T_b$).**

| | 13:21 pm (Day 144) | 15:00 pm (Day 144) |
|---|---|---|
| $d_{water}$ [cm] | 0.33 | 0.50 |
| $\varepsilon_r$ | 16.48-j6.74 | 29.14-j2.87 |
| $T_s$ [K] | 290.48 | 290.53 |
| $T_b$ [K] | 162.00 | 154.80 |

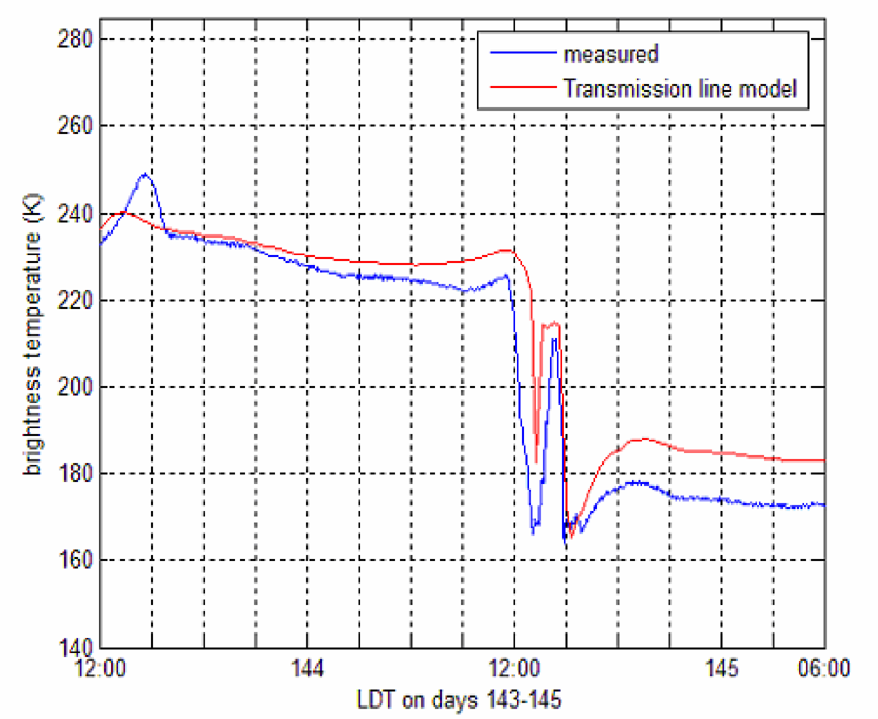

Figure 7. Modeled brightness temperature through the transmission line model. Ponding and roughness correction are included. $\alpha$=0.6.

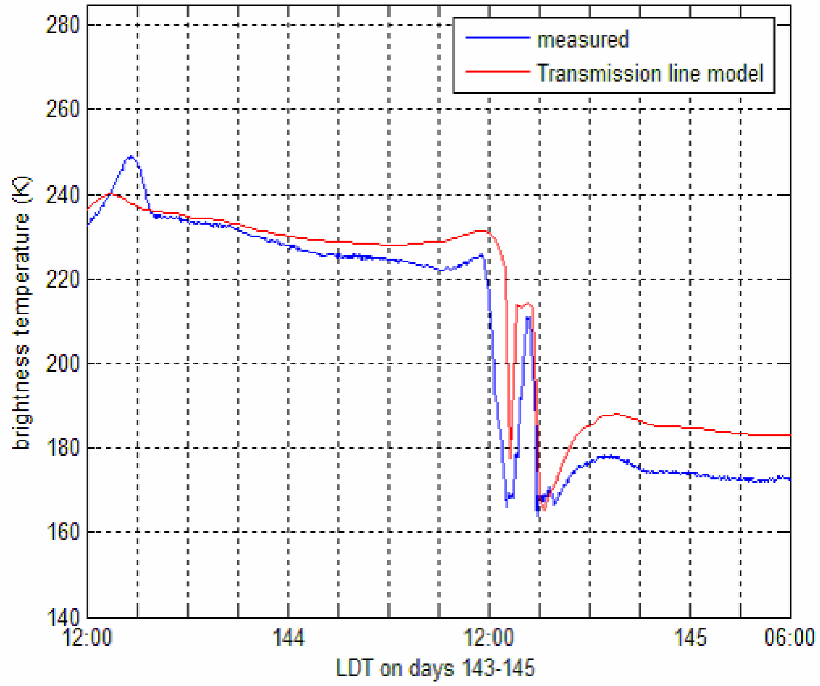

Figure 8. Modeled brightness temperature through the transmission line model. Ponding and roughness correction are included. $\alpha$=0.7.

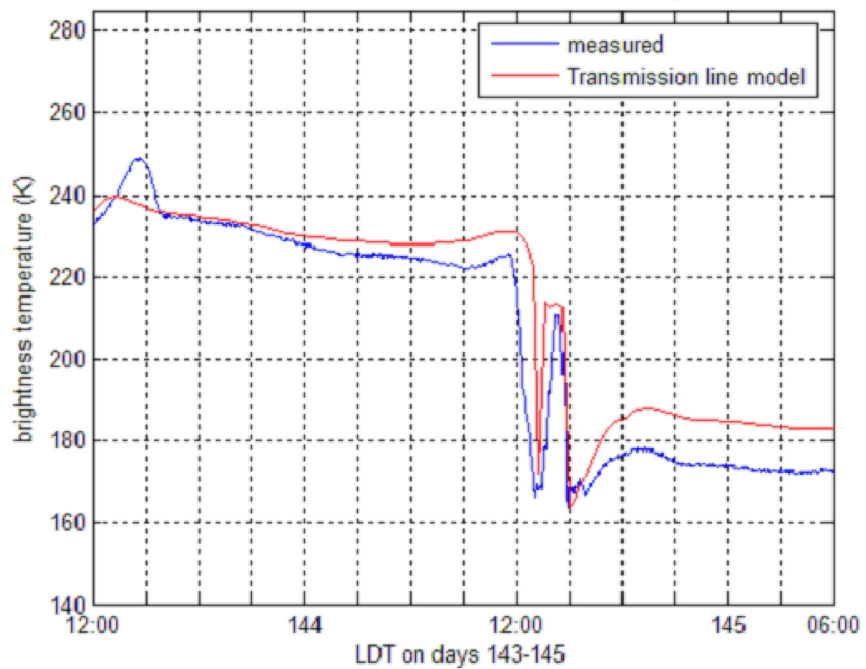

**Figure 9. Modeled brightness temperature through the transmission line model. Ponding and roughness correction are included.$\alpha$=0.8.**

For all $\alpha$ values, there is a close agreement between transmission line model result and the measured brightness temperatures. The model follows the two sharp decreases in the brightness temperature at 13:21 pm and 15:00 pm on day 144, by taking into account two ponding events. As $\alpha$ increases, the decrease in the brightness temperature for these two time steps becomes more noticeable since the total ponded area in the field increases.

The same analysis is performed for the incoherent model that was developed by Burke. Figure 10 illustrates the brightness temperature as a function of the 2 ppt water depth for 15:00 pm on day 144 respectively.

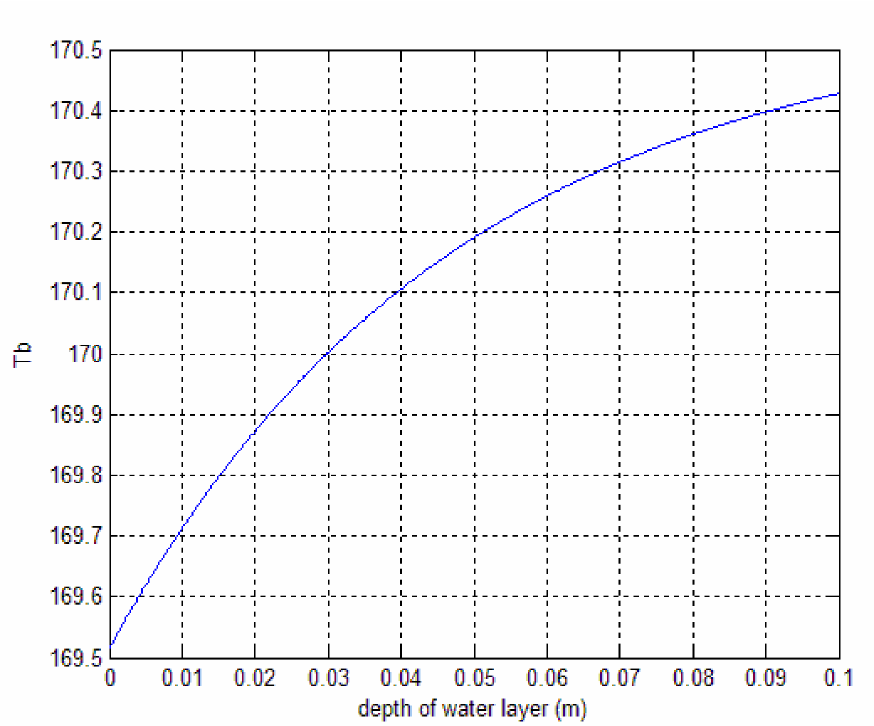

**Figure 10. Modeled brightness temperature through the incoherent model for 15:00 pm on day 144.**

Table 2 shows the 2 ppt water depth ($d_{water}$), soil surface temperature ($T_s$), efficient relative permittivity of soil, and the brightness temperature that is returned by the incoherent model ($T_b$) for the two time steps that take into account the ponding event.

**Table 2. Parameters used in the incoherent model to model ponding: Water depth ($d_{water}$) , efficient relative dielectric constant of soil ($\varepsilon_r$), average temperature of the first 10 cm of soil ($T_s$), and modeled brightness temperature ($T_b$).**

| | 13:21 pm (Day 144) | 15:00 pm (Day 144) |
|---|---|---|
| $d_{water}$ [cm] | 0.33 | 0.50 |
| $\varepsilon_r$ | 16.48-j6.74 | 29.14-j2.87 |
| $T_s$ [K] | 289.78 | 289.67 |
| $T_b$ [K] | 168.30 | 169.60 |

Figure 11, Figure 12, and Figure 13 show the measured and the modeled brightness temperatures for α=0.6, α=0.7 and α=0.8, respectively.

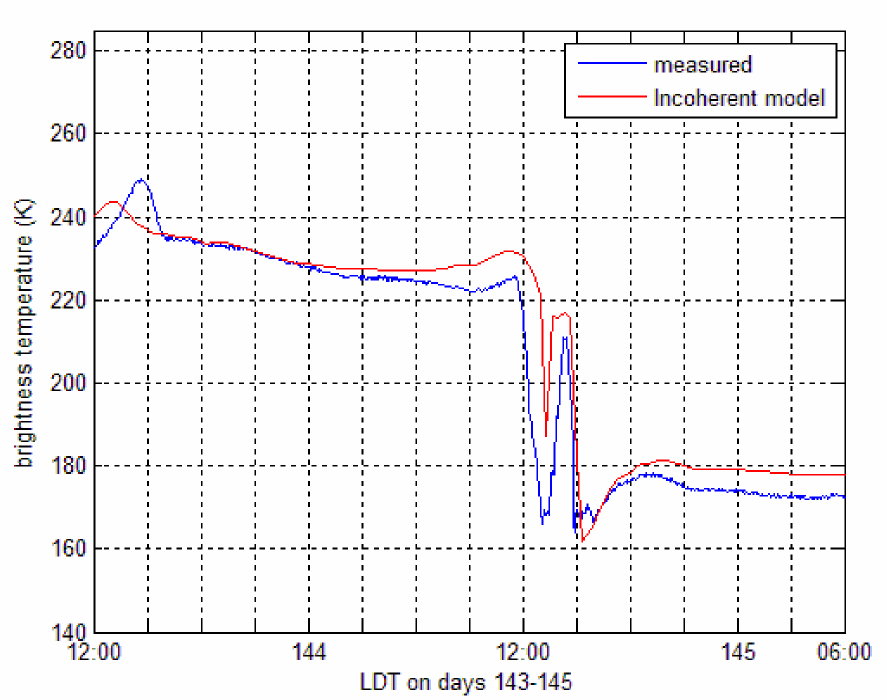

**Figure 11. Modeled brightness temperature through the incoherent model. Ponding and roughness correction are included. α=0.6.**

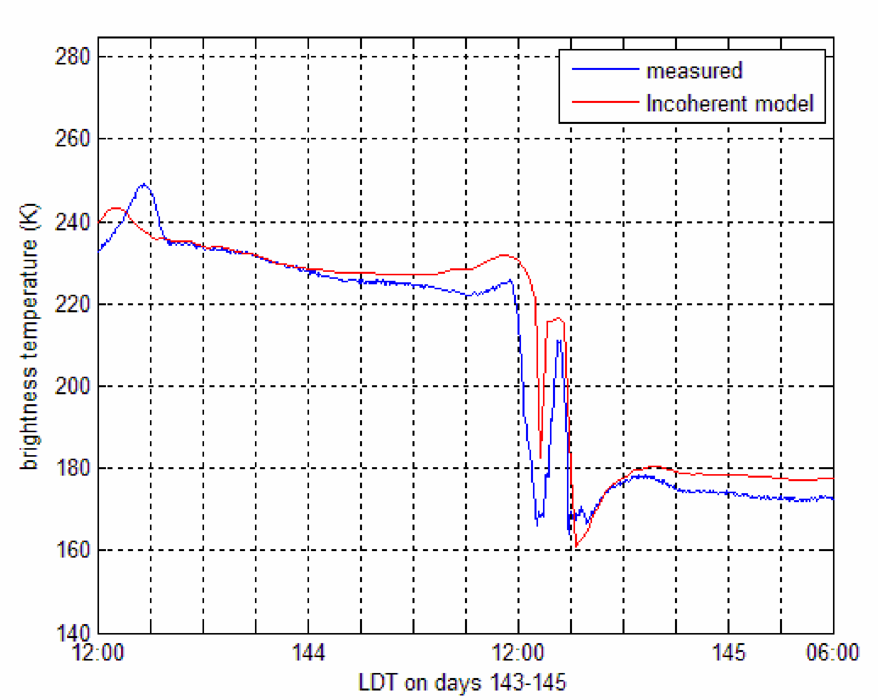

**Figure 12. Modeled brightness temperature through the incoherent model. Ponding and roughness correction are included. α=0.7.**

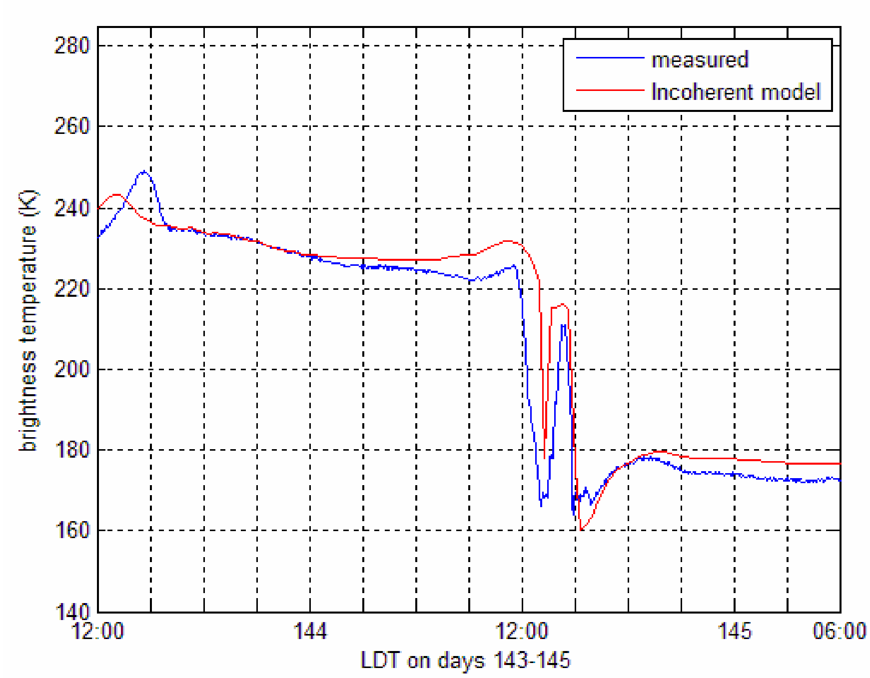

**Figure 13. Modeled brightness temperature through the inocherent model. Ponding and roughness correction are included. α=0.8.**

## 4.4 Error Analysis

We carry out an error analysis in order to determine the relative error between the measured brightness temperature, and the models applied. We perform the error analysis for the transmission line model and the incoherent model, which are capable of modeling a ponding event. The relative error $\delta T_b$ represents the difference between the measured and the modeled brightness temperatures relative to the measured brightness temperature.

$$\delta T_b = \frac{T_{bmeasured} - T_{b\,\mathrm{mod}\,eled}}{T_{bmeasured}} \tag{5}$$

The relative errors for the transmission line model and the incoherent model for α=0.6 are plotted in Figure 14.

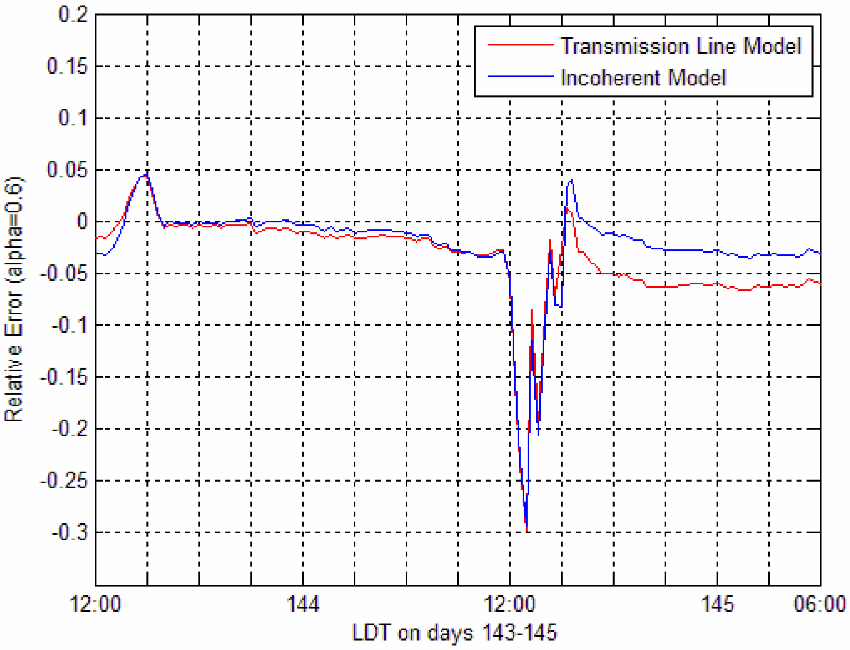

**Figure 14. Relative error variation for the transmission line and the incoherent model with α=0.6.**

It is clear that the relative error varies diurnally. The absolute value of the relative error reaches a maximum because of the assumption that the ponding occurs only at two time steps, and no other time step takes into account the ponding event. In fact, ponding might have a transitional variation, which means it might occur at other time steps also. The amount of ponding might be different at other time steps.

Another measure of the error is the root mean square error (rmse), which is defined as

$$rmse=\sqrt{\frac{\left(T_{bmeasured}(1)-T_{b\mathrm{modeled}}(1)\right)^{2}+\left(T_{bmeasured}(2)-T_{b\mathrm{modeled}}(2)\right)^{2}+\ldots+\left(T_{bmeasured}(N)-T_{b\mathrm{modeled}}(N)\right)^{2}}{N}} \qquad (6)$$

The root mean square error for the transmission line model with $\alpha$=0.6 is 9.4748 K, while the mean square error for the incoherent model with $\alpha$=0.6 is 9.1366 K. While the root mean square errors are close, it is lower for the incoherent model.

## 4.5 Conclusion

Two ponding events and their effects on the brightness temperature variation are investigated. Fresnel model, which assumes a uniform soil moisture profile and a uniform soil temperature profile is applied. It is verified that the Fresnel model cannot model a ponding event. Then, the transmission line model with the average temperature of the first 10 cm of soil, and the incoherent model are applied and the ponding event is modeled. Error analysis is also provided. Relative error and the root mean square error results show that the relative error vary diurnally, and the root mean square error of the incoherent model is lower.

# BIBLIOGRAPHY

[1] Schmugge, T. J., Gloersen, P., Wilheit, T., Geiger, F. (1974). Remote sensing of soil moisture with microwave radiometers. *Journal of Geophysical Research*. 79. pp. 317–323.

[2] Koster, R. D., Suarez, M. J., Higgins, R. W., Van den Dool, H. M. (2003). Observational evidence that soil moisture variations affect precipitation. *Geophysical Research Letters.* 30(5). p. 1241.

[3] Kerr, Y. H., Waldteufel, P., Wigneron, J. P., Martinuzzi, J. M., Font, J., Berger, M. (2001). Soil moisture retrieval from space: The soil moisture and ocean salinity (SMOS) mission. *IEEE Transactions on Geoscience and Remote Sensing*. 39(8). pp. 1729–1735.

[4] Njoku, E. G., Entekhabi, D. (1996). Passive microwave remote sensing of soil moisture. *Journal of Hydrology*. 184. pp. 101–129.

[5] Hornbuckle, B. K., England, A. W. (2004). Radiometric sensitivity to soil moisture at 1.4 GHz through a corn crop at maximum biomass. *Water Resour. Res.*40.

[6] Jackson, T. J., Schmugge, T. J. (1989). Passive microwave remote sensing system for soil moisture: Some supporting research. *IEEE Transactions on Geoscience and Remote Sensing*. 27. pp. 225–235.

[7] Hornbuckle, B. K., England, A. W., De Roo, R. D., Fischman, M. A., Boprie, D. L. (2003). Vegetation canopy anisotropy at 1.4 GHz. *IEEE Transactions on Geoscience and Remote Sensing*. 41(10). pp. 2211–2223.

[8] Hornbuckle, B. K., England, A. W., Anderson, M. C., Viner, B. J. (2006). The effect of free water in a maize canopy on microwave emission at 1.4 GHz. *Agric. For. Meteorol.* 138(1-4). pp. 180–191.

[9] Anderson, M. C., Norman, J. M., Meyers, T. P., Diak, G. D. (2000). An analytical model for estimating canopy transpiration and carbon assimilations fluxes based on canopy light–use efficiency. *Agric. For. Meteorol.* 101. pp. 265–289.

[10] Stogryn A. (1971). Equations for calculating the dielectric constant of saline water. *IEEE Transactions on Microwave Theory and Techniques.* pp.733-736.

# CHAPTER 5. SUMMARY AND DISCUSSION

This chapter highlights the contribution that this dissertation provides to the microwave remote sensing community. Several unique investigations are performed and results are presented in this study. A list of these investigations is as follows.

- World’ s first truly ground-based system is introduced. The Iowa State University Direct Sampling Digital Radiometer (DSDR) is described. Components of the DSDR are explained. Noise characterization of devices, and other types of radiometers are also presented.
- Modifications to the incoherent model and the coherent model are made. Semi-infinite layer effect is included in the incoherent model equations. It is shown that the semi-infinite layer effect could be significant in reflectivity (therefore brightness temperature) computations. A FORTRAN subroutine for the coherent model is modified for the air-water-soil test case so that the agreement between the radiative transfer models could be performed.
- An abrupt change in a time-varying brightness temperature measurement is analyzed. The data were collected in Michigan in 2001. Through the application of the two radiative transfer models, the incoherent model and the transmission line model, it is concluded that the reason for the abrupt change in the brightness temperature is ponding.
- An error analysis is carried out. Relative error as well as the root mean square error results are presented. The root mean square error of the incoherent model is found to

be slightly smaller than that of the transmission line model. Through the error analysis, it is verified that the relative error varies diurnally, and a negative peak occurs in the relative error plot. The negative peak is thought to be because of the transitional nature of ponding, while ponding is modeled in two discrete time steps in our case.

- A MATLAB tool is created in order to run all the radiative transfer models in one main program. There are several flags in the program to choose a radiative transfer model, a dielectric mixing model, a soil surface roughness model, and a plot option. It is possible to combine different options to produce the brightness temperature for a specular surface, and the brightness temperature for a rough surface. The program is written such that future contribution for different models/options could be done.

This work could be a starting point for the determination of an optimal overpass time for future satellite missions. There is still an uncertainty in the optimal overpass time, and current overpass times are not based on a rigorous analyses. Satellite overpass time is an important consideration if the most accurate soil moisture estimation is to be made. Microwave emission from a soil/vegetation system is largely affected by the diurnal variations such as soil/vegetation temperature and soil moisture changes as well as the vegetation water content and the presence of dew and intercepted precipitation. In order to estimate an optimal overpass time, it is advantageous to consider every parameter so that it will be possible to analyze constructive and destructive effects of simultaneous changes. By determining the minimum error ranges in the diurnal error variation for long periods of time, it might be possible to estimate an accurate satellite overpass time.

This is a small-scale analysis for bare soil. Future work might include a larger scale analysis and/or an investigation with vegetation. Furthermore, validation of the future satellite observations could be performed.

# APPENDIX A.  SEMI-INFINITE LAYER CONTRIBUTION

Total energy received at the bottom of a boundary i (denoted by $i^-$) due to emission by all strata in layer i is given as [1]

$$T_s(i) = T_i\left(1-\frac{1}{L_i}\right)$$

(1)

where $T_i$ is the physical temperature of layer i, and $L_i$ is the power loss factor. For a two-layer system, the geometry is shown in Figure 1.

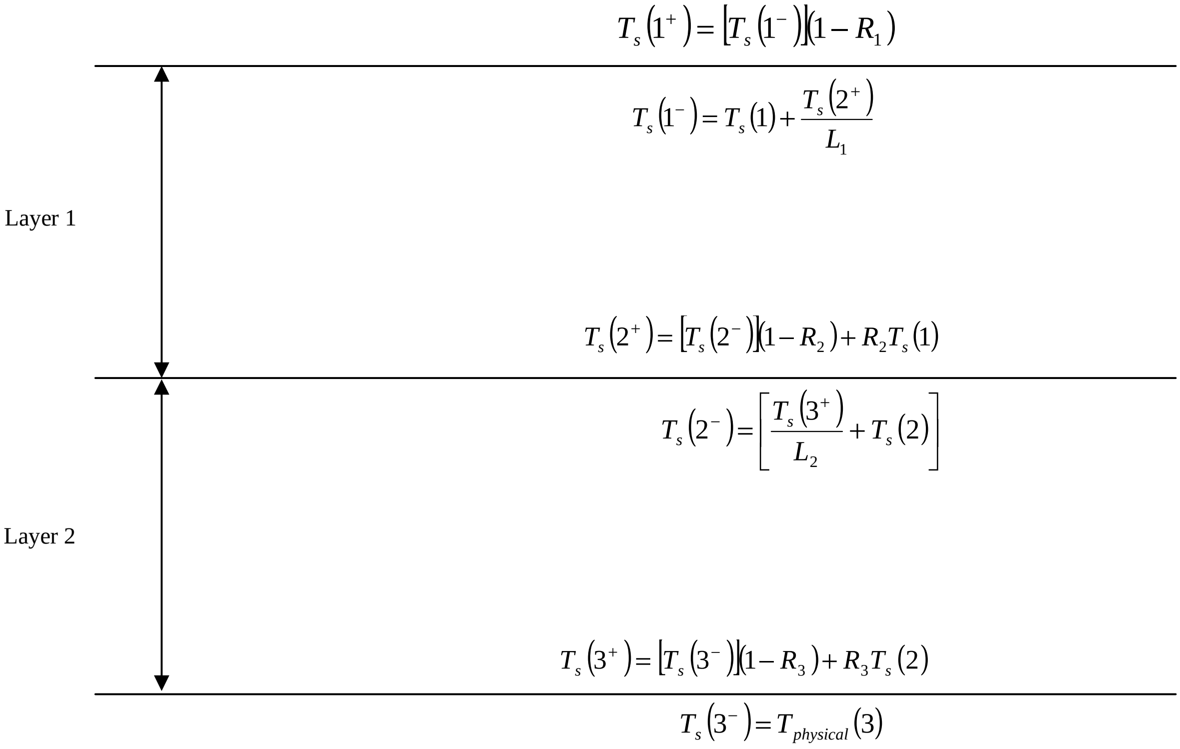

**Figure 1.  A two-layer system geometry.**

Rearranging the equations in Figure 1, we obtain

$$T_s\left(1^+\right) = \left[T_s\left(1^-\right)\right]\left(1 - R_1\right) \tag{2}$$

$$T_s\left(1^-\right) = T_s(1) + \frac{T_s\left(2^+\right)}{L_1} \tag{3}$$

$$T_s\left(2^+\right) = \left[T_s\left(2^-\right)\right]\left(1 - R_2\right) + R_2 T_s(1) \tag{4}$$

$$T_s\left(2^-\right) = \left[\frac{T_s\left(3^+\right)}{L_2} + T_s(2)\right] \tag{5}$$

$$T_s\left(3^+\right) = \left[T_s\left(3^-\right)\right]\left(1 - R_3\right) + R_3 T_s(2) \tag{6}$$

$$T_s\left(3^-\right) = T_{physical}(3) \tag{7}$$

Using Equation (7) in Equation (6)

$$T_s\left(3^+\right) = \left[T_{physical}(3)\right]\left(1 - R_3\right) + R_3 T_s(2) \tag{8}$$

Using Equation (8) in Equation (5)

$$T_s\left(2^-\right) = \frac{T_{physical}(3)\left(1 - R_3\right) + R_3 T_s(2)}{L_2} + T_s(2) \tag{9}$$

Using Equation (9) in Equation (4)

$$\left(\frac{T_{physical}(3)\left(1 - R_3\right) + R_3 T_s(2)}{L_2} + T_s(2)\right)\left(1 - R_2\right) + R_2 T_s(1) \tag{10}$$

Using Equation (10) in Equation (3)

$$T_s\left(1^-\right) = T_s(1) + \frac{1}{L_1}\left[\left(\frac{T_{physical}(3)\left(1 - R_3\right) + R_3 T_s(2)}{L_2} + T_s(2)\right)\left(1 - R_2\right) + R_2 T_s(1)\right] \tag{11}$$

Using Equation (11) in Equation (2)

$$T_s\left(1^+\right)=\left(1-R_1\right)\left[T_s\left(1\right)+\frac{1}{L_1}\left[\left(\frac{T_{physical}\left(3\right)\left(1-R_3\right)+R_3T_s\left(2\right)}{L_2}+T_s\left(2\right)\right)\left(1-R_2\right)+R_2T_s\left(1\right)\right]\right] \quad (12)$$

Rearranging Equation (12)

$$T_s\left(1^+\right)=T_s\left(1\right)\left(1+\frac{R_2}{L_1}\right)\left(1-R_1\right)+T_s\left(2\right)\left(1+\frac{R_3}{L_2}\right)\left(\frac{\left(1-R_1\right)\left(1-R_2\right)}{L_1}\right)+T_{physical}\left(3\right)\frac{\left(1-R_1\right)\left(1-R_2\right)\left(1-R_3\right)}{L_1L_2} \quad (13)$$

The last term in Equation (13) is neglected in Burke approach. Following a similar approach, $T_s(1^+)$ expression can be calculated for a three layer system.

$$\begin{aligned}T_s\left(1^+\right)=&T_s\left(1\right)\left(1+\frac{R_2}{L_1}\right)\left(1-R_1\right)+T_s\left(2\right)\left(1+\frac{R_3}{L_2}\right)\left(\frac{\left(1-R_1\right)\left(1-R_2\right)}{L_1}\right)+T_s\left(3\right)\left(1+\frac{R_4}{L_3}\right)\frac{\left(1-R_1\right)\left(1-R_2\right)\left(1-R_3\right)}{L_1L_2}\\&+T_{physical}\left(4\right)\frac{\left(1-R_1\right)\left(1-R_2\right)\left(1-R_3\right)\left(1-R_4\right)}{L_1L_2L_3}\end{aligned} \quad (14)$$

Again, the last term in Equation (14) is neglected in Burke approach.

For an N-layer system

$$\begin{aligned}T_B\left(1^+,\theta\right)=&T_s\left(1\right)\left(1+\frac{R_2}{L_1}\right)\left(1-R_1\right)+T_s\left(2\right)\left(1+\frac{R_3}{L_2}\right)\left(\frac{\left(1-R_1\right)\left(1-R_2\right)}{L_1}\right)+\ldots\ldots\ldots\ldots\ldots\\&+T_s\left(N\right)\left(1+\frac{R_{N+1}}{L_N}\right)\left(\frac{\left(1-R_1\right)\left(1-R_2\right)\ldots\ldots\left(1-R_N\right)}{L_1L_2\ldots\ldots L_{N-1}}\right)\\&+T_s\left(N+1\right)\frac{\left(1-R_1\right)\left(1-R_2\right)\left(1-R_3\right)\left(1-R_4\right)\ldots\ldots\left(1-R_N\right)}{L_1L_2L_3\ldots\ldots L_{N-1}}\frac{\left(1-R_{N+1}\right)}{L_N}\end{aligned} \quad (15)$$

The last term in Equation (15) is ignored in Burke approach. We call the neglected part as the *semi-infinite layer effect* because the layer number points to the layer that follows the last layer that is considered in Burke approach.

# BIBLIOGRAPHY

[1] Ulaby, F. T., Moore, R. K., Fung A. K. (1981). *Microwave Remote Sensing: Active and Passive*. Reading: Addison-Wesley.

# APPENDIX B. PROGRAMMING CODES

**Main program for the incoherent model:**

```
clear all

format long

N=91; %no of air layer + soil layers

M=1; %number of time steps

freq=1.4*10^9;                    %frequemcy in Hz

step = (min(1.0,1./freq))*(10^7);   %layer thickness in [m]

p=2;                              %(p=1 --> v-pol, p=2 --> h-pol)

theta_deg=35;                     %observation angle in degrees

 er = [1.00000000000000 + 0.00000000000000i;11.0787960000000 -
2.15701100000000i;11.0760170000000 - 2.15901500000000i;11.1003010000000 -
2.16486900000000i;11.2037190000000 - 2.18203700000000i;12.8172440000000 -
2.41775100000000i;13.3847310000000 - 2.50262500000000i;13.4111470000000 -
2.50728600000000i;13.4077440000000 - 2.50733700000000i;13.4128620000000 -
2.50857200000000i;13.4104470000000 - 2.50860800000000i;13.4082790000000 -
2.50864100000000i;13.4068560000000 - 2.50866200000000i;13.4251880000000 -
2.51157400000000i;13.4529810000000 - 2.51584400000000i;13.4687810000000 -
2.51842100000000i;13.4779480000000 - 2.51997200000000i;13.4816210000000 -
2.52066700000000i;13.4809970000000 - 2.52067700000000i;13.4803730000000 -
2.52068600000000i;13.4797490000000 - 2.52069600000000i;13.4791240000000 -
2.52070500000000i;13.4784990000000 - 2.52071400000000i;13.4780620000000 -
2.52072100000000i;13.4776870000000 - 2.52072600000000i;13.4770630000000 -
```

2.52073600000000i;13.4766880000000 - 2.52074100000000i;13.4763760000000 - 2.52074600000000i;13.4760640000000 - 2.52075100000000i;13.5265360000000 - 2.52844300000000i;13.5499420000000 - 2.53203600000000i;13.5541690000000 - 2.53272400000000i;13.5538540000000 - 2.53272800000000i;13.5944110000000 - 2.53889000000000i;13.6247490000000 - 2.54351100000000i;13.6244330000000 - 2.54351600000000i;13.6297930000000 - 2.54437700000000i;13.6317460000000 - 2.54472400000000i;13.6314290000000 - 2.54472900000000i;13.6311120000000 - 2.54473300000000i;13.6310480000000 - 2.54473400000000i;13.6309210000000 - 2.54473600000000i;13.6306050000000 - 2.54474100000000i;13.6445790000000 - 2.54689200000000i;13.6585530000000 - 2.54904300000000i;13.6725280000000 - 2.55119400000000i;13.6865020000000 - 2.55334500000000i;13.7004760000000 - 2.55549700000000i;13.7144500000000 - 2.55764800000000i;13.7284250000000 - 2.55979900000000i;13.7423990000000 - 2.56195000000000i;13.7563730000000 - 2.56410100000000i;13.7703480000000 - 2.56625300000000i;13.7843220000000 - 2.56840400000000i;13.7982960000000 - 2.57055500000000i;13.8122700000000 - 2.57270600000000i;13.8262440000000 - 2.57485700000000i;13.8402190000000 - 2.57700800000000i;13.8541930000000 - 2.57916000000000i;13.8681670000000 - 2.58131100000000i;13.8821420000000 - 2.58346200000000i;13.8961160000000 - 2.58561300000000i;13.9100900000000 - 2.58776500000000i;13.9240650000000 - 2.58991600000000i;13.9380390000000 - 2.59206700000000i;13.9520130000000 - 2.59421800000000i;13.9659870000000 - 2.59636900000000i;13.9799620000000 - 2.59852100000000i;13.9939370000000 - 2.60067200000000i;14.0079110000000 - 2.60282300000000i;14.0218850000000 - 2.60497400000000i;14.0315150000000 -

```
2.60647000000000i;14.0411440000000 - 2.60796500000000i;14.0507750000000 -
2.60946100000000i;14.0604050000000 - 2.61095600000000i;14.0700350000000 -
2.61245200000000i;14.0796640000000 - 2.61394700000000i;14.0892940000000 -
2.61544300000000i;14.0989250000000 - 2.61693800000000i;14.1085550000000 -
2.61843400000000i;14.1181840000000 - 2.61992900000000i;14.1278130000000 -
2.62142500000000i;14.1374440000000 - 2.62292100000000i;14.1470740000000 -
2.62441600000000i;14.1567040000000 - 2.62591100000000i;14.1663340000000 -
2.62740700000000i;14.1759630000000 - 2.62890300000000i;14.1855940000000 -
2.63039800000000i;14.1952240000000 - 2.63189400000000i;14.2048540000000 -
2.63338900000000i;14.2144830000000 - 2.63488500000000i];
             %first er is the er of air
            tsoil =
[290.831431000000;288.299994000000;288.542870000000;289.032865000000;289.392859
000000;289.507147000000;289.738589000000;289.912875000000;290.030005000000;290.
072861000000;290.161444000000;290.225724000000;290.254300000000;290.3014380000
00;290.335713000000;290.350012000000;290.378590000000;290.402878000000;290.4228
75000000;290.437153000000;290.451432000000;290.465718000000;290.480017000000;29
0.494296000000;290.504296000000;290.512871000000;290.527150000000;290.535725000
000;290.542866000000;290.549994000000;290.564293000000;290.574290000000;290.581
423000000;290.588572000000;290.595723000000;290.602864000000;290.609991000000;2
90.617142000000;290.624291000000;290.631441000000;290.638590000000;290.64002100
0000;290.642872000000;290.650000000000;290.654642000000;290.659285000000;290.66
3929000000;290.668572000000;290.673214000000;290.677859000000;290.682501000000;
```

```
290.687144000000;290.691788000000;290.696431000000;290.701073000000;290.7057160
00000;290.710360000000;290.715002000000;290.719645000000;290.724287000000;290.7
28932000000;290.733574000000;290.738217000000;290.742861000000;290.74750400000
0;290.752146000000;290.756789000000;290.761433000000;290.766076000000;290.77072
0000000;290.775362000000;290.780005000000;290.782576000000;290.785147000000;290
.787720000000;290.790291000000;290.792862000000;290.795433000000;290.7980050000
00;290.800576000000;290.803147000000;290.805718000000;290.808289000000;290.8108
60000000;290.813431000000;290.816004000000;290.818575000000;290.821146000000;29
0.823717000000;290.826289000000;290.828860000000];
          %first tsoil is arbitrary  -- temperature of air
         [tbh_vector] =
Burke_Njoku_michigan_actualtemp_loop_seminf_unix_cor_defense(er,tsoil,N,M,step,theta_
deg,freq,p); %tbh_vector: first column is the Tb for a specular surface
              %just above air-soil interface
             %tbh_vector: second column is the Tb for a specular surface
            %just below air_soil interface
```

**Subroutine for the incoherent model:**

```
        function [tbh_vector] =
Burke_Njoku_michigan_actualtemp_loop_seminf_unix_cor_defense(er,tsoil,N,M,step,theta_
deg,freq,p)
        j=sqrt(-1);
        mu1=cosd(theta_deg);  %direction cosine for the incidence angle
```

```
        mu0=4*pi*10^-7;       %free space permeability
        eps0=8.854*10^-12;    %free space permittivity
        c=1/sqrt(mu0*eps0);   %speed of light
        lambda0=c/freq;       %free space wavelength
         mur=1
          for i=1:N
             for k=1:M
             alpha(i,k)=(2*pi/lambda0)*abs(imag(sqrt(er(i,k))));  %attenuation constant
             end
          end
            for k=1:M
               for i=1:N-1
               er_first(i,k)=er(i,k);
               er_second(i,k)=er(i+1,k);
[mu2(i,k),gamma(i,k),R(i,k)]=trb_cihan_for_incoherent(mu1,er_first(i,k),er_second(i,k),p,fre
q); %compute mu2, gamma (reflection coefficient) and R (reflectivity)
               mu1=mu2(i,k);
              end
               mu1=cosd(theta_deg);
            end
            for k=1:M
                mu(1,k)=cosd(theta_deg);
            end
```

```
     for i=2:N
       for k=1:M
          mu(i,k)=mu2(i-1,k);
       end
    end
  %-------------------
      for i=1:N
       for k=1:M
       L(i,k)=exp(2*alpha(i,k)*step/mu(i,k)); %power loss factor
       factor(i,k)=(1-1/L(i,k));    % a multiplier
       end
    end
%--------------------
    for i=1:N-1
       for k=1:M
       factornew(i,k)=factor(i+1,k);     %air is now excluded
       Lnew(i,k)=L(i+1,k);              %air is now excluded
       end
    end


 %--------------------
 for i=1:N-1
    for k=1:M
```

```
        Ts(i,k)=tsoil(i+1,k)*factornew(i,k);
        end
    end
  %-------------------
   for k=1:M
        multip_term(1,k) = (1-R(1,k)); %another multiplier
    end
    for i=2:N-1
        for k=1:M
        multip_term(i,k) = multip_term(i-1,k)*(1-R(i,k))/Lnew(i-1,k);
        end
    end
   %-------------Layer contribution---(Burke's equation)---------------
    for k=1:M
       Tb(1,k) = Ts(1,k)*(1+R(2,k)/Lnew(1,k))*multip_term(1,k); %layer contribution
for the brightness temperature (no semi-infinite yet)
    end
      for i=2:N-2
         for k=1:M
          Tb(i,k) = Tb(i-1,k) + (Ts(i,k))*(1+(R(i+1,k)/Lnew(i,k)))*multip_term(i,k);
         end
      end
```

```
              %---------- Semi-infinite layer contribution----------------------
                 for k=1:M
                     seminf_term(1,k) = (1-R(2,k))*(1-R(1,k))/Lnew(1,k);
                     seminf_tb(1,k) = tsoil(2,k)*seminf_term(1,k);
                 end
                for k=1:M
                    for i=2:N-2
                        seminf_term(i,k) = seminf_term(i-1,k)*(1-R(i+1,k))/Lnew(i,k);
                        seminf_tb(i,k) = tsoil(i+1,k)*seminf_term(i,k);
                    end
                end
                 %------------------------------------------------------------
                for k=1:M
                    tbh(k) = Tb(N-2,k) + seminf_tb(N-2,k);   %brightness temperature of the
specular surface above air-soil interface (layer contribution + semi-infinite layer
contribution)
                end
    tbh_below = tbh /(1-R(1));   %brightness temperature of the specular surface just below
air-soil interface (layer contribution + semi-infinite layer contribution)

                tbh_vector = [tbh tbh_below]; %a vector that includes tbh and tbh_below that are
described above
```

**Main program for the transmission line model:**

```
clear all

format long


N=91; %no of air layer + soil layers

M=1; %number of time steps

freq=1.4*10^9;                    %frequemcy in Hz

step = (min(1.0,1./freq))*(10^7);   %layer thickness in [m]

p=2;                             %(p=1 --> v-pol, p=2 --> h-pol)

theta_deg=35;


ts = [289.683838000000];  %average soil temperature

er = [1.00000000000000 + 0.00000000000000i;12.2572870000000 -
2.20867900000000i;12.2666100000000 - 2.21047600000000i;12.2843060000000 -
2.21620500000000i;12.3133990000000 - 2.23340500000000i;13.9172920000000 -
2.47118400000000i;14.4906390000000 - 2.55672600000000i;14.5214150000000 -
2.56136200000000i;14.5214150000000 - 2.56136200000000i;14.5293920000000 -
2.56256500000000i;14.5293920000000 - 2.56256500000000i;14.5293920000000 -
2.56256500000000i;14.5293920000000 - 2.56256500000000i;14.5487710000000 -
2.56548700000000i;14.5772680000000 - 2.56978500000000i;14.5943640000000 -
2.57236500000000i;14.6046230000000 - 2.57391300000000i;14.6091830000000 -
2.57460100000000i;14.6091830000000 - 2.57460100000000i;14.6091830000000 -
2.57460100000000i;14.6091830000000 - 2.57460100000000i;14.6091830000000 -
```

```
2.57460100000000i;14.6091830000000 - 2.57460100000000i;14.6091830000000 -
2.57460100000000i;14.6091830000000 - 2.57460100000000i;14.6091830000000 -
2.57460100000000i;14.6091830000000 - 2.57460100000000i;14.6091830000000 -
2.57460100000000i;14.6091830000000 - 2.57460100000000i;14.6604770000000 -
2.58235100000000i;14.6844130000000 - 2.58596800000000i;14.6889720000000 -
2.58665700000000i;14.6889720000000 - 2.58665700000000i;14.7300070000000 -
2.59286600000000i;14.7607830000000 - 2.59752300000000i;14.7607830000000 -
2.59752300000000i;14.7664830000000 - 2.59838600000000i;14.7687640000000 -
2.59873100000000i;14.7687640000000 - 2.59873100000000i;14.7687640000000 -
2.59873100000000i;14.7687640000000 - 2.59873100000000i;14.7687640000000 -
2.59873100000000i;14.7687640000000 - 2.59873100000000i;14.7830110000000 -
2.60089800000000i;14.7972590000000 - 2.60306400000000i;14.8115080000000 -
2.60523000000000i;14.8257560000000 - 2.60739700000000i;14.8400040000000 -
2.60956300000000i;14.8542520000000 - 2.61172900000000i;14.8685010000000 -
2.61389600000000i;14.8827490000000 - 2.61606200000000i;14.8969970000000 -
2.61822800000000i;14.9112450000000 - 2.62039500000000i;14.9254930000000 -
2.62256100000000i;14.9397410000000 - 2.62472700000000i;14.9539900000000 -
2.62689400000000i;14.9682380000000 - 2.62906000000000i;14.9824860000000 -
2.63122700000000i;14.9967340000000 - 2.63339300000000i;15.0109820000000 -
2.63555900000000i;15.0252310000000 - 2.63772600000000i;15.0394780000000 -
2.63989200000000i;15.0537270000000 - 2.64205800000000i;15.0679750000000 -
2.64422500000000i;15.0822230000000 - 2.64639100000000i;15.0964710000000 -
2.64855700000000i;15.1107190000000 - 2.65072300000000i;15.1249690000000 -
```

```
2.65289000000000i;15.1392160000000 - 2.65505600000000i;15.1534640000000 -
2.65722300000000i;15.1677120000000 - 2.65938900000000i;15.1775150000000 -
2.66089500000000i;15.1873180000000 - 2.66240100000000i;15.1971210000000 -
2.66390800000000i;15.2069230000000 - 2.66541400000000i;15.2167260000000 -
2.66692000000000i;15.2265290000000 - 2.66842600000000i;15.2363310000000 -
2.66993200000000i;15.2461350000000 - 2.67143900000000i;15.2559370000000 -
2.67294500000000i;15.2657390000000 - 2.67445100000000i;15.2755420000000 -
2.67595700000000i;15.2853450000000 - 2.67746400000000i;15.2951470000000 -
2.67897000000000i;15.3049510000000 - 2.68047600000000i;15.3147540000000 -
2.68198200000000i;15.3245560000000 - 2.68348800000000i;15.3343580000000 -
2.68499500000000i;15.3441620000000 - 2.68650100000000i;15.3539650000000 -
2.68800700000000i;15.3637670000000 - 2.68951300000000i];
        %er profile including er of air
         [tbh_vector] =
coherent_tline_michigan_data_loop_final1_defense(er,ts,N,M,step,theta_deg,freq,p)
```

**Subroutine for the transmission line model:**

```
        % Same as 'coherent_tline_michigan_data_loop_final1.m'
        %Transmission line model
        function [tbh_vector] =
coherent_tline_michigan_data_loop_final1_defense(er,ts,N,M,step,theta_deg,freq,p)
        j=sqrt(-1);
        mu1=cosd(theta_deg);  %direction cosine for the incidence angle
```

```
      mu0=4*pi*10^-7;        %free space permeability

      eps0=8.854*10^-12;     %free space permittivity

      c=1/sqrt(mu0*eps0);    %speed of light

      lambda0=c/freq;        %free space wavelength

      mur=1;


        for i=1:N

          for k=1:M

          alpha(i,k)=(2*pi/lambda0)*abs(imag(sqrt(er(i,k))));  %attenuation constant

          end

        end


        for k=1:M

          for i=1:N-1

           er_first(i,k)=er(i,k);

          er_second(i,k)=er(i+1,k);

[mu2(i,k),gamma(i,k),R(i,k)]=trb_cihan_for_incoherent(mu1,er_first(i,k),er_second(i,k),p,freq); %compute mu2, gamma (reflection coefficient) and R (reflectivity)

          mu1=mu2(i,k);

           end

          mu1=cosd(theta_deg);

          end
```

```
for k=1:M
   mu(1,k)=cosd(theta_deg);
end
    for i=2:N
       for k=1:M
       mu(i,k)=mu2(i-1,k);
       end
    end
    for i=1:N
       for k=1:M
       etarr(i,k)=sqrt(mur/er(i,k)); %intrinsic impedance
       Z(i,k)=etarr(i,k)/mu(i,k); %impedance
       L(i,k)=exp(2*alpha(i,k)*step/mu(i,k));   %power loss
       end
    end
     %-------------------
   for i=1:N
       for k=1:M
       beta(i,k)=(2*pi/lambda0)*real(sqrt(er(i,k)));
       betaprime(i,k)=beta(i,k)*(1/mu(i,k));
       end
    end
 %-----------------
```

```
for i=1:N
    for k=1:M
    Znew(i,k)=Z(N-i+1,k);   %update Z, L and betaprime
    Lnew(i,k)=L(N-i+1,k);
    betaprimenew(i,k)=betaprime(N-i+1,k);
    end
end

      for i=1:N-1
          for k=1:M
           Refl(i,k) = (Znew(i,k)-Znew(i+1,k))/(Znew(i,k)+Znew(i+1,k)); %reflection coefficient
          ZIN(i,k) = Zin(Znew(i+1,k),Refl(i,k),Lnew(i+1,k),betaprimenew(i+1,k),step); %update input impedance
          Znew(i+1,k) = ZIN(i,k);
        end
      end

     for k=1:M
     gammacoh(k)=(abs(Refl(N-1,k)))^2; %coherent reflectivity
     emisscoh(k)=1-gammacoh(k);   %coherent emissivity
```

```
                 tbh(k)=ts(k)*emisscoh(k); %brightness temperature of the specular surface above air-soil interface
                 end
                 tbh_below = tbh /(1-R(1));   %brightness temperature of the specular surface just below air-soil interface
                tbh_vector = [tbh tbh_below];  % a vector that contains tbh and tbh_below that are described above
```

**Main program for the coherent model:**

```
            clear all
            format long
              mex btt_below.f
              tbh_below = btt_below; %tb for a flat surface (below air-soil boundary)
               mex btt_above1.f
               tbh_above = btt_above1; %tb for a flat surface (above air-soil boundary)
               tb_vector = [tbh_above(1) tbh_below(1)] %a vector that includes tbh_above and tbh_below
```

**Code for the coherent model:**

```
            #include "fintrf.h"
C Explictly declare the program here, so that the computation can
            C be turned into a subroutine.  When the MEX file is invoked in
            C Matlab, this routine does NOT run.
```

```
program brighttemp
            real array(1)
            call computation(array)
            end
C This is the routine that is invoked by Matlab.  It takes no
C inputs, and produces a 393 element array which contains all
C of the results produced by the routine.  Note that 393 corresponds
C to M in the computation function. It would be nice to parameterize
C this in a global variable, or even better, to determine it based
C on reading the file.  Such steps would be rather invasive for
C what we are doing at this point.

C     The standard MEX header
   subroutine mexFunction(nlhs, plhs, nrhs, prhs)

C  The type declaration
   integer nlhs, nrhs, code
   mwpointer plhs(*), prhs(*), r_pr
   real array(1)

C  Invoke the computation to get the array
            call computation(array)
```

```
C             Allocate a matrix to return in Matlab
              nlhs = 1
              code = mxClassIDFromClassName('single')
              plhs(1)=mxCreateNumericMatrix(393,1,code,0)
              r_pr = mxGetPr(plhs(1))

C             Copy the data from computation to the Matlab matrix
              call mxCopyReal4ToPtr(array, r_pr, 1)

              end
              subroutine computation(array)
              real array(*)

C          PARAMETER (IROW=1)
C           PARAMETER (ICOL=)
        PARAMETER (NTOT=1)
        PARAMETER (NZTEMP=44)
       PARAMETER (M=393)
       PARAMETER (N=44)
C           PARAMETER (NLAY=21)
C           PARAMETER (ROWS=8253)
C           PARAMETER (K=1)
```

```
      PARAMETER (NUMB=17292)
      INTEGER I,J,LOOP1,LOOP2

C        INTEGER M,N
      REAL SMP(NUMB), SOILMOIS(N,M),TEMPP(NUMB), TEMPER(N,M)
      REAL SMT1(N),TEMPT1(N),POROSITY(N+1)
C        REAL DUMMY(21)
      REAL FWAT(N,NTOT),SMT11(N,NTOT),POROS(N+1,NTOT)
      REAL TS(N,NTOT),DZTEMP_MINE(NZTEMP+2)
      REAL DZTEMP(NZTEMP+2,NTOT), DZZ(N+2,NTOT)
      REAL
WBOUND(NTOT),BULK_DEN(N+1),BDEN(N+1,NTOT),PAR_DEN(N+1)
      REAL SS_ALB(NTOT),TV(NTOT),WV(NTOT),BV(NTOT)
      REAL SSIG(NTOT),SANDPER(NTOT),CLAYPER(NTOT)
      REAL FREQ,THETA_DEG
      INTEGER MASK(NTOT),DC_OPTION
      REAL YR(N+2,NTOT),TBHT(NTOT),TBVT(NTOT)
      REAL SUMMATION(M),AVG_TEMP(M)

      FREQ=1.4
      DC_OPTION=1
      THETA_DEG=35
```

```
C          M=393

C          N=21

C          U=M*N


c          open and read the  soil temperature measurement depths (0-16 cm--
dimension=NZTEMP+2

c     element 1 = element 2 = 0 cm and element 22 = element 23 = 16 cm)

      OPEN (UNIT=20, FILE='dztemp_ksat.dat',STATUS='OLD')

      DO I=1,NZTEMP+2

      READ (20,30) DZTEMP_MINE(I)

   30 FORMAT(f4.1)

       END DO

C     set DZTEMP_MINE equal to DZTEMP (DZTEMP is 2D, DZTEMP_MINE is 1D)

c     set DZZ to DZTEMP

       DO I=1,NZTEMP+2

        DO J=1,NTOT

      DZTEMP(I,J)=DZTEMP_MINE(I)

       DZZ(I,J)=DZTEMP(I,J)

        END DO

         END DO

c          open the  soil moisture profile--column vector

C      OPEN (UNIT=2, FILE='ipond0_sm_lowerksat.dat',STATUS='OLD') !ipond=0,
Ksat=0.000005
```

```
          OPEN (UNIT=2, FILE='sm_lowerksat.dat',STATUS='OLD') !ipond=1,
Ksat=0.000005
     C      OPEN(UNIT=2, FILE='smprofile_0.000040_ipond0.dat', STATUS='OLD')
!ipond=0, Ksat=0.000040
     C      OPEN(UNIT=2, FILE='sm_0.000040_ipond1_decimal.dat', STATUS='OLD')
            !ipond=1, Ksat=0.000040
     C       OPEN(UNIT=2, FILE='sm_lowerksat.dat', STATUS='OLD')
     c             read the  soil moisture profile--column vector

          DO I=1,17292
          READ (2,3) SMP(I)
       3   FORMAT(f6.5)
           END DO
      c    print the contents of SMT1
     c          DO J=1,1000
    c           PRINT *,SMP(J)
    c         END DO
     c    arrange soil moisture vector as a 2D matrix
     c    columns: sm values at layers, rows: time steps
     c    (each column represents a soil moisture profile at a certain time step)
          DO I=1,N  !21
          DO J=1,M  !393
         SOILMOIS(I,J)=SMP(I+N*(J-1))
```

```
          END DO
          END DO
 c          open the  temperature profile file--column vector
 C       OPEN (UNIT=22, FILE='ipond0_temp_lowerksat.dat',STATUS='OLD') !ipond=0, Ksat=0.000005
          OPEN(UNIT=22, FILE='temp_lowerksat.dat',STATUS='OLD')  !ipond=1, Ksat=0.000005
 C       OPEN(UNIT=22, FILE='temp_0.000040_ipond0.dat',STATUS='OLD') !ipond=0, Ksat=0.000040
 C       OPEN(UNIT=22, FILE='temp_0.000040_ipond1.dat',STATUS='OLD') !ipond=1, Ksat=0.000040
 C        OPEN(UNIT=22, FILE='temp_lowerksat.dat', STATUS='OLD')
 c          read the  temperature profile--column vector
         DO I=1,17292
         READ (22,9) TEMPP(I)
       9  FORMAT(f6.5)
         END DO
 c     arrange soil moisture vector as a 2D matrix
 c     columns: sm values at layers, rows: time steps
 c     (each column represents a soil moisture profile at a certain time step)

         DO I=1,N  !21
          DO J=1,M  !393
```

```
  TEMPER(I,J)=TEMPP(I+N*(J-1))


  END DO

  END DO


 DO I=1,NTOT

WBOUND(I)=0.02

END  DO

 DO I=1,N+1

BULK_DEN(I)=1210  !for low areas (for high areas it is 1090)

END DO

  DO I=1,N+1

  PAR_DEN(I)=2650

  END DO

 DO I=1,N+1

  POROSITY(I) = 1 - BULK_DEN(I)/PAR_DEN(I)

 END DO

 DO I=1,N+1

 DO J=1,NTOT

POROS(I,J)=POROSITY(I)

END DO

 END DO

 DO I=1,N+1
```

```
 DO J=1,NTOT


 BDEN(I,J)=BULK_DEN(I)
  END DO
  END DO
 DO I=1,NTOT
 SS_ALB(I)=0.5
  TV(I)=300
   MASK(I)=1
   WV(I)=2
   BV(I)=0.6
   SSIG(I)=1.5
   SANDPER(I)=16.1
   CLAYPER(I)=28.9
  END DO
C   OPEN (UNIT=70,FILE='tbht.dat')
    DO LOOP1=1,1
    DO J=1,NTOT
    DO LOOP2=1,N !21
  SMT1(LOOP2)=SOILMOIS(LOOP2,LOOP1)
  SMT11(LOOP2,J)=SMT1(LOOP2)
  FWAT(LOOP2,J)=SMT11(LOOP2,J)/POROS(LOOP2,J)
  TEMPT1(LOOP2)=TEMPER(LOOP2,LOOP1)
```

```
      TS(LOOP2,J)=TEMPT1(LOOP2)
c       TS(LOOP2,J)=AVG_TEMP(LOOP1)

     END DO
      END DO
   CALL rtm_grid_v18(NTOT,N,NZTEMP,FREQ,MASK,TV,TS,FWAT,
POROS,WBOUND,SS_ALB,WV,BV,SSIG,SANDPER,CLAYPER,
DC_OPTION,THETA_DEG,DZZ,DZTEMP,BDEN,YR,TBHT,TBVT,array,LOOP1)

     END DO
C      OPEN (UNIT=70,FILE='tbht.dat')
C         DO I=1,M
C          WRITE(70,*) TBHT(I)
C         END DO
c       STOP
                 close(unit=2)
                 close(unit=20)
                 close(unit=22)
       END
       subroutine rtm_grid_v18(ntot,nlay,nztemp,freq,mask,tv,ts,fwat,
     +  poros,wbound,ss_alb,wv,bv,ssig,sandper,clayper,
     +  dc_option,theta_deg,dzz,dztemp,bden,yr,tbht,tbvt,array,loop1)
```

```
c       Calculates soil dielectric constant profile and microwave
c       brightness temperature, given soil temperature and moisture profiles.
c       This version operates on a grid.
c       Handles only one frequency and one view angle at one time.
c       Uses linear interpolation on temperatures and dielectric constants.
        parameter (nzz=90)
c                   = number of layers over which integration is performed
c                   setting nzz = 60 results in integration over 2 wavelengths.
       implicit complex(a-h,o-z)
      complex m1,m2,m3,m4

        real array(*)
        integer dc_option,mask(ntot),loop1
        real alpha,step,t1,t1v,t2,t2v,t3,t3v,t5,t5v
         real ewr,ewi,xlmd,sh,qkc,sht,rqz
        real thtt,thttv,tf
        real epi,eit,ebr,ebi,theta_deg,theta,qk,tauv,pi,densmin
        real ezte,eztm,qiz,dl1,a1,a1v,b1,b1v,temp,tempv,veg,qx,freq
        real wv(ntot),bv(ntot),ssig(ntot)
        real sandper(ntot),clayper(ntot),vwc_trans,wilt,gam
        real ts(nztemp,ntot),wbound(ntot),tv(ntot),ss_alb(ntot)
        real fwat(nlay,ntot),poros(nlay+1,ntot),bden(nlay+1,ntot)
        real tbh(ntot),tbht(ntot),tbh_below(ntot)
```

```
       real tbv(ntot),tbvt(ntot)
       real gpsi(nzz+1),gpsr(nzz+1),tz(nzz+2),muz(nzz+2)
       real yi(nlay+2),air(nlay+2),ddz(nzz+2)
       real sm(nlay+2),vs(nlay+2),tc(nztemp),tsfc,tt,relax
       real eps_water,eps_min,eps_ice,eps_air,eps_inf
      real dzz(nlay+2,ntot),dztemp(nztemp+2,ntot),yr(nlay+2,ntot)
       dimension a(nzz+1),b(nzz+1),c(nzz+1),d(nzz+1),rpss(nlay+2),
      epss(nzz+2),bi(2,2),bo(2,2),bt(2,2),pe(nzz+1),pm(nzz+1),
      re(nzz+1),rm(nzz+1),ce1(nzz+1),ce2(nzz+1),cep1(nzz+1),
      cep2(nzz+1),ve2(nzz+1,2),vm1(nzz+1,2),vm2(nzz+1,2),
      qz(nzz+2),ve1(nzz+1,2),con(200),son(200)
     c     Input variables:
c    ntot = total number of grid cells
c    nlay = number of soil layers for which moisture values are input
c    nztemp = number of layers at which measured soil temperatures are available
c    mask = indicator of whether grid point should be processed
c         = 1 for points to be processed
c         = 0 for points to be excluded
c    freq = microwave frequency  (GHz)
c    tv = vegetation temperature (K)
c    ts = soil temperature profile (K)
c    fwat = volumetric soil water content (as proportion of saturation)
c    poros = porosity of soil (unitless)
```

```
c     wbound = amount of bound water in soil (volumetric water content, m^3/m^3)
c     ss_alb = single scattering albedo (unitless)
c     wv = vegetation water content (kg/m^2)
c     bv = empirical coefficient relating veg. water content to transmittance (m^2/kg)
c     ssig = standard deviation of surface height (cm)
c     sandper = sand content (%)
c     clayper = clay content (%)
c     dc_option = option for calculation of dielectric constant
c               1 = Dobson, 2 = Wang and Schmugge
c     theta_deg = view angle (degrees)
c     dzz = soil moisture measurement depths (cm)
c     dztemp = soil temperature measurement depths (cm)     ! Note that dztemp(1) is not used!
c     bden = bulk soil density (kg/m^3)
c
c     Definitions:
c
c     tc = soil temperature at measurement depths (deg. C)
c     tsfc = surface temperature (K)
c     ro = smooth surface reflectivity (unitless)
c     step = thickness of soil layers in integration (cm)
c     theta = view angle (radians)
c     ddz = soil layer depths at model levels (equal intervals) (cm)
```

```
c    rpss = complex dielectric constant at measurement depths
c    yi = imaginary part of dielectric constant at measurement depths
c    tz = soil temperature interpolated to model depths (deg. C)
c    ewr = real part of dielectric constant for free water
c    ewi = imaginary part of dielectric constant for free water
c    ebr = real part of dielectric constant for bound water
c    ebi = imaginary part of dielectric constant for bound water
c    densmin = density of mineral matter
c    tauv = vegetation transmittance
c    epss = complex dielectric constant at model levels
c    tbh = Horizontally polarized brightness temperature w/o corrections (K)
c    tbv = Vertically polarized brightness temperature w/o corrections (K)
c    vwc_trans = 'transition' soil water content (unitless)
c    wilt = soil wilting point (unitless)
c    gam = term used in dielectric constant formulation (unitless)
c    eps_min = dielectric content of mineral matter (unitless)
c    eps_ice = dielectric content of ice (unitless)
c    eps_air = dielectric content of air(unitless)
c    eps_inf = high frequency dielectric content (unitless)
c
c    Output variables:
c
c    yr = real part of dielectric constant at measurement depths
```

```
c    tbht = Horizontally polarized brightness temperature w/ corrections (K)
c    tbvt = Vertically polarized brightness temperature w/ corrections (K)

     data ebr,ebi,ewi,densmin/35.0,14.5,14.5,2650./
     data alpha/0.65/
     data eps_min/5.5/
     data eps_ice/3.2/
     data eps_air/1.0/
     data eps_inf/4.9/
      data veg/1.0/

C      OPEN (UNIT=70,FILE='tbht_lowksat_ipond1_ssig15_unix_dobson.dat')
C     OPEN (UNIT=70,FILE='tbht_highksat_ipond0_ssig08_unix.dat')
C     OPEN (UNIT=92,FILE='er_profile_highksat_ipond0_unix.dat')
c     OPEN (UNIT=70,FILE='tbht334_lowksat_ipond1_ssig15_unix.dat')
c     OPEN (UNIT=92,FILE='er334_lowksat_ipond1_ssig15_unix.dat')
c     OPEN (UNIT=92,FILE='er_lowksat_ipond1_ssig15_unix_dobson.dat')
c     Define step size depending on frequency
c
      step = amin1(1.0,1./freq)
      nzz1=nzz+1
      pi=acos(-1.0)
      theta=theta_deg*pi/180.0
```

```
       ci=cmplx(0,1)
       do 100 i=1,nzz+2
 100      ddz(i)=(i-1)*step
      do 9000 ix = 1,ntot
      if(mask(ix) .ge. 1) then
c       Fill profile arrays of air, temperature and soil moisture
c          Calculate vs(1) using bulk density at level 2 since level 1 is not defined.
       vs(1) = bden(2,ix)/densmin
       do iz=2,nlay+1
          vs(iz)=bden(iz,ix)/densmin
          sm(iz) = fwat(iz-1,ix)*poros(iz-1,ix)
         air(iz)=amax1(0.0,poros(iz-1,ix) - sm(iz))
       end do
c       Define soil moisture at level 1 as value at level 2.
c       Also define air(1).
       sm(1)=sm(2)
       air(1) = amax1(0.0,poros(1,1) - sm(1))
       do iz = 1,nztemp
         tc(iz) = ts(iz,ix) - 273.15
       end do
       do i=1,nzz1
         call interp(dztemp(2,ix),tc,nztemp,ddz(i),tz(i))
       end do
```

```
      tz(nzz+2)=tz(nzz1)
c       OPEN (UNIT=63,FILE='tempprofile_subroutine_dobson.dat')
c       DO i=1,nzz+1
c       WRITE (63,65) tz(i)
c65      FORMAT (1f10.6)
c       END DO
      t2=(1.01+0.44*0.001*densmin)**2-0.062
c      Define variables used in Wang and Schmugge mixing model.
      wilt = 0.06774 - 0.00064*sandper(ix) + 0.00478*clayper(ix)
      vwc_trans = 0.165 + 0.49*wilt
      gam = -0.57*wilt + 0.481
c      Calculate dielectric constant at measurement depths.
c      Use either Dobson or Wang and Schmugge mixing model.
      do 210 j=1,nlay+1
c      Call interp to interpolate soil temperatures (tc) to moisture measurement depths.
        call interp(dztemp(2,ix),tc,nztemp,dzz(j,ix),tt)
        ewr=88.045-0.4147*tt + 6.295e-4*tt*tt + 1.075e-5*tt**3
        relax = 1.1109e-10 - 3.824e-12*tt          ! Relaxation time
     + 6.938e-14*tt**2 - 5.096e-16*tt**3
        eps_water =eps_inf+(ewr-eps_inf)/(1.+(freq*1.e9*relax)**2)
        t3=sm(j) - wbound(ix)
        ew=eps_water+ci*ewi
        epso=t2
```

```
      rpss(j)=t3*(ew**(alpha))+vs(j)*(epso**(alpha))
          +air(j)+((ebr+ci*ebi)**(alpha))*wbound(ix)
      rpss(j)=rpss(j)**(1.0/alpha)
      if (dc_option .eq. 1) then    ! Dobson mixing model
        yr(j,ix)=real(rpss(j))

  ! Wang and Schmugge mixing modelc
c     Wang and Schmugge Dielectric constant calculation - real part only
       if (sm(j) .lt. vwc_trans) then
            eps1 =eps_ice+(eps_water-eps_ice)*(sm(j)/vwc_trans)*gam
            yr(j,ix) = sm(j)*eps1 + air(j)*eps_air
             + (1. - poros(j,ix))*eps_min
     else
            eps1 = eps_ice + (eps_water-eps_ice)*gam
            yr(j,ix)= vwc_trans*eps1 + (sm(j)-vwc_trans)*eps_water
  + (poros(j,ix) - sm(j))*eps_air + (1. - poros(j,ix))*eps_min
        end if
      end if
c     For both mixing models, use imaginary part calculated from Dobson model
      yi(j)=imag(rpss(j))
 210  continue
c      Set dielectric constant for layer nlay+2 to that of nlay+1
```

```
        yr(nlay+2,ix) = yr(nlay+1,ix)
        yi(nlay+2) = yi(nlay+1)
c     Interpolate dielectric constant to model layers
      do i=1,nzz1
        call interp(dzz(1,ix),yr(1,ix),nlay+2,ddz(i),gpsr(i))
        gpsr(i) = amax1(gpsr(i),2.0)
        call interp(dzz(1,ix),yi,nlay+2,ddz(i),gpsi(i))
        gpsi(i) = amax1(gpsi(i),0.3)
c             write(*,*) gpsr(i),gpsi(i)
c         epss(i)=cmplx(gpsr(i),gpsi(i))
      end do
c        epss(nzz+2)=cmplx(-4.0,gpsi(nzz1))
c        epss(1)=1.0
c        WRITE(92,94) epss
c 94     FORMAT(1f10.6)

CCCCCCCCCCCCCCCCCCCCCCCCCCCCCCCCCCCCCCCCCCCCCCCC
          OPEN (UNIT=25, FILE='er_time1.dat',STATUS='OLD')
          DO I=1,92
          READ (25,9) epss(I)
    9 FORMAT(f10.6)
      END DO
```

```
CCCCCCCCCCCCCCCCCCCCCCCCCCCCCCCCCCCCCCCCCCCCCCCC
      ezte=1.0
      eztm=1.0
      xlmd=30.0/freq
      sh=4.*ssig(ix)*ssig(ix)*((2.*pi/xlmd)**2)
      sht=exp(-sh*cos(theta)**2)
      qk=2.*pi/(xlmd)
      qx=qk*sin(theta)
      do 500 i=1,nzz+2
        muz(i)=1.0
        qz2=qk*qk*muz(i)*epss(i)-qx*qx
500       qz(i)=sqrt(qz2)
      do 600 i=1,nzz1
        pe(i)= muz(i)*qz(i+1)/(muz(i+1) *qz(i))
        pm(i)=epss(i)*qz(i+1)/(epss(i+1)*qz(i))
        re(i)=(1.0-pe(i))/(1.0+pe(i))
        rm(i)=(1.0-pm(i))/(1.0+pm(i))
600     continue
      do 700 i=1,nzz1
        ce1(i)=exp(-ci*qz(i)*ddz(i)*2.)
        ce2(i)=1.0/ce1(i)
        cep1(i)=exp(-ci*qz(i+1)*ddz(i)*2.)
700       cep2(i)=1.0/cep1(i)
```

```
c   Compute reflection coefficients
        abne=re(nzz1)*ce2(nzz1)
        abnm=rm(nzz1)*ce2(nzz1)
        con(nzz)=abne
        son(nzz)=abnm
        do 800 j=1,nzz-1
           i=nzz-j+1
           con(i)=ce2(i)*(re(i)+con(i+1)*cep1(i))/
            (1.0+re(i)*con(i+1)*cep1(i))
           son(i)=ce2(i)*(rm(i)+son(i+1)*cep1(i))/
          (1.0+rm(i)*son(i+1)*cep1(i))

 800    continue
        con(1)=(re(1)+con(2)*cep1(1))/(1.0+re(1)*con(2)*cep1(1))
        son(1)=(rm(1)+son(2)*cep1(1))/(1.0+rm(1)*son(2)*cep1(1))
        abie=con(1)
        abim=son(1)
c Compute transfer matrices and a b c d
        do 900 i=1,nzz1
           ct1=0.5*(1.+1./pe(i))
          t1m=0.5*(1.+1./pm(i))*(qk*sqrt(epss(i)))/(qk*sqrt(epss(i+1)))
           ct2=ci*qz(i+1)*(ddz(i+1)-ddz(i))
           ve1(i,1)=       exp(-ct2)*ct1
```

```
        vm1(i,1)=      exp(-ct2)*t1m
        ve2(i,1)=-re(i)*exp(-ct2)*ct1
        vm2(i,1)=-rm(i)*exp(-ct2)*t1m
        ve1(i,2)=-re(i)*exp(ct2)*ct1
        vm1(i,2)=-rm(i)*exp(ct2)*t1m
        ve2(i,2)=      exp(ct2)*ct1
900       vm2(i,2)=      exp(ct2)*t1m
      bi(1,1) = 1.0
      bi(2,2) = 1.0
      bi(1,2) = 0.0
      bi(2,1) = 0.0
      do 2000 i=1,nzz1
        do 2100 k=1,2
          bt(k,1)=ve1(i,k)
2100        bt(k,2)=ve2(i,k)
c      Compute bo=bt*bi
        do 2110 ib=1,2
          do 2110 jb=1,2
           temp=0.0
            do 2130 kb=1,2
2130            temp=temp+bt(ib,kb)*bi(kb,jb)
2110          bo(ib,jb)=temp
        do 2140 ib=1,2
```

```
          do 2140 jb=1,2
2140          bi(ib,jb)=bo(ib,jb)
2000  continue
        ct1=exp(ci*qz(1)*ddz(1))
      if ( (cabs(bo(1,1)) .ge. 1.0e-6) ) then
          ct2=(bo(1,1)*bo(2,2)-bo(1,2)*bo(2,1))/bo(1,1)
      else
          ct2=bo(2,2)
        end if
        tte=ct2*ct1
        bi(1,1) = 1.0
        bi(2,2) = 1.0
        bi(1,2) = 0.0
        bi(2,1) = 0.0
        do 4000 i=1,nzz1
          do 4100 k=1,2
              bt(k,1)=vm1(i,k)
4100          bt(k,2)=vm2(i,k)
          do 4110 ib=1,2
            do 4110 jb=1,2
              temp=0.0
              do 4130 kb=1,2
4130              temp=temp+bt(ib,kb)*bi(kb,jb)
```

```
4110          bo(ib,jb)=temp
          do ib=1,2
            do jb=1,2
              bi(ib,jb)=bo(ib,jb)
            end do
          end do
4000   continue
      if ( (cabs(bo(1,1)) .ge. 1.0e-6) ) then
          ct2=(bo(1,1)*bo(2,2)-bo(1,2)*bo(2,1))/bo(1,1)
      else
          ct2=bo(2,2)
      end if
        ttm=ct2*ct1
        a(1)=abie*ezte
        b(1)=ezte
        c(1)=abim*eztm
        d(1)=eztm
        do 5000 i=2,nzz1
          a(i)=ve1(i-1,1)*a(i-1)+ve2(i-1,1)*b(i-1)
          b(i)=ve1(i-1,2)*a(i-1)+ve2(i-1,2)*b(i-1)
          c(i)=vm1(i-1,1)*c(i-1)+vm2(i-1,1)*d(i-1)
5000      d(i)=vm1(i-1,2)*c(i-1)+vm2(i-1,2)*d(i-1)
```

```
        do 6000 i=1,nzz1
          a(i)=a(i)*exp(ci*qz(i)*ddz(i))
          b(i)=b(i)*exp(-ci*qz(i)*ddz(i))
          c(i)=c(i)*exp(ci*qz(i)*ddz(i))
 6000     d(i)=d(i)*exp(-ci*qz(i)*ddz(i))
c compute brightness temperatures for horizontal polarization
        qkc=qk/cos(theta)
        t2=qkc*imag(epss(nzz+2))*(tz(nzz+2)+273.15)*abs(tte)**2
        t3=imag(qz(nzz+2))
        thtt=exp(-2.*t3*ddz(nzz1))/(2.*t3)*t2
       write(20,*) ' initial term in TBH=',thtt
       write(20,*) 're(1)=',real(re(1)),'pe(1)=',real(pe(1))
        temp=0.0
        do 7000 i=2,nzz1
          epi=imag(epss(i))
          eit=epi*(tz(i)+273.15)
          ct3=a(i)*exp(-ci*qz(i)*ddz(i))
          qiz=imag(qz(i))
          t5=abs(ct3)**2/(2.*qiz)
          dl1=ddz(i-1)-ddz(i)
          t3=1.0-exp(2.*qiz*dl1)
          a1=t3*t5
          ct1=b(i)*exp(ci*qz(i)*ddz(i))
```

```
         t1=(abs(ct1)**2)/(2.*qiz)

         t2=1.0-exp(-2.*qiz*dl1)

         b1=-t1*t2

         ct1=a(i)*exp(-ci*qz(i)*ddz(i))

         ct2=conjg(b(i)*exp(ci*qz(i)*ddz(i)))

         rqz=real(qz(i))

         ct1=ct1*ct2/(2.*ci*rqz)

         ab1=-ct1*(1.0-exp(-2.*ci*rqz*dl1))

         ct1=conjg(a(i)*exp(-ci*qz(i)*ddz(i)))

         ct2=b(i)*exp(ci*qz(i)*ddz(i))

         ct1=ct1*ct2/(2.*ci*rqz)

         ab2=ct1*(1.0-exp(ci*2.*rqz*dl1))

 7000      temp=temp+eit*(a1+b1+real(ab1+ab2))

         temp=temp*qkc

       tbh(ix)=thtt+temp


           tbh_below(ix) = tbh(ix)/(1-abs(con(1))*abs(con(1)))

c     Add the effects of vegetation and roughness for horizontal polarization


C      tauv=bv(ix)*wv(ix)

C       veg=sqrt(exp(-2.*tauv/cos(theta))) !! Transmissivity, not squared.

       tsfc = tc(1)+273.15

       ro = 1. -  tbh(ix)/tsfc
```

```
          tbht(ix) = (1.-veg)*(1.-ss_alb(ix))*tv(ix)*(1.+veg*ro*sht)
           + veg*tsfc*(1.-ro*sht)
      C Now that the file prints to matlab, we no longer write to the text
      C file or the screen (you can continue to do this, if you wish).

      C      PRINT *,tbht(ix)
      C      WRITE(70,*) tbht(ix)
            array(loop1) = tbh_below(ix)

      c compute brightness temperatures for vertical polarization   !! This section added
11/3/04

          t2v=qkc*imag(epss(nzz+2))*(tz(nzz+2)+273.15)*abs(ttm)**2
          t3v=imag(qz(nzz+2))
          thttv=exp(-2.*t3v*ddz(nzz1))/(2.*t3v)*t2v
          m3=qz(nzz+2)*qz(nzz+2)+qx*qx
          m4=epss(nzz+2)*qk*qk*1.0
          tf=thttv*(m3/m4)
          tempv=0.0
         do 1515 i=2,nzz1
            epi=imag(epss(i))
            eit=epi*(tz(i)+273.15)
            ct3v=c(i)*exp(-ci*qz(i)*ddz(i))
```

```
      qiz=imag(qz(i))
      t5v=abs(ct3v)**2/(2.*qiz)
      dl1=ddz(i)-ddz(i-1)
      t3v=1.0-exp(-2.*qiz*dl1)
      a1v=t3v*t5v
      ct1v=d(i)*exp(ci*qz(i)*ddz(i))
      t1v=(abs(ct1v)**2)/(2.*qiz)
      t2v=1.0-exp(2.*qiz*dl1)
      b1v=-t1v*t2v
      ct1v=c(i)*exp(-ci*qz(i)*ddz(i))
      ct2v=conjg(d(i)*exp(ci*qz(i)*ddz(i)))
      rqz=real(qz(i))
      ct1v=ct1v*ct2v/(2.*ci*rqz)
      ab1v=ct1v*(1.0-exp(2.*ci*rqz*dl1))
      ct1v=conjg(c(i)*exp(-ci*qz(i)*ddz(i)))
      ct2v=d(i)*exp(ci*qz(i)*ddz(i))
      ct1v=ct1v*ct2v/(2.*ci*rqz)
      ab2v=-ct1v*(1.0-exp(-2.*ci*rqz*dl1))
      m1=(qz(i)*qz(i)+qx*qx)/(epss(i)*qk*qk*1.0)
     m2=(qz(i)*qz(i)-qx*qx)/(qz(i)*qz(i)+qx*qx)
1515      tempv=tempv+eit*m1*(a1v+b1v+m2*real(ab1v+ab2v))
    tempv=tempv*qkc
    tbv(ix)=tf+tempv
```

```
c     Add the effects of vegetation and roughness for vertical polarization
       rov = 1. -  tbv(ix)/tsfc
       tbvt(ix) = (1.-veg)*(1.-ss_alb(ix))*tv(ix)*(1.+veg*rov*sht)
      + veg*tsfc*(1.-rov*sht)
       end if                      ! For mask .ge. 1
 9000   continue
      return
      end
       subroutine interp(xin,yin,n,x,y)
c      Performs linear interpolation
c      Input:
c      xin, yin = input values of x, y.
c      Assumed that xin is in increasing order, i.e. xin(i) > xin(i-1).
c      n = number of elements in x and y
c      x = value of x at which an interpolated y-value is desired
c      Output:
c      y = interpolated value of y at the given value of x
       dimension xin(n),yin(n)
       klo=1
       khi=n
1      if(khi-klo.gt.1) then
         k=(khi+kLo)/2
         if(xin(k).gt.x) then
```

```
    khi=k
  else
    klo=k
  end if
go to 1
end if
h=xin(khi)-xin(klo)
a=(xin(khi)-x)/h
b=(x-xin(klo))/h
y=a*yin(klo) + b*yin(khi)
return
end
```

# APPENDIX C. ALEX INPUT FILE

```
41.93 -83.82 -90.00          (XLAT XLONG STDLNG  AZALIA, MI)

0                            (IPOND)

4                            (REFHTW)

3.2                (REFHTT)

9         0.10      0.01      0.10  0.75        (ITYPE XL Z0DH DISPDH CLUMP)

6                            (NGDAY)

140   0.01     0.01      0.01  (GDOY DLAI DFG DHEIGHT)

141   0.01     0.01      0.01  (GDOY DLAI DFG DHEIGHT)

142   0.01     0.01      0.01  (GDOY DLAI DFG DHEIGHT)

143   0.01     0.01      0.01  (GDOY DLAI DFG DHEIGHT)

144   0.01     0.01      0.01  (GDOY DLAI DFG DHEIGHT)

145   0.01     0.01      0.01  (GDOY DLAI DFG DHEIGHT)

0.85      0.15      0.97      (ALEAFV ALEAFN ALEAFL)

0.60      0.15      0.97      (ADEADV ADEADN ADEADL)

2.0     0.15        0.2        0.1       (DROOT PINTMXLF FWETMX FWETMN)

44  0. .005 .010 .015 .020 .025 .030 .035 .040 .045 .050 .055 .060 .065 .070 .075 .080 .085 .090 .095 .10 .11 .12
.13 .14 .15 .16 .17 .18 .19 .20 .21 .22 .23 .24 .25 .26 .27 .28 .29 .30 .50 1.0 2.0 (NDSOIL ZSOIL(NDSOIL))

0.26 0.26 0.26 0.26 0.26 0.26 0.26 0.29 0.29 0.29 0.29 0.29 0.29 0.29 0.29 0.29 0.29 0.29 0.29 0.29 0.291 0.291
0.291 0.291 .291 .291 .291 .291 .291 .291 .291 .293 .291 .293 .293 .293 .293 .293 .293 .293 .293 .30 .31 .31
(WTI(NDSOIL))

18.0                         (TSOLBC)

0.15      0.25      0.96      (RSOILV RSOILN EMSOIL)

1                            (NLSOIL)

0.30   1.5    0.161  0.55  0.289   0.00  -3.3     6.6   0.000005 (ONE LINE PER LAYER: ZLSOIL BD SAND SILT
CLAY QRTZ PE BX DAK)

0     6     2.5    2.2  (IDOROC IROCLY AKROCK CPROCK)


        2001      140       0.000     2.1        14.48     14.08     0.00       307.44   0.00       0.00       988.00
```

| | | | | | | | | | | |
|---|---|---|---|---|---|---|---|---|---|---|
| 2001 | 140 | 0.333 | 1.8 | 14.86 | 13.70 | 0.00 | 307.93 | 0.00 | 0.00 | 988.00 |
| 2001 | 140 | 0.667 | 2.3 | 15.51 | 12.85 | 0.00 | 309.32 | 0.00 | 0.00 | 988.00 |
| 2001 | 140 | 1.000 | 1.7 | 15.45 | 12.29 | 0.00 | 307.46 | 0.00 | 0.00 | 988.00 |
| 2001 | 140 | 1.333 | 1.2 | 14.31 | 12.74 | 0.00 | 304.29 | 0.00 | 0.00 | 988.00 |
| 2001 | 140 | 1.667 | 1.5 | 13.82 | 12.79 | 0.00 | 305.57 | 0.00 | 0.00 | 988.00 |
| 2001 | 140 | 2.000 | 1.2 | 13.29 | 12.83 | 0.00 | 304.92 | 0.00 | 0.00 | 988.00 |
| 2001 | 140 | 2.333 | 1.3 | 13.52 | 12.75 | 0.00 | 303.49 | 0.00 | 0.00 | 988.00 |
| 2001 | 140 | 2.667 | 1.7 | 12.83 | 12.75 | 0.00 | 302.27 | 0.00 | 0.00 | 988.00 |
| 2001 | 140 | 3.000 | 1.1 | 12.38 | 12.65 | 0.00 | 304.48 | 0.00 | 0.00 | 988.00 |
| 2001 | 140 | 3.333 | 0.7 | 12.15 | 12.39 | 0.00 | 307.28 | 0.00 | 0.00 | 988.00 |
| 2001 | 140 | 3.667 | 1.0 | 12.07 | 12.19 | 0.00 | 310.10 | 0.00 | 0.00 | 988.00 |
| 2001 | 140 | 4.000 | 1.3 | 11.68 | 12.30 | 0.00 | 305.64 | 0.00 | 0.00 | 988.00 |
| 2001 | 140 | 4.333 | 1.4 | 11.47 | 12.24 | 0.00 | 308.42 | 0.00 | 0.00 | 988.00 |
| 2001 | 140 | 4.667 | 1.8 | 11.39 | 11.94 | 0.00 | 303.47 | 0.00 | 0.00 | 988.00 |
| 2001 | 140 | 5.000 | 1.5 | 11.33 | 12.07 | 0.00 | 300.07 | 0.00 | 0.00 | 988.00 |
| 2001 | 140 | 5.333 | 2.1 | 11.15 | 12.02 | 0.00 | 296.79 | 0.00 | 0.00 | 988.00 |
| 2001 | 140 | 5.667 | 1.6 | 10.68 | 11.66 | 0.00 | 295.44 | 0.00 | 0.00 | 988.00 |
| 2001 | 140 | 6.000 | 1.5 | 10.70 | 11.71 | 0.00 | 296.23 | 0.00 | 0.00 | 988.00 |
| 2001 | 140 | 6.333 | 1.6 | 10.81 | 11.53 | 0.77 | 295.11 | 0.00 | 0.00 | 988.00 |
| 2001 | 140 | 6.667 | 1.6 | 10.51 | 11.39 | 9.51 | 294.03 | 0.00 | 0.00 | 988.00 |
| 2001 | 140 | 7.000 | 1.5 | 10.40 | 11.47 | 31.25 | 294.90 | 0.00 | 0.00 | 988.00 |
| 2001 | 140 | 7.333 | 1.7 | 10.75 | 11.65 | 67.31 | 295.70 | 0.00 | 0.00 | 988.00 |
| 2001 | 140 | 7.667 | 1.3 | 11.14 | 12.00 | 78.32 | 295.52 | 0.00 | 0.00 | 988.00 |
| 2001 | 140 | 8.000 | 1.8 | 11.99 | 12.40 | 185.87 | 304.96 | 0.00 | 0.00 | 988.00 |
| 2001 | 140 | 8.333 | 2.3 | 12.63 | 12.79 | 140.77 | 304.87 | 0.00 | 0.00 | 988.00 |
| 2001 | 140 | 8.667 | 2.2 | 13.45 | 13.18 | 255.04 | 318.57 | 0.00 | 0.00 | 988.00 |
| 2001 | 140 | 9.000 | 2.9 | 14.33 | 13.22 | 373.58 | 325.53 | 0.00 | 0.00 | 988.00 |
| 2001 | 140 | 9.333 | 2.7 | 14.79 | 13.71 | 342.96 | 315.55 | 0.00 | 0.00 | 988.00 |

| | | | | | | | | | | |
|---|---|---|---|---|---|---|---|---|---|---|
| 2001 | 140 | 9.667 | 3.1 | 15.77 | 14.10 | 533.31 | 323.23 | 0.00 | 0.00 | 988.00 |
| 2001 | 140 | 10.000 | 3.2 | 16.50 | 14.38 | 595.45 | 332.96 | 0.00 | 0.00 | 988.00 |
| 2001 | 140 | 10.333 | 3.5 | 17.37 | 14.56 | 581.72 | 339.96 | 0.00 | 0.00 | 988.00 |
| 2001 | 140 | 10.667 | 3.1 | 18.32 | 14.65 | 535.18 | 345.96 | 0.00 | 0.00 | 988.00 |
| 2001 | 140 | 11.000 | 3.4 | 19.14 | 14.07 | 671.60 | 349.75 | 0.00 | 0.00 | 988.00 |
| 2001 | 140 | 11.333 | 3.8 | 19.75 | 13.76 | 812.17 | 346.03 | 0.00 | 0.00 | 988.00 |
| 2001 | 140 | 11.667 | 3.8 | 20.20 | 14.32 | 847.94 | 348.82 | 0.00 | 0.00 | 988.00 |
| 2001 | 140 | 12.000 | 4.4 | 20.55 | 14.38 | 839.78 | 349.36 | 0.00 | 0.00 | 988.00 |
| 2001 | 140 | 12.333 | 4.6 | 21.10 | 13.93 | 921.27 | 351.51 | 0.00 | 0.00 | 988.00 |
| 2001 | 140 | 12.667 | 4.4 | 21.24 | 13.51 | 936.75 | 352.52 | 0.00 | 0.00 | 988.00 |
| 2001 | 140 | 13.000 | 4.2 | 21.53 | 14.15 | 948.90 | 356.13 | 0.00 | 0.00 | 988.00 |
| 2001 | 140 | 13.333 | 4.8 | 21.70 | 14.02 | 953.41 | 356.78 | 0.00 | 0.00 | 988.00 |
| 2001 | 140 | 13.667 | 4.9 | 21.91 | 13.27 | 961.19 | 357.57 | 0.00 | 0.00 | 988.00 |
| 2001 | 140 | 14.000 | 5.0 | 22.01 | 13.41 | 958.91 | 356.42 | 0.00 | 0.00 | 988.00 |
| 2001 | 140 | 14.333 | 5.5 | 22.32 | 13.63 | 943.68 | 354.38 | 0.00 | 0.00 | 988.00 |
| 2001 | 140 | 14.667 | 5.4 | 22.69 | 13.73 | 952.09 | 355.19 | 0.00 | 0.00 | 988.00 |
| 2001 | 140 | 15.000 | 6.2 | 22.73 | 13.60 | 784.16 | 354.27 | 0.00 | 0.00 | 988.00 |
| 2001 | 140 | 15.333 | 5.9 | 22.99 | 13.43 | 885.16 | 356.12 | 0.00 | 0.00 | 988.00 |
| 2001 | 140 | 15.667 | 6.2 | 23.12 | 13.25 | 842.36 | 351.64 | 0.00 | 0.00 | 988.00 |
| 2001 | 140 | 16.000 | 6.5 | 23.41 | 13.23 | 785.16 | 351.37 | 0.00 | 0.00 | 988.00 |
| 2001 | 140 | 16.333 | 6.7 | 23.09 | 13.25 | 648.79 | 352.78 | 0.00 | 0.00 | 988.00 |
| 2001 | 140 | 16.667 | 6.4 | 22.90 | 13.56 | 501.03 | 353.83 | 0.00 | 0.00 | 988.00 |
| 2001 | 140 | 17.000 | 6.0 | 22.57 | 13.87 | 534.24 | 361.77 | 0.00 | 0.00 | 988.00 |
| 2001 | 140 | 17.333 | 6.4 | 22.19 | 13.57 | 454.79 | 350.36 | 0.00 | 0.00 | 988.00 |
| 2001 | 140 | 17.667 | 6.3 | 21.90 | 13.41 | 402.26 | 350.23 | 0.00 | 0.00 | 988.00 |
| 2001 | 140 | 18.000 | 6.9 | 21.63 | 13.22 | 366.98 | 341.03 | 0.00 | 0.00 | 988.00 |
| 2001 | 140 | 18.333 | 6.3 | 21.47 | 13.07 | 303.21 | 336.51 | 0.00 | 0.00 | 988.00 |
| 2001 | 140 | 18.667 | 6.4 | 20.77 | 12.77 | 194.90 | 338.82 | 0.00 | 0.00 | 988.00 |

| | | | | | | | | | | |
|---|---|---|---|---|---|---|---|---|---|---|
| 2001 | 140 | 19.000 | 5.4 | 20.38 | 12.62 | 177.51 | 343.12 | 0.00 | 0.00 | 988.00 |
| 2001 | 140 | 19.333 | 4.7 | 20.10 | 12.73 | 162.30 | 345.04 | 0.00 | 0.00 | 988.00 |
| 2001 | 140 | 19.667 | 4.0 | 19.88 | 12.88 | 110.30 | 347.53 | 0.00 | 0.00 | 988.00 |
| 2001 | 140 | 20.000 | 4.1 | 19.52 | 12.94 | 71.52 | 347.00 | 0.00 | 0.00 | 988.00 |
| 2001 | 140 | 20.333 | 3.6 | 18.96 | 13.15 | 40.83 | 339.50 | 0.00 | 0.00 | 988.00 |
| 2001 | 140 | 20.667 | 3.3 | 18.45 | 13.12 | 11.57 | 337.86 | 0.00 | 0.00 | 988.00 |
| 2001 | 140 | 21.000 | 3.7 | 18.18 | 12.70 | 0.93 | 335.14 | 0.00 | 0.00 | 988.00 |
| 2001 | 140 | 21.333 | 3.6 | 17.80 | 12.64 | 0.00 | 332.90 | 0.00 | 0.00 | 988.00 |
| 2001 | 140 | 21.667 | 4.7 | 17.54 | 12.67 | 0.00 | 332.87 | 0.00 | 0.00 | 988.00 |
| 2001 | 140 | 22.000 | 4.1 | 17.16 | 13.29 | 0.00 | 336.35 | 0.00 | 0.00 | 988.00 |
| 2001 | 140 | 22.333 | 3.7 | 16.86 | 13.81 | 0.00 | 341.59 | 0.00 | 0.00 | 988.00 |
| 2001 | 140 | 22.667 | 3.5 | 16.71 | 14.19 | 0.00 | 347.90 | 0.00 | 0.00 | 988.00 |
| 2001 | 140 | 23.000 | 2.9 | 16.68 | 14.50 | 0.00 | 342.19 | 0.00 | 0.00 | 988.00 |
| 2001 | 140 | 23.333 | 2.1 | 16.46 | 14.67 | 0.00 | 336.31 | 0.00 | 0.00 | 988.00 |
| 2001 | 140 | 23.667 | 2.1 | 15.97 | 14.84 | 0.00 | 341.29 | 0.00 | 0.00 | 988.00 |
| 2001 | 141 | 0.000 | 2.1 | 15.81 | 14.87 | 0.00 | 343.79 | 0.00 | 0.00 | 988.00 |
| 2001 | 141 | 0.333 | 2.0 | 15.67 | 14.90 | 0.00 | 347.40 | 0.00 | 0.00 | 988.00 |
| 2001 | 141 | 0.667 | 2.1 | 15.08 | 14.79 | 0.00 | 343.66 | 0.00 | 0.00 | 988.00 |
| 2001 | 141 | 1.000 | 2.3 | 15.10 | 14.90 | 0.00 | 342.18 | 0.00 | 0.00 | 988.00 |
| 2001 | 141 | 1.333 | 2.0 | 14.51 | 14.56 | 0.00 | 343.69 | 0.00 | 0.00 | 988.00 |
| 2001 | 141 | 1.667 | 2.1 | 14.28 | 14.49 | 0.00 | 349.17 | 0.00 | 0.00 | 988.00 |
| 2001 | 141 | 2.000 | 1.5 | 14.17 | 14.47 | 0.00 | 355.59 | 0.00 | 0.00 | 988.00 |
| 2001 | 141 | 2.333 | 1.3 | 14.21 | 14.51 | 0.00 | 357.88 | 0.00 | 0.00 | 988.00 |
| 2001 | 141 | 2.667 | 2.2 | 14.42 | 14.63 | 0.00 | 359.37 | 0.00 | 0.00 | 988.00 |
| 2001 | 141 | 3.000 | 1.9 | 14.56 | 14.84 | 0.00 | 359.40 | 0.00 | 0.00 | 988.00 |
| 2001 | 141 | 3.333 | 1.4 | 14.47 | 15.05 | 0.00 | 359.05 | 0.00 | 0.00 | 988.00 |
| 2001 | 141 | 3.667 | 1.9 | 14.65 | 15.45 | 0.00 | 369.49 | 0.00 | 0.00 | 988.00 |
| 2001 | 141 | 4.000 | 1.9 | 14.89 | 15.86 | 0.00 | 370.24 | 0.00 | 0.00 | 988.00 |

| | | | | | | | | | | |
|---|---|---|---|---|---|---|---|---|---|---|
| 2001 | 141 | 4.333 | 1.9 | 15.22 | 16.38 | 0.00 | 381.83 | 0.00 | 0.00 | 988.00 |
| 2001 | 141 | 4.667 | 2.1 | 16.44 | 17.70 | 0.00 | 386.79 | 0.00 | 0.00 | 988.00 |
| 2001 | 141 | 5.000 | 2.2 | 17.17 | 18.23 | 0.00 | 376.76 | 0.00 | 0.00 | 988.00 |
| 2001 | 141 | 5.333 | 2.1 | 17.45 | 18.51 | 0.00 | 382.87 | 0.00 | 0.00 | 988.00 |
| 2001 | 141 | 5.667 | 2.3 | 17.60 | 18.75 | 0.00 | 385.99 | 0.00 | 0.00 | 988.00 |
| 2001 | 141 | 6.000 | 2.7 | 17.97 | 19.19 | 0.00 | 394.18 | 0.00 | 0.00 | 988.00 |
| 2001 | 141 | 6.333 | 3.4 | 18.32 | 19.43 | 0.41 | 399.61 | 0.00 | 0.00 | 988.00 |
| 2001 | 141 | 6.667 | 3.7 | 18.69 | 19.75 | 3.92 | 389.23 | 0.00 | 0.00 | 988.00 |
| 2001 | 141 | 7.000 | 3.8 | 18.69 | 19.85 | 16.78 | 385.88 | 0.00 | 0.00 | 988.00 |
| 2001 | 141 | 7.333 | 3.5 | 18.94 | 20.10 | 34.65 | 393.26 | 0.00 | 0.00 | 988.00 |
| 2001 | 141 | 7.667 | 4.1 | 19.17 | 20.32 | 75.75 | 387.39 | 0.00 | 0.00 | 988.00 |
| 2001 | 141 | 8.000 | 4.4 | 19.51 | 20.57 | 103.87 | 388.76 | 0.00 | 0.00 | 988.00 |
| 2001 | 141 | 8.333 | 4.1 | 19.71 | 20.68 | 11.86 | 404.55 | 0.51 | 0.00 | 988.00 |
| 2001 | 141 | 8.667 | 4.3 | 18.97 | 20.24 | 17.69 | 399.47 | 1.02 | 0.00 | 988.00 |
| 2001 | 141 | 9.000 | 2.1 | 18.20 | 19.51 | 19.80 | 399.70 | 2.03 | 0.00 | 988.00 |
| 2001 | 141 | 9.333 | 1.8 | 17.79 | 19.15 | 74.76 | 404.47 | 0.25 | 0.00 | 988.00 |
| 2001 | 141 | 9.667 | 1.6 | 18.27 | 19.44 | 120.16 | 407.98 | 0.00 | 0.00 | 988.00 |
| 2001 | 141 | 10.000 | 2.3 | 18.90 | 20.14 | 193.00 | 409.14 | 0.00 | 0.00 | 988.00 |
| 2001 | 141 | 10.333 | 3.0 | 19.67 | 20.95 | 360.11 | 403.52 | 0.00 | 0.00 | 988.00 |
| 2001 | 141 | 10.667 | 2.7 | 20.90 | 22.18 | 370.31 | 407.31 | 0.00 | 0.00 | 988.00 |
| 2001 | 141 | 11.000 | 2.8 | 21.98 | 23.14 | 469.26 | 408.56 | 0.00 | 0.00 | 988.00 |
| 2001 | 141 | 11.333 | 3.3 | 22.77 | 23.27 | 264.28 | 418.17 | 0.00 | 0.00 | 988.00 |
| 2001 | 141 | 11.667 | 3.3 | 23.12 | 23.32 | 277.81 | 423.14 | 0.00 | 0.00 | 988.00 |
| 2001 | 141 | 12.000 | 3.8 | 23.38 | 23.57 | 274.47 | 422.61 | 0.00 | 0.00 | 988.00 |
| 2001 | 141 | 12.333 | 3.9 | 23.77 | 23.43 | 393.26 | 416.39 | 0.00 | 0.00 | 988.00 |
| 2001 | 141 | 12.667 | 4.4 | 24.14 | 23.01 | 519.94 | 417.62 | 0.00 | 0.00 | 988.00 |
| 2001 | 141 | 13.000 | 5.1 | 24.84 | 22.78 | 523.09 | 420.36 | 0.00 | 0.00 | 988.00 |
| 2001 | 141 | 13.333 | 4.8 | 24.54 | 22.60 | 185.43 | 416.57 | 0.00 | 0.00 | 988.00 |

| | | | | | | | | | | |
|---|---|---|---|---|---|---|---|---|---|---|
| **2001** | **141** | **13.667** | **5.0** | **24.26** | **21.88** | **260.96** | **416.82** | **0.00** | **0.00** | **988.00** |
| **2001** | **141** | **14.000** | **6.2** | **23.96** | **21.37** | **251.95** | **413.20** | **0.00** | **0.00** | **988.00** |
| **2001** | **141** | **14.333** | **5.5** | **23.57** | **21.71** | **308.70** | **412.09** | **0.00** | **0.00** | **988.00** |
| **2001** | **141** | **14.667** | **6.2** | **23.76** | **21.57** | **448.08** | **414.48** | **0.00** | **0.00** | **988.00** |
| **2001** | **141** | **15.000** | **6.9** | **23.87** | **21.59** | **336.43** | **415.97** | **0.00** | **0.00** | **988.00** |
| **2001** | **141** | **15.333** | **7.2** | **23.49** | **22.03** | **213.32** | **411.64** | **0.00** | **0.00** | **988.00** |
| **2001** | **141** | **15.667** | **7.3** | **23.21** | **20.04** | **217.81** | **411.29** | **0.00** | **0.00** | **988.00** |
| **2001** | **141** | **16.000** | **6.2** | **22.66** | **19.90** | **96.08** | **406.31** | **0.00** | **0.00** | **988.00** |
| **2001** | **141** | **16.333** | **5.0** | **21.40** | **20.64** | **71.71** | **400.35** | **0.00** | **0.00** | **988.00** |
| **2001** | **141** | **16.667** | **4.2** | **20.42** | **20.96** | **146.30** | **402.09** | **0.51** | **0.00** | **988.00** |
| **2001** | **141** | **17.000** | **6.3** | **20.37** | **21.17** | **143.56** | **399.20** | **0.25** | **0.00** | **988.00** |
| **2001** | **141** | **17.333** | **5.6** | **20.26** | **20.67** | **181.10** | **398.02** | **0.25** | **0.00** | **988.00** |
| **2001** | **141** | **17.667** | **7.0** | **20.51** | **20.58** | **156.12** | **400.54** | **0.00** | **0.00** | **988.00** |
| **2001** | **141** | **18.000** | **6.8** | **20.11** | **20.92** | **126.80** | **397.37** | **0.00** | **0.00** | **988.00** |
| **2001** | **141** | **18.333** | **6.2** | **20.90** | **21.37** | **259.79** | **391.16** | **0.00** | **0.00** | **988.00** |
| **2001** | **141** | **18.667** | **7.3** | **21.52** | **20.28** | **186.39** | **389.87** | **0.00** | **0.00** | **988.00** |
| **2001** | **141** | **19.000** | **6.3** | **21.38** | **20.04** | **74.10** | **406.99** | **0.00** | **0.00** | **988.00** |
| **2001** | **141** | **19.333** | **8.8** | **20.87** | **19.95** | **36.38** | **403.43** | **0.00** | **0.00** | **988.00** |
| **2001** | **141** | **19.667** | **7.4** | **20.18** | **20.08** | **83.06** | **396.65** | **0.00** | **0.00** | **988.00** |
| **2001** | **141** | **20.000** | **7.4** | **20.25** | **19.65** | **85.03** | **397.10** | **0.00** | **0.00** | **988.00** |
| **2001** | **141** | **20.333** | **7.4** | **20.20** | **19.48** | **30.70** | **404.25** | **0.00** | **0.00** | **988.00** |
| **2001** | **141** | **20.667** | **9.9** | **19.74** | **18.44** | **8.68** | **400.13** | **0.00** | **0.00** | **988.00** |
| **2001** | **141** | **21.000** | **9.2** | **19.19** | **17.87** | **2.99** | **396.98** | **0.00** | **0.00** | **988.00** |
| **2001** | **141** | **21.333** | **8.6** | **18.68** | **17.79** | **0.00** | **395.89** | **0.00** | **0.00** | **988.00** |
| **2001** | **141** | **21.667** | **9.9** | **17.59** | **17.55** | **0.00** | **387.54** | **0.00** | **0.00** | **988.00** |
| **2001** | **141** | **22.000** | **7.2** | **16.86** | **17.42** | **0.00** | **388.13** | **0.00** | **0.00** | **988.00** |
| **2001** | **141** | **22.333** | **6.6** | **17.12** | **17.07** | **0.00** | **391.30** | **0.00** | **0.00** | **988.00** |
| **2001** | **141** | **22.667** | **5.3** | **17.32** | **16.91** | **0.00** | **390.95** | **0.00** | **0.00** | **988.00** |

| | | | | | | | | | | |
|---|---|---|---|---|---|---|---|---|---|---|
| 2001 | 141 | 23.000 | 4.8 | 17.33 | 16.78 | 0.00 | 390.40 | 0.00 | 0.00 | 988.00 |
| 2001 | 141 | 23.333 | 4.6 | 17.23 | 16.67 | 0.00 | 388.53 | 0.00 | 0.00 | 988.00 |
| 2001 | 141 | 23.667 | 4.7 | 17.20 | 16.52 | 0.00 | 386.79 | 0.00 | 0.00 | 988.00 |
| 2001 | 142 | 0.000 | 5.2 | 17.06 | 16.40 | 0.00 | 385.80 | 0.00 | 0.00 | 988.00 |
| 2001 | 142 | 0.333 | 5.1 | 16.91 | 16.36 | 0.00 | 384.80 | 0.00 | 0.00 | 988.00 |
| 2001 | 142 | 0.667 | 5.1 | 16.82 | 16.22 | 0.00 | 384.64 | 0.00 | 0.00 | 988.00 |
| 2001 | 142 | 1.000 | 5.0 | 16.84 | 15.99 | 0.00 | 377.01 | 0.00 | 0.00 | 988.00 |
| 2001 | 142 | 1.333 | 5.3 | 16.68 | 15.68 | 0.00 | 371.81 | 0.00 | 0.00 | 988.00 |
| 2001 | 142 | 1.667 | 4.7 | 16.60 | 15.54 | 0.00 | 375.20 | 0.00 | 0.00 | 988.00 |
| 2001 | 142 | 2.000 | 4.6 | 16.43 | 15.62 | 0.00 | 376.81 | 0.00 | 0.00 | 988.00 |
| 2001 | 142 | 2.333 | 4.5 | 16.31 | 15.81 | 0.00 | 373.83 | 0.00 | 0.00 | 988.00 |
| 2001 | 142 | 2.667 | 5.0 | 16.29 | 15.40 | 0.00 | 353.52 | 0.00 | 0.00 | 988.00 |
| 2001 | 142 | 3.000 | 4.7 | 16.12 | 14.78 | 0.00 | 359.25 | 0.00 | 0.00 | 988.00 |
| 2001 | 142 | 3.333 | 4.6 | 15.92 | 14.31 | 0.00 | 334.03 | 0.00 | 0.00 | 988.00 |
| 2001 | 142 | 3.667 | 4.2 | 15.37 | 14.14 | 0.00 | 319.64 | 0.00 | 0.00 | 988.00 |
| 2001 | 142 | 4.000 | 4.7 | 15.16 | 13.66 | 0.00 | 344.49 | 0.00 | 0.00 | 988.00 |
| 2001 | 142 | 4.333 | 4.0 | 14.89 | 13.47 | 0.00 | 335.86 | 0.00 | 0.00 | 988.00 |
| 2001 | 142 | 4.667 | 4.0 | 14.69 | 13.24 | 0.00 | 334.56 | 0.00 | 0.00 | 988.00 |
| 2001 | 142 | 5.000 | 3.3 | 14.37 | 13.24 | 0.00 | 322.68 | 0.00 | 0.00 | 988.00 |
| 2001 | 142 | 5.333 | 3.0 | 13.84 | 13.59 | 0.00 | 334.64 | 0.00 | 0.00 | 988.00 |
| 2001 | 142 | 5.667 | 3.5 | 14.07 | 13.92 | 0.00 | 353.35 | 0.00 | 0.00 | 988.00 |
| 2001 | 142 | 6.000 | 4.2 | 14.32 | 13.69 | 0.00 | 355.08 | 0.00 | 0.00 | 988.00 |
| 2001 | 142 | 6.333 | 4.1 | 14.24 | 13.40 | 0.46 | 358.92 | 0.00 | 0.00 | 988.00 |
| 2001 | 142 | 6.667 | 3.9 | 14.06 | 13.35 | 4.30 | 363.63 | 0.00 | 0.00 | 988.00 |
| 2001 | 142 | 7.000 | 3.2 | 13.98 | 13.29 | 13.07 | 360.72 | 0.00 | 0.00 | 988.00 |
| 2001 | 142 | 7.333 | 3.3 | 14.10 | 13.23 | 20.46 | 367.18 | 0.00 | 0.00 | 988.00 |
| 2001 | 142 | 7.667 | 3.6 | 14.19 | 13.11 | 22.75 | 365.89 | 0.00 | 0.00 | 988.00 |
| 2001 | 142 | 8.000 | 3.4 | 14.21 | 12.77 | 31.40 | 365.20 | 0.00 | 0.00 | 988.00 |

| | | | | | | | | | | |
|---|---|---|---|---|---|---|---|---|---|---|
| **2001** | **142** | **8.333** | **3.2** | **14.11** | **12.93** | **38.53** | **363.97** | **0.00** | **0.00** | **988.00** |
| **2001** | **142** | **8.667** | **3.6** | **14.14** | **12.65** | **50.97** | **364.53** | **0.00** | **0.00** | **988.00** |
| **2001** | **142** | **9.000** | **3.9** | **14.16** | **12.46** | **52.89** | **364.43** | **0.00** | **0.00** | **988.00** |
| **2001** | **142** | **9.333** | **3.8** | **14.09** | **12.49** | **73.24** | **364.34** | **0.00** | **0.00** | **988.00** |
| **2001** | **142** | **9.667** | **4.2** | **14.08** | **12.19** | **83.23** | **363.43** | **0.00** | **0.00** | **988.00** |
| **2001** | **142** | **10.000** | **4.2** | **14.04** | **12.09** | **93.64** | **362.28** | **0.00** | **0.00** | **988.00** |
| **2001** | **142** | **10.333** | **4.8** | **14.06** | **12.08** | **158.02** | **361.84** | **0.00** | **0.00** | **988.00** |
| **2001** | **142** | **10.667** | **5.3** | **13.94** | **11.70** | **154.17** | **359.48** | **0.00** | **0.00** | **988.00** |
| **2001** | **142** | **11.000** | **5.4** | **13.94** | **11.17** | **243.65** | **358.06** | **0.00** | **0.00** | **988.00** |
| **2001** | **142** | **11.333** | **5.0** | **14.23** | **11.36** | **302.21** | **355.51** | **0.00** | **0.00** | **988.00** |
| **2001** | **142** | **11.667** | **4.9** | **14.51** | **11.44** | **458.70** | **336.76** | **0.00** | **0.00** | **988.00** |
| **2001** | **142** | **12.000** | **6.2** | **15.23** | **11.35** | **916.27** | **327.72** | **0.00** | **0.00** | **988.00** |
| **2001** | **142** | **12.333** | **5.9** | **15.86** | **11.14** | **763.42** | **337.41** | **0.00** | **0.00** | **988.00** |
| **2001** | **142** | **12.667** | **6.0** | **16.39** | **11.36** | **843.41** | **342.52** | **0.00** | **0.00** | **988.00** |
| **2001** | **142** | **13.000** | **6.4** | **16.09** | **10.49** | **574.82** | **337.80** | **0.00** | **0.00** | **988.00** |
| **2001** | **142** | **13.333** | **7.2** | **16.37** | **10.48** | **998.34** | **334.96** | **0.00** | **0.00** | **988.00** |
| **2001** | **142** | **13.667** | **7.5** | **16.44** | **10.25** | **610.65** | **344.85** | **0.00** | **0.00** | **988.00** |
| **2001** | **142** | **14.000** | **7.1** | **16.63** | **10.27** | **667.10** | **349.15** | **0.00** | **0.00** | **988.00** |
| **2001** | **142** | **14.333** | **7.3** | **16.85** | **9.71** | **854.08** | **351.18** | **0.00** | **0.00** | **988.00** |
| **2001** | **142** | **14.667** | **7.4** | **17.13** | **9.93** | **736.51** | **346.42** | **0.00** | **0.00** | **988.00** |
| **2001** | **142** | **15.000** | **6.9** | **17.23** | **9.91** | **469.52** | **346.94** | **0.00** | **0.00** | **988.00** |
| **2001** | **142** | **15.333** | **7.0** | **17.57** | **9.91** | **661.77** | **348.85** | **0.00** | **0.00** | **988.00** |
| **2001** | **142** | **15.667** | **7.6** | **17.79** | **9.93** | **653.92** | **338.19** | **0.00** | **0.00** | **988.00** |
| **2001** | **142** | **16.000** | **7.4** | **17.95** | **9.54** | **708.00** | **322.87** | **0.00** | **0.00** | **988.00** |
| **2001** | **142** | **16.333** | **6.9** | **17.84** | **9.25** | **627.20** | **333.18** | **0.00** | **0.00** | **988.00** |
| **2001** | **142** | **16.667** | **7.4** | **18.14** | **8.70** | **645.14** | **322.63** | **0.00** | **0.00** | **988.00** |
| **2001** | **142** | **17.000** | **7.0** | **18.12** | **8.80** | **526.62** | **321.01** | **0.00** | **0.00** | **988.00** |
| **2001** | **142** | **17.333** | **6.6** | **18.08** | **8.81** | **471.31** | **323.61** | **0.00** | **0.00** | **988.00** |

| | | | | | | | | | | |
|---|---|---|---|---|---|---|---|---|---|---|
| **2001** | **142** | **17.667** | **6.1** | **17.93** | **8.80** | **381.89** | **318.87** | **0.00** | **0.00** | **988.00** |
| **2001** | **142** | **18.000** | **6.5** | **17.43** | **8.74** | **284.19** | **317.78** | **0.00** | **0.00** | **988.00** |
| **2001** | **142** | **18.333** | **6.5** | **17.85** | **8.72** | **463.47** | **321.92** | **0.00** | **0.00** | **988.00** |
| **2001** | **142** | **18.667** | **6.4** | **17.55** | **8.82** | **216.66** | **317.95** | **0.00** | **0.00** | **988.00** |
| **2001** | **142** | **19.000** | **7.2** | **17.53** | **8.72** | **357.64** | **338.02** | **0.00** | **0.00** | **988.00** |
| **2001** | **142** | **19.333** | **6.4** | **17.20** | **8.58** | **223.47** | **297.79** | **0.00** | **0.00** | **988.00** |
| **2001** | **142** | **19.667** | **5.6** | **17.09** | **8.70** | **174.10** | **296.42** | **0.00** | **0.00** | **988.00** |
| **2001** | **142** | **20.000** | **5.3** | **16.67** | **8.63** | **118.33** | **292.80** | **0.00** | **0.00** | **988.00** |
| **2001** | **142** | **20.333** | **5.0** | **16.28** | **8.59** | **54.21** | **288.22** | **0.00** | **0.00** | **988.00** |
| **2001** | **142** | **20.667** | **3.7** | **15.58** | **9.02** | **20.34** | **286.01** | **0.00** | **0.00** | **988.00** |
| **2001** | **142** | **21.000** | **2.8** | **14.84** | **9.04** | **2.84** | **286.29** | **0.00** | **0.00** | **988.00** |
| **2001** | **142** | **21.333** | **2.0** | **14.23** | **9.49** | **0.00** | **285.50** | **0.00** | **0.00** | **988.00** |
| **2001** | **142** | **21.667** | **2.1** | **13.62** | **9.97** | **0.00** | **285.13** | **0.00** | **0.00** | **988.00** |
| **2001** | **142** | **22.000** | **2.2** | **13.23** | **9.78** | **0.00** | **285.26** | **0.00** | **0.00** | **988.00** |
| **2001** | **142** | **22.333** | **2.9** | **13.05** | **9.81** | **0.00** | **285.25** | **0.00** | **0.00** | **988.00** |
| **2001** | **142** | **22.667** | **3.8** | **13.25** | **9.59** | **0.00** | **285.92** | **0.00** | **0.00** | **988.00** |
| **2001** | **142** | **23.000** | **4.1** | **12.94** | **9.50** | **0.00** | **284.72** | **0.00** | **0.00** | **988.00** |
| **2001** | **142** | **23.333** | **5.5** | **12.91** | **9.33** | **0.00** | **285.71** | **0.00** | **0.00** | **988.00** |
| **2001** | **142** | **23.667** | **4.3** | **12.84** | **9.43** | **0.00** | **286.06** | **0.00** | **0.00** | **988.00** |
| **2001** | **143** | **0.000** | **3.6** | **12.21** | **9.66** | **0.00** | **282.66** | **0.00** | **0.00** | **988.00** |
| **2001** | **143** | **0.333** | **3.2** | **11.68** | **9.65** | **0.00** | **280.93** | **0.00** | **0.00** | **988.00** |
| **2001** | **143** | **0.667** | **3.1** | **11.46** | **9.82** | **0.00** | **279.01** | **0.00** | **0.00** | **988.00** |
| **2001** | **143** | **1.000** | **2.9** | **10.95** | **9.96** | **0.00** | **276.00** | **0.00** | **0.00** | **988.00** |
| **2001** | **143** | **1.333** | **3.3** | **10.92** | **9.82** | **0.00** | **275.81** | **0.00** | **0.00** | **988.00** |
| **2001** | **143** | **1.667** | **2.9** | **10.57** | **9.91** | **0.00** | **275.70** | **0.00** | **0.00** | **988.00** |
| **2001** | **143** | **2.000** | **2.3** | **10.35** | **9.92** | **0.00** | **275.78** | **0.00** | **0.00** | **988.00** |
| **2001** | **143** | **2.333** | **2.7** | **10.12** | **9.91** | **0.00** | **276.35** | **0.00** | **0.00** | **988.00** |
| **2001** | **143** | **2.667** | **2.8** | **9.99** | **9.94** | **0.00** | **275.40** | **0.00** | **0.00** | **988.00** |

| | | | | | | | | | | |
|---|---|---|---|---|---|---|---|---|---|---|
| 2001 | 143 | 3.000 | 3.9 | 10.25 | 9.77 | 0.00 | 276.61 | 0.00 | 0.00 | 988.00 |
| 2001 | 143 | 3.333 | 3.8 | 10.07 | 9.78 | 0.00 | 276.05 | 0.00 | 0.00 | 988.00 |
| 2001 | 143 | 3.667 | 3.4 | 9.89 | 9.69 | 0.00 | 276.32 | 0.00 | 0.00 | 988.00 |
| 2001 | 143 | 4.000 | 3.0 | 9.93 | 9.74 | 0.00 | 277.32 | 0.00 | 0.00 | 988.00 |
| 2001 | 143 | 4.333 | 2.5 | 9.51 | 9.72 | 0.00 | 281.64 | 0.00 | 0.00 | 988.00 |
| 2001 | 143 | 4.667 | 2.8 | 9.30 | 9.75 | 0.00 | 278.69 | 0.00 | 0.00 | 988.00 |
| 2001 | 143 | 5.000 | 2.9 | 9.37 | 9.73 | 0.00 | 280.17 | 0.00 | 0.00 | 988.00 |
| 2001 | 143 | 5.333 | 2.3 | 9.02 | 9.67 | 0.00 | 283.99 | 0.00 | 0.00 | 988.00 |
| 2001 | 143 | 5.667 | 2.1 | 8.93 | 9.76 | 0.00 | 287.09 | 0.00 | 0.00 | 988.00 |
| 2001 | 143 | 6.000 | 2.3 | 8.86 | 9.78 | 0.00 | 282.53 | 0.00 | 0.00 | 988.00 |
| 2001 | 143 | 6.333 | 2.0 | 8.81 | 9.82 | 3.96 | 282.69 | 0.00 | 0.00 | 988.00 |
| 2001 | 143 | 6.667 | 2.0 | 8.68 | 9.87 | 17.52 | 278.91 | 0.00 | 0.00 | 988.00 |
| 2001 | 143 | 7.000 | 1.7 | 8.71 | 9.93 | 50.30 | 286.30 | 0.00 | 0.00 | 988.00 |
| 2001 | 143 | 7.333 | 2.1 | 9.01 | 10.11 | 105.89 | 285.70 | 0.00 | 0.00 | 988.00 |
| 2001 | 143 | 7.667 | 2.8 | 9.45 | 10.32 | 123.69 | 299.20 | 0.00 | 0.00 | 988.00 |
| 2001 | 143 | 8.000 | 3.5 | 9.87 | 10.55 | 144.58 | 317.57 | 0.00 | 0.00 | 988.00 |
| 2001 | 143 | 8.333 | 4.0 | 10.24 | 10.60 | 151.74 | 303.12 | 0.00 | 0.00 | 988.00 |
| 2001 | 143 | 8.667 | 3.8 | 10.62 | 10.64 | 285.38 | 296.82 | 0.00 | 0.00 | 988.00 |
| 2001 | 143 | 9.000 | 4.0 | 11.16 | 10.84 | 443.43 | 293.55 | 0.00 | 0.00 | 988.00 |
| 2001 | 143 | 9.333 | 3.7 | 12.07 | 10.98 | 520.94 | 294.78 | 0.00 | 0.00 | 988.00 |
| 2001 | 143 | 9.667 | 4.1 | 12.38 | 11.11 | 520.84 | 292.48 | 0.00 | 0.00 | 988.00 |
| 2001 | 143 | 10.000 | 4.0 | 12.90 | 10.91 | 584.72 | 299.11 | 0.00 | 0.00 | 988.00 |
| 2001 | 143 | 10.333 | 4.0 | 13.30 | 10.64 | 689.15 | 305.79 | 0.00 | 0.00 | 988.00 |
| 2001 | 143 | 10.667 | 3.0 | 13.78 | 10.30 | 630.08 | 308.49 | 0.00 | 0.00 | 988.00 |
| 2001 | 143 | 11.000 | 3.3 | 13.74 | 10.46 | 552.49 | 309.88 | 0.00 | 0.00 | 988.00 |
| 2001 | 143 | 11.333 | 3.3 | 14.21 | 10.36 | 704.24 | 314.72 | 0.00 | 0.00 | 988.00 |
| 2001 | 143 | 11.667 | 3.3 | 14.80 | 9.67 | 848.58 | 317.09 | 0.00 | 0.00 | 988.00 |
| 2001 | 143 | 12.000 | 4.3 | 15.34 | 9.24 | 918.81 | 316.70 | 0.00 | 0.00 | 988.00 |

| | | | | | | | | | | |
|---|---|---|---|---|---|---|---|---|---|---|
| 2001 | 143 | 12.333 | 4.6 | 15.99 | 9.26 | 921.76 | 323.34 | 0.00 | 0.00 | 988.00 |
| 2001 | 143 | 12.667 | 4.3 | 16.91 | 9.35 | 975.56 | 329.38 | 0.00 | 0.00 | 988.00 |
| 2001 | 143 | 13.000 | 4.6 | 17.29 | 9.25 | 868.74 | 344.17 | 0.00 | 0.00 | 988.00 |
| 2001 | 143 | 13.333 | 5.3 | 17.55 | 8.68 | 765.78 | 353.65 | 0.00 | 0.00 | 988.00 |
| 2001 | 143 | 13.667 | 5.4 | 17.03 | 8.59 | 451.10 | 356.23 | 0.00 | 0.00 | 988.00 |
| 2001 | 143 | 14.000 | 4.3 | 17.06 | 8.61 | 304.55 | 354.29 | 0.00 | 0.00 | 988.00 |
| 2001 | 143 | 14.333 | 3.7 | 16.82 | 8.72 | 98.32 | 356.22 | 0.00 | 0.00 | 988.00 |
| 2001 | 143 | 14.667 | 3.9 | 16.70 | 8.00 | 154.72 | 358.89 | 0.00 | 0.00 | 988.00 |
| 2001 | 143 | 15.000 | 3.0 | 16.34 | 7.89 | 58.46 | 357.92 | 0.00 | 0.00 | 988.00 |
| 2001 | 143 | 15.333 | 4.8 | 15.34 | 8.34 | 81.29 | 354.76 | 0.00 | 0.00 | 988.00 |
| 2001 | 143 | 15.667 | 4.5 | 15.44 | 7.97 | 195.09 | 360.59 | 0.00 | 0.00 | 988.00 |
| 2001 | 143 | 16.000 | 7.0 | 15.68 | 8.42 | 192.35 | 357.45 | 0.00 | 0.00 | 988.00 |
| 2001 | 143 | 16.333 | 7.1 | 15.77 | 8.88 | 159.35 | 356.91 | 0.00 | 0.00 | 988.00 |
| 2001 | 143 | 16.667 | 6.9 | 15.69 | 8.87 | 158.47 | 354.17 | 0.00 | 0.00 | 988.00 |
| 2001 | 143 | 17.000 | 6.1 | 15.31 | 8.16 | 205.51 | 353.84 | 0.00 | 0.00 | 988.00 |
| 2001 | 143 | 17.333 | 4.6 | 15.13 | 7.98 | 202.02 | 356.20 | 0.00 | 0.00 | 988.00 |
| 2001 | 143 | 17.667 | 3.0 | 14.89 | 8.14 | 60.86 | 356.77 | 0.00 | 0.00 | 988.00 |
| 2001 | 143 | 18.000 | 2.8 | 14.34 | 8.12 | 29.90 | 358.22 | 0.00 | 0.00 | 988.00 |
| 2001 | 143 | 18.333 | 3.1 | 14.11 | 8.56 | 37.03 | 360.27 | 0.00 | 0.00 | 988.00 |
| 2001 | 143 | 18.667 | 3.7 | 14.16 | 8.79 | 167.02 | 355.57 | 0.00 | 0.00 | 988.00 |
| 2001 | 143 | 19.000 | 4.4 | 14.28 | 8.87 | 134.73 | 349.53 | 0.00 | 0.00 | 988.00 |
| 2001 | 143 | 19.333 | 4.2 | 14.37 | 9.14 | 152.65 | 316.70 | 0.00 | 0.00 | 988.00 |
| 2001 | 143 | 19.667 | 5.0 | 14.27 | 9.81 | 93.14 | 321.33 | 0.00 | 0.00 | 988.00 |
| 2001 | 143 | 20.000 | 5.6 | 13.83 | 10.38 | 52.16 | 350.15 | 0.00 | 0.00 | 988.00 |
| 2001 | 143 | 20.333 | 4.5 | 13.59 | 10.55 | 16.35 | 356.49 | 0.00 | 0.00 | 988.00 |
| 2001 | 143 | 20.667 | 2.8 | 13.45 | 10.78 | 4.25 | 358.03 | 0.00 | 0.00 | 988.00 |
| 2001 | 143 | 21.000 | 1.9 | 13.48 | 11.08 | 0.00 | 354.27 | 0.00 | 0.00 | 988.00 |
| 2001 | 143 | 21.333 | 2.4 | 13.26 | 11.36 | 0.00 | 334.87 | 0.00 | 0.00 | 988.00 |

| | | | | | | | | | | |
|---|---|---|---|---|---|---|---|---|---|---|
| 2001 | 143 | 21.667 | 1.5 | 13.06 | 11.57 | 0.00 | 296.40 | 0.00 | 0.00 | 988.00 |
| 2001 | 143 | 22.000 | 2.0 | 12.50 | 11.75 | 0.00 | 292.68 | 0.00 | 0.00 | 988.00 |
| 2001 | 143 | 22.333 | 2.4 | 12.00 | 11.79 | 0.00 | 291.24 | 0.00 | 0.00 | 988.00 |
| 2001 | 143 | 22.667 | 2.7 | 12.05 | 11.86 | 0.00 | 291.15 | 0.00 | 0.00 | 988.00 |
| 2001 | 143 | 23.000 | 2.5 | 11.86 | 11.87 | 0.00 | 290.27 | 0.00 | 0.00 | 988.00 |
| 2001 | 143 | 23.333 | 2.4 | 11.63 | 11.84 | 0.00 | 292.21 | 0.00 | 0.00 | 988.00 |
| 2001 | 143 | 23.667 | 2.0 | 11.53 | 11.85 | 0.00 | 300.23 | 0.00 | 0.00 | 988.00 |
| 2001 | 144 | 0.000 | 2.4 | 11.59 | 11.94 | 0.00 | 312.16 | 0.00 | 0.00 | 988.00 |
| 2001 | 144 | 0.333 | 2.9 | 11.58 | 11.94 | 0.00 | 319.19 | 0.00 | 0.00 | 988.00 |
| 2001 | 144 | 0.667 | 2.6 | 11.49 | 11.79 | 0.00 | 308.41 | 0.00 | 0.00 | 988.00 |
| 2001 | 144 | 1.000 | 2.4 | 11.25 | 11.69 | 0.00 | 309.10 | 0.00 | 0.00 | 988.00 |
| 2001 | 144 | 1.333 | 2.6 | 11.34 | 11.62 | 0.00 | 303.80 | 0.00 | 0.00 | 988.00 |
| 2001 | 144 | 1.667 | 2.4 | 11.42 | 11.58 | 0.00 | 302.80 | 0.00 | 0.00 | 988.00 |
| 2001 | 144 | 2.000 | 2.5 | 11.11 | 11.56 | 0.00 | 317.01 | 0.00 | 0.00 | 988.00 |
| 2001 | 144 | 2.333 | 2.7 | 10.95 | 11.52 | 0.00 | 318.88 | 0.00 | 0.00 | 988.00 |
| 2001 | 144 | 2.667 | 1.8 | 10.94 | 11.42 | 0.00 | 322.16 | 0.00 | 0.00 | 988.00 |
| 2001 | 144 | 3.000 | 2.0 | 10.97 | 11.38 | 0.00 | 340.52 | 0.00 | 0.00 | 988.00 |
| 2001 | 144 | 3.333 | 2.2 | 10.81 | 11.46 | 0.00 | 344.19 | 0.00 | 0.00 | 988.00 |
| 2001 | 144 | 3.667 | 2.0 | 10.73 | 11.42 | 0.00 | 332.37 | 0.00 | 0.00 | 988.00 |
| 2001 | 144 | 4.000 | 2.2 | 10.71 | 11.36 | 0.00 | 327.14 | 0.00 | 0.00 | 988.00 |
| 2001 | 144 | 4.333 | 2.1 | 10.56 | 11.36 | 0.00 | 321.30 | 0.00 | 0.00 | 988.00 |
| 2001 | 144 | 4.667 | 3.0 | 10.55 | 11.31 | 0.00 | 330.72 | 0.00 | 0.00 | 988.00 |
| 2001 | 144 | 5.000 | 3.5 | 10.81 | 11.29 | 0.00 | 333.30 | 0.00 | 0.00 | 988.00 |
| 2001 | 144 | 5.333 | 3.1 | 10.87 | 11.39 | 0.00 | 341.02 | 0.00 | 0.00 | 988.00 |
| 2001 | 144 | 5.667 | 2.5 | 10.84 | 11.54 | 0.00 | 341.84 | 0.00 | 0.00 | 988.00 |
| 2001 | 144 | 6.000 | 1.9 | 10.92 | 11.71 | 0.00 | 346.30 | 0.00 | 0.00 | 988.00 |
| 2001 | 144 | 6.333 | 2.0 | 10.88 | 11.77 | 3.35 | 344.91 | 0.00 | 0.00 | 988.00 |
| 2001 | 144 | 6.667 | 2.3 | 10.97 | 11.86 | 24.26 | 344.92 | 0.00 | 0.00 | 988.00 |

| | | | | | | | | | | |
|---|---|---|---|---|---|---|---|---|---|---|
| 2001 | 144 | 7.000 | 3.2 | 11.19 | 11.91 | 35.85 | 350.92 | 0.00 | 0.00 | 988.00 |
| 2001 | 144 | 7.333 | 3.5 | 11.30 | 11.85 | 35.82 | 349.48 | 0.00 | 0.00 | 988.00 |
| 2001 | 144 | 7.667 | 3.4 | 11.55 | 11.90 | 54.68 | 348.40 | 0.00 | 0.00 | 988.00 |
| 2001 | 144 | 8.000 | 3.0 | 11.59 | 11.86 | 82.54 | 349.91 | 0.00 | 0.00 | 988.00 |
| 2001 | 144 | 8.333 | 3.3 | 11.79 | 12.04 | 116.61 | 350.37 | 0.00 | 0.00 | 988.00 |
| 2001 | 144 | 8.667 | 2.3 | 11.97 | 12.04 | 90.99 | 352.17 | 0.00 | 0.00 | 988.00 |
| 2001 | 144 | 9.000 | 2.7 | 11.80 | 11.95 | 59.20 | 351.90 | 0.00 | 0.00 | 988.00 |
| 2001 | 144 | 9.333 | 2.4 | 11.83 | 12.12 | 91.12 | 351.73 | 0.00 | 0.00 | 988.00 |
| 2001 | 144 | 9.667 | 2.9 | 12.18 | 12.36 | 140.46 | 350.69 | 0.00 | 0.00 | 988.00 |
| 2001 | 144 | 10.000 | 2.8 | 12.37 | 12.33 | 209.02 | 348.79 | 0.00 | 0.00 | 988.00 |
| 2001 | 144 | 10.333 | 2.8 | 12.80 | 12.61 | 266.11 | 347.13 | 0.00 | 0.00 | 988.00 |
| 2001 | 144 | 10.667 | 3.7 | 12.86 | 12.56 | 251.55 | 353.44 | 0.00 | 0.00 | 988.00 |
| 2001 | 144 | 11.000 | 4.1 | 13.29 | 12.74 | 329.31 | 352.58 | 0.00 | 0.00 | 988.00 |
| 2001 | 144 | 11.333 | 4.1 | 13.50 | 12.72 | 198.46 | 353.69 | 0.00 | 0.00 | 988.00 |
| 2001 | 144 | 11.667 | 3.7 | 13.46 | 12.67 | 117.57 | 355.26 | 0.00 | 0.00 | 988.00 |
| 2001 | 144 | 12.000 | 3.0 | 13.15 | 12.75 | 107.06 | 356.42 | 0.25 | 0.00 | 988.00 |
| 2001 | 144 | 12.333 | 3.1 | 12.61 | 12.53 | 103.50 | 356.73 | 0.51 | 0.00 | 988.00 |
| 2001 | 144 | 12.667 | 2.8 | 12.74 | 12.89 | 102.65 | 356.76 | 0.25 | 0.00 | 988.00 |
| 2001 | 144 | 13.000 | 3.3 | 12.75 | 13.03 | 103.50 | 357.68 | 0.51 | 0.00 | 988.00 |
| 2001 | 144 | 13.333 | 4.7 | 12.54 | 12.53 | 131.40 | 355.82 | 0.51 | 0.00 | 988.00 |
| 2001 | 144 | 13.667 | 4.9 | 12.87 | 12.78 | 231.86 | 358.05 | 0.00 | 0.00 | 988.00 |
| 2001 | 144 | 14.000 | 5.5 | 13.22 | 12.84 | 364.15 | 359.53 | 0.25 | 0.00 | 988.00 |
| 2001 | 144 | 14.333 | 5.6 | 13.39 | 12.97 | 312.23 | 361.32 | 0.00 | 0.00 | 988.00 |
| 2001 | 144 | 14.667 | 4.9 | 13.26 | 12.92 | 80.03 | 358.69 | 0.25 | 0.00 | 988.00 |
| 2001 | 144 | 15.000 | 3.3 | 12.11 | 12.07 | 49.15 | 359.78 | 4.57 | 0.00 | 988.00 |
| 2001 | 144 | 15.333 | 0.8 | 11.21 | 11.36 | 275.25 | 364.57 | 0.25 | 0.00 | 988.00 |
| 2001 | 144 | 15.667 | 2.3 | 12.62 | 12.70 | 369.65 | 368.52 | 0.00 | 0.00 | 988.00 |
| 2001 | 144 | 16.000 | 3.8 | 13.03 | 12.79 | 175.27 | 368.43 | 0.00 | 0.00 | 988.00 |

| | | | | | | | | | | |
|---|---|---|---|---|---|---|---|---|---|---|
| 2001 | 144 | 16.333 | 5.6 | 13.87 | 11.60 | 826.18 | 331.08 | 0.00 | 0.00 | 988.00 |
| 2001 | 144 | 16.667 | 6.6 | 14.11 | 11.47 | 733.38 | 319.96 | 0.00 | 0.00 | 988.00 |
| 2001 | 144 | 17.000 | 5.3 | 14.50 | 11.61 | 700.18 | 313.91 | 0.00 | 0.00 | 988.00 |
| 2001 | 144 | 17.333 | 4.8 | 14.85 | 11.87 | 565.70 | 316.91 | 0.00 | 0.00 | 988.00 |
| 2001 | 144 | 17.667 | 4.3 | 14.69 | 11.70 | 279.40 | 302.22 | 0.00 | 0.00 | 988.00 |
| 2001 | 144 | 18.000 | 3.6 | 14.94 | 11.34 | 323.37 | 305.66 | 0.00 | 0.00 | 988.00 |
| 2001 | 144 | 18.333 | 2.5 | 15.37 | 11.21 | 353.33 | 323.25 | 0.00 | 0.00 | 988.00 |
| 2001 | 144 | 18.667 | 2.7 | 15.47 | 11.50 | 346.80 | 323.38 | 0.00 | 0.00 | 988.00 |
| 2001 | 144 | 19.000 | 2.7 | 15.51 | 11.08 | 192.13 | 302.21 | 0.00 | 0.00 | 988.00 |
| 2001 | 144 | 19.333 | 2.9 | 15.49 | 10.80 | 237.41 | 303.56 | 0.00 | 0.00 | 988.00 |
| 2001 | 144 | 19.667 | 2.1 | 15.42 | 10.71 | 158.20 | 300.59 | 0.00 | 0.00 | 988.00 |
| 2001 | 144 | 20.000 | 1.7 | 15.30 | 11.08 | 83.53 | 298.34 | 0.00 | 0.00 | 988.00 |
| 2001 | 144 | 20.333 | 1.3 | 15.17 | 11.65 | 33.99 | 294.36 | 0.00 | 0.00 | 988.00 |
| 2001 | 144 | 20.667 | 1.5 | 14.51 | 11.71 | 14.70 | 293.00 | 0.00 | 0.00 | 988.00 |
| 2001 | 144 | 21.000 | 1.7 | 14.10 | 11.50 | 3.02 | 294.53 | 0.00 | 0.00 | 988.00 |
| 2001 | 144 | 21.333 | 1.3 | 14.13 | 11.20 | 0.00 | 295.70 | 0.00 | 0.00 | 988.00 |
| 2001 | 144 | 21.667 | 1.5 | 13.29 | 11.26 | 0.00 | 297.60 | 0.00 | 0.00 | 988.00 |
| 2001 | 144 | 22.000 | 1.5 | 13.01 | 11.40 | 0.00 | 325.83 | 0.00 | 0.00 | 988.00 |
| 2001 | 144 | 22.333 | 3.3 | 13.28 | 11.29 | 0.00 | 348.97 | 0.00 | 0.00 | 988.00 |
| 2001 | 144 | 22.667 | 1.6 | 13.27 | 11.12 | 0.00 | 318.87 | 0.00 | 0.00 | 988.00 |
| 2001 | 144 | 23.000 | 2.5 | 12.86 | 11.10 | 0.00 | 333.54 | 0.00 | 0.00 | 988.00 |
| 2001 | 144 | 23.333 | 2.0 | 12.33 | 11.88 | 0.00 | 333.97 | 0.00 | 0.00 | 988.00 |
| 2001 | 144 | 23.667 | 1.6 | 12.10 | 11.69 | 0.00 | 335.23 | 0.00 | 0.00 | 988.00 |
| 2001 | 145 | 0.000 | 1.4 | 12.03 | 11.34 | 0.00 | 332.24 | 0.00 | 0.00 | 988.00 |
| 2001 | 145 | 0.333 | 2.2 | 11.90 | 11.20 | 0.00 | 316.48 | 0.00 | 0.00 | 988.00 |
| 2001 | 145 | 0.667 | 2.5 | 11.61 | 10.96 | 0.00 | 316.86 | 0.00 | 0.00 | 988.00 |
| 2001 | 145 | 1.000 | 1.8 | 11.11 | 10.99 | 0.00 | 306.96 | 0.00 | 0.00 | 988.00 |
| 2001 | 145 | 1.333 | 1.5 | 10.98 | 10.74 | 0.00 | 302.34 | 0.00 | 0.00 | 988.00 |

| | | | | | | | | | | |
|---|---|---|---|---|---|---|---|---|---|---|
| 2001 | 145 | 1.667 | 1.7 | 10.83 | 10.68 | 0.00 | 292.10 | 0.00 | 0.00 | 988.00 |
| 2001 | 145 | 2.000 | 1.8 | 10.82 | 10.69 | 0.00 | 301.81 | 0.00 | 0.00 | 988.00 |
| 2001 | 145 | 2.333 | 1.9 | 10.42 | 10.73 | 0.00 | 299.27 | 0.00 | 0.00 | 988.00 |
| 2001 | 145 | 2.667 | 2.1 | 10.15 | 10.57 | 0.00 | 287.09 | 0.00 | 0.00 | 988.00 |
| 2001 | 145 | 3.000 | 1.7 | 10.34 | 10.53 | 0.00 | 284.26 | 0.00 | 0.00 | 988.00 |
| 2001 | 145 | 3.333 | 1.8 | 10.23 | 10.52 | 0.00 | 286.61 | 0.00 | 0.00 | 988.00 |
| 2001 | 145 | 3.667 | 2.0 | 9.82 | 10.42 | 0.00 | 301.78 | 0.00 | 0.00 | 988.00 |
| 2001 | 145 | 4.000 | 1.1 | 9.02 | 10.24 | 0.00 | 305.16 | 0.00 | 0.00 | 988.00 |
| 2001 | 145 | 4.333 | 1.3 | 8.35 | 10.14 | 0.00 | 299.69 | 0.00 | 0.00 | 988.00 |
| 2001 | 145 | 4.667 | 1.0 | 7.99 | 10.06 | 0.00 | 315.46 | 0.00 | 0.00 | 988.00 |
| 2001 | 145 | 5.000 | 1.6 | 8.19 | 10.28 | 0.00 | 323.75 | 0.00 | 0.00 | 988.00 |
| 2001 | 145 | 5.333 | 1.8 | 9.20 | 10.67 | 0.00 | 335.98 | 0.00 | 0.00 | 988.00 |
| 2001 | 145 | 5.667 | 1.4 | 9.82 | 10.62 | 0.00 | 326.73 | 0.00 | 0.00 | 988.00 |
| 2001 | 145 | 6.000 | 1.5 | 9.82 | 10.69 | 0.00 | 336.49 | 0.00 | 0.00 | 988.00 |
| 2001 | 145 | 6.333 | 2.4 | 9.92 | 10.85 | 0.00 | 350.11 | 0.00 | 0.00 | 988.00 |
| 2001 | 145 | 6.667 | 3.0 | 10.31 | 11.19 | 0.00 | 349.18 | 0.25 | 0.00 | 988.00 |
| 2001 | 145 | 7.000 | 3.7 | 10.09 | 11.38 | 1.14 | 350.36 | 0.76 | 0.00 | 988.00 |
| 2001 | 145 | 7.333 | 3.5 | 9.44 | 11.13 | 3.63 | 350.13 | 1.27 | 0.00 | 988.00 |
| 2001 | 145 | 7.667 | 1.9 | 9.28 | 11.12 | 23.56 | 348.73 | 0.76 | 0.00 | 988.00 |
| 2001 | 145 | 8.000 | 1.6 | 9.34 | 11.19 | 79.78 | 337.98 | 0.00 | 0.00 | 988.00 |
| 2001 | 145 | 8.333 | 1.3 | 9.43 | 11.17 | 117.63 | 339.19 | 0.00 | 0.00 | 988.00 |
| 2001 | 145 | 8.667 | 1.0 | 9.72 | 11.14 | 90.31 | 345.91 | 0.00 | 0.00 | 988.00 |
| 2001 | 145 | 9.000 | 1.2 | 10.15 | 11.27 | 260.60 | 324.48 | 0.00 | 0.00 | 988.00 |
| 2001 | 145 | 9.333 | 1.1 | 10.68 | 11.38 | 321.48 | 312.18 | 0.00 | 0.00 | 988.00 |
| 2001 | 145 | 9.667 | 2.0 | 11.29 | 11.41 | 393.34 | 337.27 | 0.00 | 0.00 | 988.00 |
| 2001 | 145 | 10.000 | 2.6 | 11.30 | 11.34 | 472.68 | 333.28 | 0.00 | 0.00 | 988.00 |
| 2001 | 145 | 10.333 | 2.3 | 11.89 | 11.76 | 576.60 | 343.46 | 0.00 | 0.00 | 988.00 |
| 2001 | 145 | 10.667 | 2.7 | 12.20 | 11.75 | 578.20 | 325.42 | 0.00 | 0.00 | 988.00 |

# ACKNOWLEDGEMENTS

I would like to thank my advisor, Dr. Brian Hornbuckle. I have learned and improved a lot with your guidance and help in the past four years. Thank you for your efforts, time, and energy and give my best regards to you and your family.

I would like to take this opportunity to thank my advisory committee members, Dr. Robert Horton, Dr. Robert Weber, Dr. Mani Mina, and Dr. James Evans for their guidance and help. Special thanks to Dr. Robert Horton for his professionality, encouragement, and inspiration.

This is a great opportunity to express my thanks to those who helped me with various aspects of conducting research and the writing of this dissertation. Thanks to Dr. Roger De Roo and David Boprie and Halim Elsaadi for their help with the radiometer issues.  I would also like to thank Dr. William Crosson, and Dr. Charles Laymon for their efforts on the theoretical aspects of my research. I would additionally like to thank Dr. Martha Anderson and Dr. John Norman for their help with learning a land-surface model and related computation issues. Thanks to Dr. Eugene Takle for the Global Change course that he taught, and the material he provided.

Thanks to my office mate Daniel Rajewski for his endless help with FORTRAN computations, and Brian Viner for his time to show me how to use a land-surface model. I am grateful to Matthew Regennitter for his critical assistance with a programming issue. Above all, I would like to express my thanks to my family and my fiancé Esen Dogusgen, who have always been with me.